Handbook of
Nanostructured Thin Films and Coatings

Nanostructured Thin Films and Coatings

Mechanical Properties

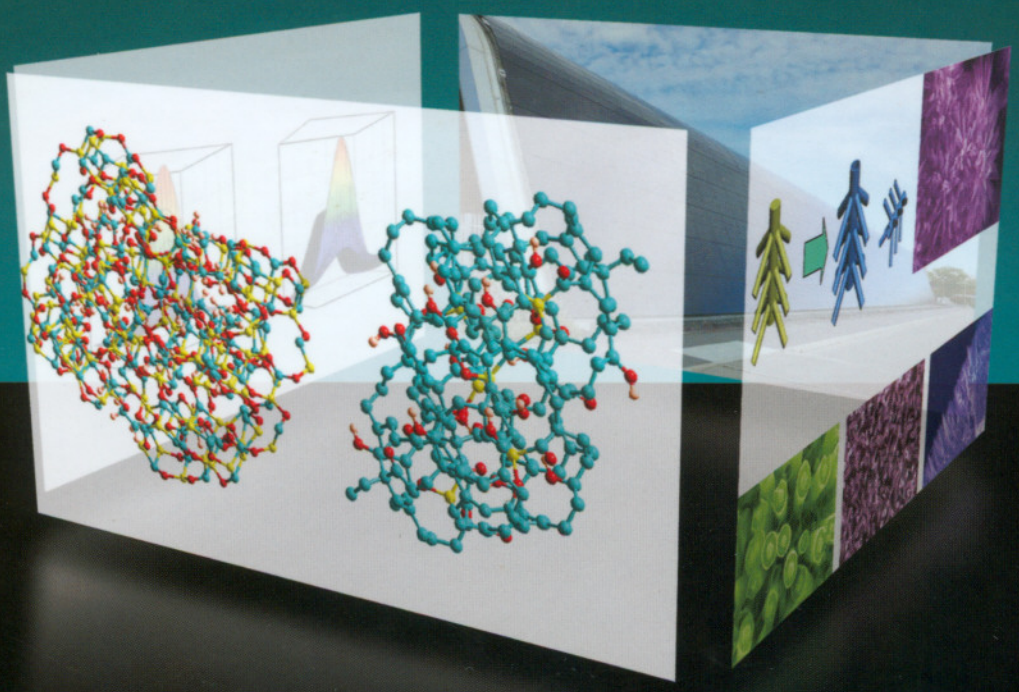

Edited by

Sam Zhang

CRC Press
Taylor & Francis Group

Handbook of
Nanostructured Thin Films and Coatings

Nanostructured Thin Films and Coatings

Mechanical Properties

Edited by
Sam Zhang

CRC Press
Taylor & Francis Group
Boca Raton London New York

CRC Press is an imprint of the
Taylor & Francis Group, an **informa** business

CRC Press
Taylor & Francis Group
6000 Broken Sound Parkway NW, Suite 300
Boca Raton, FL 33487-2742

© 2010 by Taylor and Francis Group, LLC
CRC Press is an imprint of Taylor & Francis Group, an Informa business

No claim to original U.S. Government works

Printed in the United States of America on acid-free paper
10 9 8 7 6 5 4 3 2 1

International Standard Book Number: 978-1-4200-9402-2 (Hardback)

This book contains information obtained from authentic and highly regarded sources. Reasonable efforts have been made to publish reliable data and information, but the author and publisher cannot assume responsibility for the validity of all materials or the consequences of their use. The authors and publishers have attempted to trace the copyright holders of all material reproduced in this publication and apologize to copyright holders if permission to publish in this form has not been obtained. If any copyright material has not been acknowledged please write and let us know so we may rectify in any future reprint.

Except as permitted under U.S. Copyright Law, no part of this book may be reprinted, reproduced, transmitted, or utilized in any form by any electronic, mechanical, or other means, now known or hereafter invented, including photocopying, microfilming, and recording, or in any information storage or retrieval system, without written permission from the publishers.

For permission to photocopy or use material electronically from this work, please access www.copyright.com (http://www.copyright.com/) or contact the Copyright Clearance Center, Inc. (CCC), 222 Rosewood Drive, Danvers, MA 01923, 978-750-8400. CCC is a not-for-profit organization that provides licenses and registration for a variety of users. For organizations that have been granted a photocopy license by the CCC, a separate system of payment has been arranged.

Trademark Notice: Product or corporate names may be trademarks or registered trademarks, and are used only for identification and explanation without intent to infringe.

Visit the Taylor & Francis Web site at
http://www.taylorandfrancis.com

and the CRC Press Web site at
http://www.crcpress.com

Contents

Contents

Preface

The twenty-first century is said to be the century of nanotechnologies. In a way, it is. The development of science and technology has come to a stage where "microscopic" is no longer enough to properly describe or depict a scientific phenomenon or a technological process. With the advance of nanoscience and nanotechnology, the world technological landscape changes not only affect the way scientists do research, technologists carry out development, and engineers manufacture products, but also the way ordinary people go about their daily life, through, for instance, nanomedicine, cell phones, controlled drug delivery, no-pain operations, solar cell–powered gadgets, etc. Thin films and coatings play a very important and indispensable role in all of these. This three-volume book set aims to capture the development in the films and coatings area in relation to nanoscience and nanotechnology so as to provide a timely handbook series for researchers to refer to and for newcomers to learn from, and thus contribute to the advancement of the technology.

The three-volume book set, *Handbook of Nanostructured Thin Films and Coatings*, has 25 chapters where 11 chapters in volume 1 concentrate on the mechanical properties (hardness, toughness, adhesion, etc.) of thin films and coatings, including processing, properties, and performance, as well as a detailed analysis of theories and size effect, etc., as listed here: Chapter 1, The Fundamentals of Hard and Superhard Nanocomposites and Heterostructures; Chapter 2, Determination of Hardness and Modulus of Thin Films; Chapter 3, Fracture Toughness and Interfacial Adhesion Strength of Thin Films: Indentation and Scratch Experiments and Analysis; Chapter 4, Toughness and Toughening of Hard Nanocomposite Coatings; Chapter 5, Processing and Mechanical Properties of Hybrid Sol-Gel- Derived Nanocomposite Coatings; Chapter 6, Using Nanomechanics to Optimize Coatings for Cutting Tools; Chapter 7, Electrolytic Deposition of Nanocomposite Coatings: Processing, Properties, and Applications; Chapter 8, Diamond Coatings: The Industrial Perspective; Chapter 9, Amorphous Carbon Coatings; Chapter 10, Transition Metal Nitride–Based Nanolayered Multilayer Coatings and Nanocomposite Coatings as Novel Superhard Materials; and Chapter 11, Plasma Polymer Films: From Nanoscale Synthesis to Macroscale Functionality.

Volume 2 contains eight chapters focusing on functional properties, i.e., optical, electronic, and electrical properties, and the related devices and applications: Chapter 1, Large-Scale Fabrication of Functional Thin Films with Nanoarchitecture via Chemical Routes; Chapter 2, Fabrication and Characterization of SiC Nanostructured/Nanocomposite Films; Chapter 3, Low-Dimensional Nanocomposite Fabrication and its Applications; Chapter 4, Optical and Optoelectronic Properties of Silicon Nanocrystals Embedded in SiO_2 Matrix; Chapter 5, Electrical Properties of Silicon Nanocrystals Embedded in Amorphous SiO_2 Films; Chapter 6, Properties and Applications of Sol-Gel-Derived Nanostructured Thin Films: Optical Aspects; Chapter 7, Controllably Micro/Nanostructured Films and Devices; and Chapter 8, Thin Film Shape Memory Alloy for Microsystem Applications.

Volume 3 focuses on organic nanostructured thin-film devices and coatings for clean energy with six chapters discussing the processing and properties of organic thin films, devices, and coatings for clean energy applications: Chapter 1, Thin Film Solar Cells Based on the Use of Polycrystalline Thin Film Materials; Chapter 2, Anodized Titania Nanotube Array and its Application in Dye-Sensitized Solar Cells; Chapter 3, Progress and Challenges of Photovoltaic Applications of Silicon Nanocrystalline Materials; Chapter 4, Semiconductive Nanocomposite Films for Clean Environment; Chapter 5, Thin Coating Technologies and Applications in High-Temperature Solid Oxide Fuel Cells; and Chapter 6, Nanoscale Organic Molecular Thin Films for Information Memory Applications.

A striking feature of these books is that both novice and experts have been considered while they were written: the chapters are written in such a way that for newcomers in the relevant field, the handbooks would serve as an introduction and a stepping stone to enter the field with least confusion, while for the experts, the handbooks would provide up-to-date information through the figures, tables, and images that could assist their research. I sincerely hope this aim is achieved.

The chapter authors come from all over the globe: Belgium, China, the Czech Republic, Egypt, Germany, India, Korea, Singapore, Taiwan, the Netherlands, the United Kingdom, and the United States. Being top researchers at the forefront of their relevant research fields, naturally, all the contributors are very busy. As editor, I am very grateful that they all made special efforts to ensure timely response and progress of their respective chapters. I am extremely indebted to many people who accepted my request and acted as reviewers for all the chapters—as the nature of the writing is to cater to both novice and experts, the chapters are inevitably lengthy. To ensure the highest quality of the chapters, more than 50 reviewers (at least two per chapter) painstakingly went through all the chapters and came out with sincere and frank criticism and suggestions that helped make the chapters complete. Though I am not able to list all the names, I would like to take this opportunity to say a big thank you to all of them. Last but not least, I would like to convey my gratitude to many CRC Press staff, especially Allison Shatkin and Jennifer Ahringer at Taylor & Francis Group, for their invaluable assistance rendered to me throughout the entire endeavor that made the smooth publication of the handbook set a reality.

Sam Zhang
Singapore

Editor

Sam Zhang Shanyong, better known as Sam Zhang, received his BEng in materials in 1982 from Northeastern University (Shenyang, China), his MEng in materials in 1984 from the Central Iron and Steel Research Institute (Beijing, China), and his PhD in ceramics in 1991 from the University of Wisconsin-Madison (Madison, Wisconsin). Since 2006, he has been a full professor at the School of Mechanical and Aerospace Engineering, Nanyang Technological University (Singapore).

Professor Zhang serves as editor in chief for *Nanoscience and Nanotechnology Letters* (United States) and as principal editor for the *Journal of Materials Research* (United States), among other editorial commitments for international journals. He has been involved in the fields of processing and characterization of thin films and coatings for the past 20 years, his interests ranging from hard coatings to biological coatings and from electronic thin films to energy films and coatings. He has authored/coauthored more than 200 peer-reviewed international journal articles, 14 book chapters, and guest-edited 9 journal volumes in *Surface and Coatings Technology* and *Thin Solid Films*. Including this handbook, he has authored and/or edited 6 books so far: *CRC Handbook of Nanocomposite Films and Coatings*: Vol. 1, *Nanocomposite Films and Coatings*: *Mechanical Properties*; Vol. 2, *Nanocomposite Films and Coatings*: *Functional Properties*; Vol. 3, *Organic Nanostructured Film Devices and Coatings for Clean Energy*, and *Materials Characterization Techniques* (Sam Zhang, Lin Li, Ashok Kumar, published by CRC Press/Taylor & Francis Group, 2008); *Nanocomposite Films and Coatings—Processing, Properties and Performance* (edited by Sam Zhang and Nasar Ali, Published by Imperial College Press, U.K., 2007), and *CRC Handbook of Biological and Biomedical Coatings* (scheduled for a 2010 publication by CRC Press/Taylor & Francis Group).

Professor Zhang is a fellow at the Institute of Materials, Minerals and Mining (U.K.), an honorary professor at the Institute of Solid State Physics, Chinese Academy of Sciences, and a guest professor at Zhejiang University and at Harbin Institute of Technology. He was featured in the first edition of *Who's Who in Engineering Singapore* (2007), and featured in the 26th and 27th editions of *Who's Who in the World* (2009 and 2010). Since 1998, he has been frequently invited to present plenary keynote lectures at international conferences including in Japan, the United States, France, Spain, Germany, China, Portugal, New Zealand, and Russia. He is also frequently invited by industries and universities to conduct short courses and workshops in Singapore, Malaysia, Portugal, the United States, and China.

Professor Zhang has been actively involved in organizing international conferences: 10 conferences as chairman, 12 conferences as member of the organizing committee, and 6 conferences as member of the scientific committee. The Thin Films conference series (The International Conference on Technological Advances of Thin Films & Surface Coatings), initiated and, since, chaired by Professor Zhang, has grown from 70 members in 2002 at the time of its inauguration to 800 in 2008. It has now become a biannual feature at Singapore.

Professor Zhang served as a consultant to a city government in China and to industrial organizations in China and Singapore. He also served in numerous research evaluation/advisory panels in Singapore, Israel, Estonia, China, Brunei, and Japan. Details of Professor Zhang's research and publications are easily accessible at his personal Web site: http://www.ntu.edu.sg/home/msyzhang.

Contributors

Alsayed Abdel Aal
Surface Protection and Corrosion Control Lab
Central Metallurgical Research and Development Institute
Cairo, Egypt

Ali S. Argon
Department of Mechanical Engineering
Massachusetts Institute of Technology
Cambridge, Massachusetts

Harish C. Barshilia
Surface Engineering Division
National Aerospace Laboratories (CSIR)
Bangalore, India

B.D. Beake
Micro Materials Ltd.
Wrexham, United Kingdom

S.J. Bull
School of Chemical Engineering and Advanced Materials
University of Newcastle
Newcastle upon Tyne, United Kingdom

Vladimir Cech
Institute of Materials Chemistry
Brno University of Technology
Brno, Czech Republic

Lei Chen
Department of Mechanical Engineering
National University of Singapore
Singapore, Singapore

B. Deepthi
Surface Engineering Division
National Aerospace Laboratories (CSIR)
Bangalore, India

G.S. Fox-Rabinovich
Department of Mechanical Engineering
McMaster University
Hamilton, Ontario, Canada

S.R. Goodes
Micro Materials Ltd.
Wrexham, United Kingdom

Haiyan Jiang
Department of Materials Science and Engineering
National University of Singapore
Singapore, Singapore

Ming-Chi Kan
KINIK Company
Taipei Hsien, Taiwan

Alexander M. Korsunsky
University of Oxford
Oxford, United Kingdom

Amit Kumar
Department of Mechanical Engineering
National University of Singapore
Singapore, Singapore

Sandor Nemeth
Singapore Institute of Manufacturing Technology
Singapore, Singapore

K.S. Rajam
Surface Engineering Division
National Aerospace Laboratories (CSIR)
Bangalore, India

Sahendra Pal Sharma
Department of Materials Science and Engineering
National Cheng Kung University
Tainan, Taiwan

J.F. Smith
Micro Materials Ltd.
Wrexham, United Kingdom

James Chien-Min Sung
KINIK Company
Taipei Hsien, Taiwan

and

National Taiwan University
Taipei, Taiwan

and

National Taipei University of Technology
Taipei, Taiwan

Jyh-Ming Ting
Department of Materials Science and Engineering
National Cheng Kung University
Tainan, Taiwan

S.C. Veldhuis
Department of Mechanical Engineering
McMaster University
Hamilton, Ontario, Canada

Stan Veprek
Department of Chemistry
Technical University of Munich
Garching, Germany

Maritza Veprek-Heijman
Department of Chemistry
Technical University of Munich
Garching, Germany

Huili Wang
School of Mechanical and Aerospace Engineering
Nanyang Technological University
Singapore, Singapore

Wan-Yu Wu
Department of Materials Science and Engineering
National Cheng Kung University
Tainan, Taiwan

Kong Boon Yeap
Department of Mechanical Engineering
National University of Singapore
Singapore, Singapore

Kaiyang Zeng
Department of Mechanical Engineering
National University of Singapore
Singapore, Singapore

RuiFeng Zhang
Department of Chemistry
Technical University of Munich
Garching, Germany

Sam Zhang
School of Mechanical and Aerospace Engineering
Nanyang Technological University
Singapore, Singapore

10 Transition Metal Nitride–Based Nanolayered Multilayer Coatings and Nanocomposite Coatings as Novel Superhard Materials

Harish C. Barshilia, B. Deepthi, and K.S. Rajam

CONTENTS

10.1 INTRODUCTION

To meet the ever-changing technological demands, a variety of engineering materials have been developed in the last century. In order to achieve better performance, the engineering materials, in general, should have superior mechanical properties, such as high strength, hardness, and toughness. Also, improved corrosion and friction properties are required for a given application. It is impossible to achieve all these properties in a given engineering material at a low cost. In order to do so, surface modification of the engineering materials is essential [1]. Surface modification techniques

can be used to develop a wide range of functional properties, such as physical, chemical, electrical, electronic, magnetic, mechanical, wear-resistant, and corrosion-resistant properties at the required substrate surfaces. The applications of surface modification cover a wide range of industrial sectors, such as automotive, aerospace, electronic, defense, biomedical, machine tools, etc. Surface modification or surface engineering can be accomplished either by altering the properties of the surface or by applying a protective coating to the surface [2].

Among the different types of coatings used for different purposes, hard coatings (hardness >20 GPa) are particularly important as they provide superior mechanical and tribological properties, which enhance the ability of the surface to resist deformation and wear. For example, hard coatings are an indispensable part of the cutting tool industry as they reduce costs and increase the efficiency of the cutting tools [3]. This is because tools last longer and, in many cases, can be run with minimum or no lubricant. Hard coatings also reduce friction in engine and machine components and improve their performance by reducing wear. The use of hard coatings has spread well beyond tools; they are now being used for many tribological applications and also for decorative purposes [4–6].

A variety of transition metal based hard coatings have been developed since 1980 for various dry and high-speed operations [7]. Transition metals, also called *d*-block elements, are extremely useful because of their physical or chemical properties. Most of the hard materials are formed from the high-melting elements of the transition series. For example, borides, carbides, and nitrides of transition metals (TiB_2, TiC, TiN, etc.) are generally hard materials [8]. Transition metals from the left side of the periodic table, including Sc, Ti, V, Cr, Y, Zr, Nb, Hf, and Ta form nitrides with a B1-NaCl structure [8]. Transition metal nitrides have been studied extensively due to their remarkable properties, including high hardness, wear resistance, chemical inertness, and thermal stability. The excellent mechanical properties of the transition metal nitride coatings are due to the simultaneous contributions of metallic, covalent, and ionic bonding between metal–metal pairs of atoms and metal–nonmetal pairs of atoms [7–9]. The state of the art in transition metal nitride based hard coatings has been reviewed extensively by Holleck and Sundgren and Hentzell in the late 1980s [7,9,10].

Conventionally, TiN (also known as first-generation hard coating) has been widely used as a protective coating to increase the lifetime and performance of cutting and forming tools [11–14]. These coatings are also used as diffusion barriers in microelectronic devices, and as corrosion and abrasion-resistant layers on optical components [15,16]. The main drawback of TiN, however, is its limited oxidation resistance (approximately 500°C) [17]. For many applications, the performance of the TiN coatings at higher temperatures is severely affected because of oxide formation on the surface of the coating, which degrades their wear and friction properties. Differences in the molar volumes of oxide (e.g., 18.75 cc/mol for TiO_2) and nitride (e.g., 11.85 cc/mol for TiN) coatings develop a considerable amount of stress in the coating, which eventually affects adhesion of the coating and, in extreme cases, the coating may not adhere at all to the substrate. It has been reported that the oxidation resistance of TiN is considerably improved by the presence of Al [18,19]. The ternary metallic hard coating of TiAlN has been developed as an alternative to TiN because of its higher oxidation resistance (approximately 750°C) and higher hardness (approximately 30 GPa as compared with 20–25 GPa for TiN coatings) [18–20]. The ternary metallic hard nitride and carbide coatings are commonly known as second-generation hard coatings. The wear performance of TiAlN coating under ambient conditions shows insignificant improvement due to its brittleness and high friction coefficient (e.g., 0.45 ± 0.1 for TiN and 0.65 ± 0.1 for TiAlN) [21]. Similar to TiN, chromium nitride (CrN) has also been used as a hard, protective, and wear-resistant coating for cutting tools [22]. CrN exhibits low-friction coefficient, high corrosion, and wear resistance when compared with TiN [23,24]. But the oxidation resistance of CrN is limited to about 600°C [25]. Similar to TiAlN, the presence of Al in CrN improves the oxidation resistance of CrN coatings. For the ternary nitride coatings, the Al content controls the structure and other properties [20]. For example, at low Al contents, the ternary transition metal nitrides exhibit a cubic structure, and a hexagonal structure is observed at higher Al contents [20]. Other ternary nitride coatings, such as AlTiN, AlCrN, NbAlN, ZrAlN, HfAlN, etc., have also been developed [26–29].

Improvement in the properties of ternary nitride coatings has been attributed to several factors, such as a decrease in the inter-atomic distance, an increase in the covalent nature, and a decrease in the crystallite size [7,20,30]. For example, a decrease in the lattice parameter of TiAlN coating has been observed due to the substitution of some of the Ti atoms (atomic radius = 0.1467 nm) by Al atoms (atomic radius = 0.1431 nm) in the TiN lattice, which is reported to increase the covalent band gap (E_h) according to the expression: $E_h = kd^{-2.5}$, where d is the inter-atomic distance and k is a constant [20]. The addition of Al in TiN increases the covalent bonding as TiN is a metallic hard material and AlN is a covalent bonded material [7]. Therefore, an increase in hardness is expected for TiAlN as compared to TiN due to the covalent contribution. Fine-grained microstructure, exhibiting higher hardness, is well-known for bulk materials. It is true for two-dimensional coating materials as well. Most importantly, in the case of thin coatings, the grain size can be controlled conveniently by substrate bias (V_S) during deposition [13]. Biasing leads to higher nucleation density and consequently to fine-grained morphology. No biasing or lower values of substrate bias leads to coarse grains with a high density of defect structures, consisting of sub-grains and dislocation cell boundaries and, consequently, lower hardness of the coatings [31]. Furthermore, the energy imparted to the growing surface by ion bombardment helps to anneal out imperfections in the coating [31]. But above a certain energy level, the effect of damage induced from the ion bombardment is more than that contributed by the annealing out of the imperfections, leading to a high degree of compressive stress in the coatings [31,32]. Therefore, an optimum value of the substrate bias is required to achieve better properties. In order to obtain hard coatings with superior mechanical properties, concepts other than those discussed above need to be explored.

In recent years, a number of hard coatings with hardness in the range of 40–80 GPa, also known as superhard coatings, have been developed. Attempts have also been made to develop ultrahard coatings with hardness exceeding 80 GPa. These coatings can be divided into: (1) intrinsic, such as diamond (hardness = 80–100 GPa) and cubic boron nitride (c-BN; hardness = 50–60 GPa) and (2) extrinsic, whose mechanical properties are determined by their microstructure. Diamond thin film, however, reacts with oxygen and ferrous materials at higher temperatures [33]. Cubic boron nitride is widely viewed as an ideal superhard coating, however, synthesizing c-BN coating has proved to be difficult [34]. Therefore, applications of diamond and c-BN thin films are limited. In addition, a lot of work has also been carried out on other intrinsic superhard coatings such as a-CN_x, a-B_4C, $B_{12}C_{2.88}Si_{0.35}$, $Si_3N_{2.2}C_{2.16}$, Ti-B-C-N, TiB_2, etc. [35]. However, most of these intrinsic superhard coatings could not be commercialized because of various limitations. In order to overcome the limitations of the intrinsic superhard coatings, in recent years, a number of extrinsic superhard coatings have been developed by various researchers [35–39]. The extrinsic superhard coatings are designed by engineering composite materials at the nanometric scale. Nanoscale engineering, using nanosize grains and nanolayers, results in nanostructured coatings with improved properties.

10.2 NANOSTRUCTURED SUPERHARD COATINGS

Nanostructured coatings, i.e., whose crystallites have dimensions of the order of a few nanometers, exhibit extremely fascinating and useful properties. The unique properties of the nanostructured coatings are due to small grain size and, consequently, large volume fractions of atoms in or near the grain boundaries [40]. A hard coating designed by nanoscale engineering and displaying hardness greater than 40 GPa is defined as nanostructured superhard coating [37]. Because of the complex requirements for a variety of applications, a hard coating must exhibit a combination of contradictory properties, such as high hardness, high strength and toughness, good adhesion, and improved resistance to oxidation and corrosion [1].

The field of nanostructured hard and superhard coatings includes nanocrystalline coatings, nanostructured multilayers, superlattices, nanograded coatings, and nanocomposite coatings [1]. Two of the most important developments in the area of nanostructured superhard coatings are the

preparation and characterization of nanolayered multilayer coatings and nanocomposite coatings [36–39,41]. These coatings are generally known as third-generation hard coatings. Nanostructured hard coatings exhibit hardness values significantly exceeding those given by the rule-of-mixture [37]. For example, for a two-component material, the rule-of-mixture is calculated using the following equation [42]:

$$H = V_A H_A + V_B H_B \tag{10.1}$$

where

V_A and V_B are the volume fractions of components A and B
H_A and H_B are the measured hardness values of A and B, respectively

Hardness values greater than 40 GPa have been obtained using multilayer coatings with a bilayer thickness of the order of a few nanometers [41]. By tailoring the thicknesses of the individual layers, it is possible to produce multilayer films with the desired hardness values [43]. The presence of a large number of sharp interfaces and the difference in shear moduli between the two layer materials are the main factors responsible for high hardness in the multilayer coatings [44]. Other mechanisms, namely coherency strains, Hall–Petch strengthening, etc., have also been used to explain the hardness enhancement in the nanolayered multilayer coatings and these will be discussed briefly, later [45]. Nanocomposites represent a new generation of superhard coatings. Nanocomposite coatings are in the early stages of development and are still being explored in a large way. At present, the origin of the enhanced mechanical properties of the nanocomposite coatings is not very clear. It is believed that at very small grain sizes (≤10 nm), the number of atoms in a boundary region, which surrounds the grain, is comparable to that in the grain. This hinders the generation of dislocations and prevents crack propagation due to grain boundary enhancement and suppression of grain boundary sliding [40,46]. Furthermore, a large volume fraction of grain boundaries provides ductility through grain boundary sliding and nanocracking along grain/matrix interfaces [47].

10.2.1 Nanolayered Multilayer Coatings

Since the publication of a classic paper on the "attempt to design a strong solid" by Koehler in 1970 and experimental validation by Lehoczky in 1978 for thin-layered metal laminates, a lot of research has taken place in search of new superhard materials [44,48]. Theoretically, Koehler demonstrated that by using alternate ultra-thin layers of materials with high and low elastic constants, new materials with superior mechanical properties can be produced. This concept has led to the development of nanolayered multilayer coatings or superlattice coatings [41,43]. Multilayers represent materials engineering on atomic scales, with structures made up of layers only a few atomic monolayers thick. Artificial multilayers are structures prepared by sequentially depositing two (or more) materials on a suitable substrate. A schematic diagram of a multilayer structure is shown in Figure 10.1. The choice of the component materials in a multilayer and the thicknesses of the individual layers play a key role in determining its properties. The bilayer thickness, commonly known as the modulation wavelength (Λ) critically affects the properties of the multilayer coatings. A variety of multilayers and superlattices such as metal/metal (Fe/Ni, Co/Cu, Co/Ni, Ni/Ti, Cu/Ni, etc. [49,50]) metal/ceramic (Ti/TiN, Hf/HfN, Al/AlN, Mo/NbN, etc. [51–53]), and ceramic/ceramic (TiN/CrN, TiN/VN, TiN/NbN, TiAlN/CrN, etc. [54–60]) have been studied by various researchers. The ceramic/ceramic multilayers exhibit superior mechanical and wear-resistant properties among the three multilayer systems. The general interest in the ceramic multilayer coatings has been motivated by the potential for discovering new and yet unknown physical properties, and possible technological applications in diverse fields.

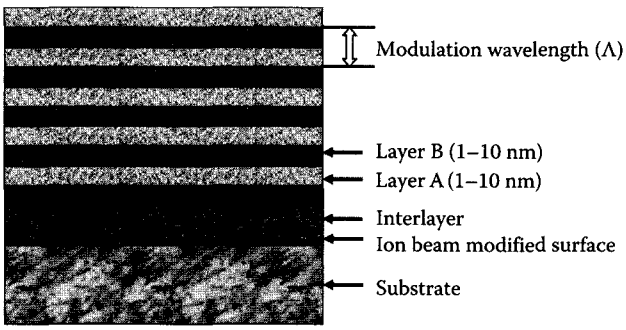

FIGURE 10.1 Schematic diagram of a nanolayered multilayer coating, indicating two different layers A and B, having thicknesses of the order of 1–10 nm. Also shown in the figure is an interlayer, which is used for improved adhesion of the coating. The ion beam modified surface has been indicated to illustrate the importance of *in situ* plasma pretreatments for improved adhesion.

In 1987, Helmersson et al. reported that single-crystal transition metal nitride superlattice films, deposited on MgO (100) substrates by reactive magnetron sputtering, showed hardness 2–3 times those of the homogeneous nitrides [57]. A maximum hardness value of 56 GPa was observed for the TiN/VN multilayer with a modulation wavelength of 5.2 nm. In addition, these multilayers showed a higher wear resistance than the homogeneous materials. This has opened up a wide range of opportunities for the deposition of "tailor-made" superhard superlattice coatings, wherein a variety of combinations can be used. A large number of ceramic/ceramic multilayer systems have been studied in recent years. The most technologically important ceramic/ceramic multilayer systems are: TiN/VN [56,57], TiN/NbN [58,59,61,62], TiN/CrN [54,63,64], TiN/(V_xNb_{1-x})N [65], TiN/AlN [66], TiAlN/TiN [59,67], TiAlN/CrN [60,68,69], CrN/NbN [70], CrN/CrAlN [71], and TiAlN/CrAlN [72].

10.2.1.1 Growth of Nanolayered Thin Coatings

Several physical vapor deposition (PVD) methods have been used to deposit transition metal nitride based nanolayered multilayer coatings. These include: ion beam deposition, sputtering, electron beam evaporation, arc evaporation, etc. Among these methods, the reactive magnetron sputtering process is the most widely used for multilayer deposition [58–60]. The sputtering can be from many different types of sources (radio frequency (RF), pulsed, direct current (DC), planar or cylindrical magnetron, triode or diode) operating at moderately high pressures (0.1–1 Pa), or can be ion-beam sputtering in which the target is bombarded by an ion beam generated independently [73,74].

While depositing nanolayered multilayer thin films using reactive magnetron sputtering, the following two issues need to be addressed carefully: first, the control of the stoichiometry of the component layers and second, the quality of the interfaces [75]. The control of the stoichiometry is a serious issue especially for transition metal nitrides as it is well-known that the heat of formation of the transition metal nitrides differ significantly [41]. For example, in the case of the TiN/NbN multilayer system, the heat of formation of NbN (56.2 kcal/mol) is considerably less than that of TiN (80.8 kcal/mol) [76]. Different partial pressures of nitrogen are thus required in the same deposition chamber to deposit stoichiometric single-phase transition metal nitride coatings. The transition metal nitrides also exist in different phases [8]. For example, niobium nitride exists in different phases: β-Nb_2N, γ-NbN_x, and δ-NbN. δ-NbN has a cubic B1 NaCl *fcc* structure with a lattice parameter of 0.439 nm. Furthermore, the homogeneity range of single phase nitrides is very narrow [8]. Therefore, optimization of deposition parameters such as, modulation wavelength, nitrogen partial pressure, substrate bias, substrate temperature, operating pressure, etc., is required to achieve high quality multilayer coatings. Control of interface quality is also very important as the properties

of the multilayer coatings greatly depend on the nature of the interface. In order to achieve the multilayer coating, the substrate is rotated in between the fixed sources. Because of overlapping of the source materials (e.g., TiN and NbN vapor fluxes in the case of the TiN/NbN multilayer), the interfaces of the multilayers are graded. In view of these issues, extreme caution is needed to achieve repeatability and uniformity across the complex shaped work pieces.

A schematic diagram of a typical semi-industrial magnetron sputtering system for the deposition of transition metal nitride multilayers is shown in Figure 10.2 [77]. The sputtering chamber houses magnetron cathodes, a substrate holder, feed-throughs, etc. A high vacuum pumping system with a turbomolecular pump is generally used to create a vacuum of the order of $1.0–5.0\times10^{-4}$ Pa in the chamber. Four direct-cooled unbalanced magnetron cathodes (circular or rectangular) mounted vertically in opposed-cathode configuration are used for co-sputtering. The cathodes are powered by DC or pulsed-DC generators. The substrates are mounted on a substrate holder plate with planetary rotation and heating facility. This ensures a uniform deposition on complex-shaped substrates. A DC power supply is used for substrate bias and thus ion bombardment. Reactive sputtering is generally carried out at a total $Ar+N_2$ gas pressure of $1.0–5.0\times10^{-1}$ Pa and a thin metallic interlayer is deposited for improved adhesion of the coating. By judicious control of target power density, reactive gas partial pressure, substrate rotation speed, and substrate temperature, it is possible to deposit multilayer coatings with the desired modulation wavelengths. Typically, in order to obtain a multilayer coating of approximately 2–4 μm thickness, the deposition is carried out for a duration of 2–4 h.

In recent years, in order to achieve transition metal nitride multilayer coatings for industrial applications wherein very high growth rates are needed, hybrid deposition systems based upon

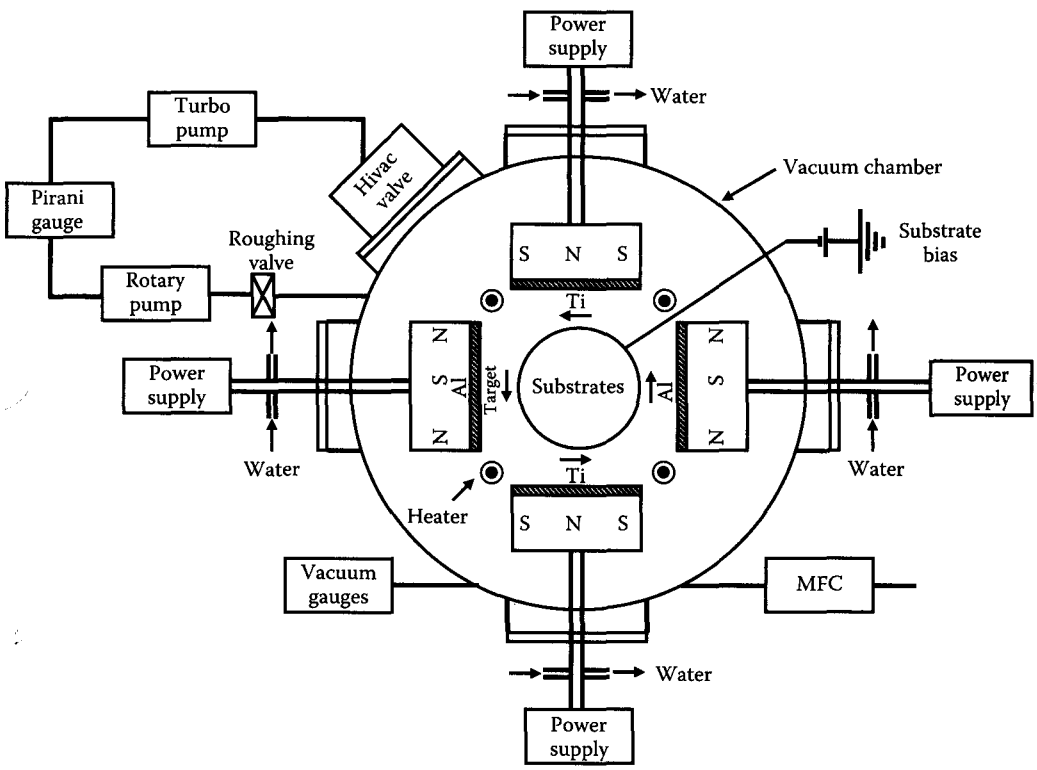

FIGURE 10.2 Schematic diagram of a four-cathode reactive direct current unbalanced magnetron sputtering system for the deposition of transition metal nitride multilayer coatings. The system can also be used to deposit nanocomposite coatings. (From Barshilia, H.C. et al., *Vacuum*, 83, 427, 2008. With permission.)

cathodic arc and magnetron sputtering have been developed [78]. These hybrid deposition systems can provide multilayer coatings with very high adhesion, uniformity, and improved mechanical properties.

10.2.1.2 Structural Characterization and Chemical Composition

X-ray diffraction (XRD) is an essential and universal tool for the structural characterization of multilayer coatings. Numerous researchers have used this technique to investigate structural properties of the nanolayered multilayer coatings [79–83]. The XRD patterns of the multilayer coatings, usually taken in the Bragg-Brentano (θ–2θ) geometry, consist of a convolution of the lattice spacing variations and the composition modulation [41,79]. Interpretation of the XRD data provides information regarding modulation wavelength, inter-planar spacing, orientation, etc. In order to illustrate the structure of a multilayer coating using the x-ray diffraction technique, we present the XRD data of the TiN/NbN multilayer system. Typical XRD patterns of a single-layer TiN coating and a single-layer NbN coating are shown in Figure 10.3. As is evident from the figure, the XRD data of TiN, NbN, and TiN/NbN multilayer coatings exhibit a prominent reflection along the (111) plane; whereas, the XRD pattern of the TiN/NbN multilayer exhibits a principal reflection (PR) flanked by additional reflections known as satellite reflections (SR), which are characteristics of the superlattice formation. The position of the satellite reflection depends on the modulation wavelength of the multilayer coating. The satellite reflection shifts toward the principal reflection with an increase in the modulation wavelength [80]. At very high modulation wavelengths, the satellite reflections merge with the principal reflection, indicating a loss in the superlattice structure. The intensities, the width, and the orders of satellite reflections in a multilayer depend on a variety of factors such as the nature of the coating (epitaxial or polycrystalline), interface width, interface roughness, and individual layer thicknesses [83]. For example, for epitaxially grown TiN/NbN multilayer coatings on MgO substrates, Shinn et al., have reported the appearance of as many as 9 orders of satellite reflections in their XRD data [62]. However, for non-epitaxially grown multilayer coatings, the satellite reflections are usually hidden in the background and only a few orders of satellite reflections are observed in the XRD data. The intensity of the satellite reflection is related to the magnitude of the composition modulation [41]. If

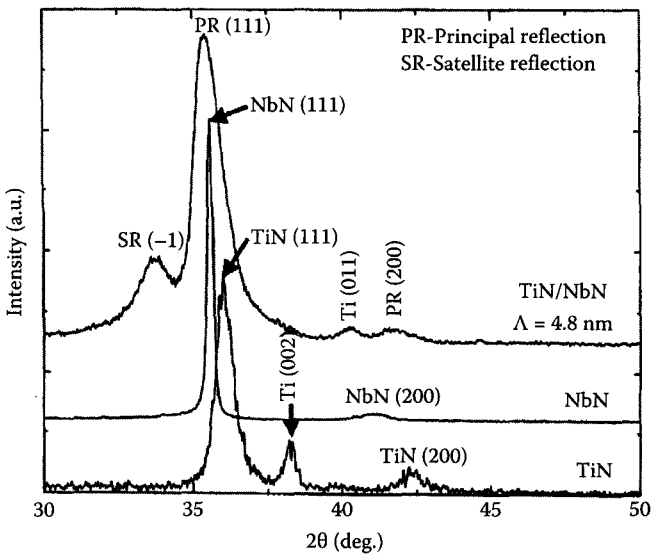

FIGURE 10.3 XRD patterns of single layer TiN coating, single layer NbN coating and TiN/NbN multilayer coating with a modulation wavelength of 4.8 nm. (From Barshilia, H.C. and Rajam, K.S., *Surf. Coat. Technol.*, 183, 174, 2004. With permission.)

the coating does not possess an ideal square wave composition modulation, the intensities of the satellite reflections decrease, with high order peaks being more affected than the low order peaks. Furthermore, the intensities of the positive and negative satellite reflections along the principal reflection depend upon the x-ray scattering efficiency and the lattice mismatch of the component layers [62].

The average lattice spacing ($\bar{d}$) of a multilayer with an ideal interface (i.e., zero width) can be calculated using [81]

$$\bar{d} = \frac{\sum_{i=1}^{n_1} d_{Ai} + \sum_{i=1}^{n_2} d_{Bi}}{n_A + n_B} \tag{10.2}$$

where

$n_{A,B}$ is the number of atomic planes of A, B per bilayer
$d_{Ai,Bi}$ is the growth direction atomic plane spacing of A and B

The average inter-planar spacing of a multilayer lies in between that of the inter-planar spacings of the component layers.

The modulation wavelength of the multilayer coatings can be calculated from the XRD data using the following equation [65]:

$$\Lambda = \frac{\pm m\lambda}{2(\sin\theta_{SR} - \sin\theta_{PR})} \tag{10.3}$$

where

m is the order of the satellite reflection
θ_{PR} is the position of the principal Bragg reflection
θ_{SR} is the position of the satellite reflection
λ is the wavelength of the x-rays

The structure of a superlattice critically depends on the modulation wavelength and the substrate bias. Numerous studies have been presented in the literature regarding the effect of these parameters on the structure of a variety of multilayer coatings [63–65]. It has been reported that the superlattice structure is observed only within a limited range of modulation wavelength (typically 3–20 nm for transition metal nitride multilayers) [41,43]. XRD data from the TiN/NbN multilayer coatings deposited at different modulation wavelengths are shown in Figure 10.4, displaying a superlattice structure for $10.6\,\text{nm} \geq \Lambda \geq 3.0\,\text{nm}$ (data shown only up to 7.0 nm) [58]. The substrate bias, resulting in ion bombardment of the deposited coating, is used for densification of the transition metal nitride multilayer coatings. It has been widely reported that an optimal value of the substrate bias is required to achieve the best mechanical properties [54,56]. Structural analyses of the multilayer coatings deposited at various substrate bias voltages indicate that the substrate bias not only affects the modulation wavelength, but also affects the interface quality. A higher substrate bias leads to a decrease in the modulation wavelength because of re-sputtering of the deposited material. It has been reported that at low substrate bias values, the superlattice layers are generally rough, leading to weak and broad satellite reflections [63]. XRD patterns of polycrystalline TiN/CrN multilayer coatings deposited at different substrate bias voltages are shown in Figure 10.5 [63]. First order satellite reflections can be seen for $V_S \geq 130\,\text{V}$. It must be emphasized here that simulations are required in order to obtain precise quantitative structural information from the XRD data of a multilayer coating. Kinematical and dynamical diffraction theories have been used to simulate the XRD data of multilayer coatings, the details of which can be found elsewhere [41,79–83].

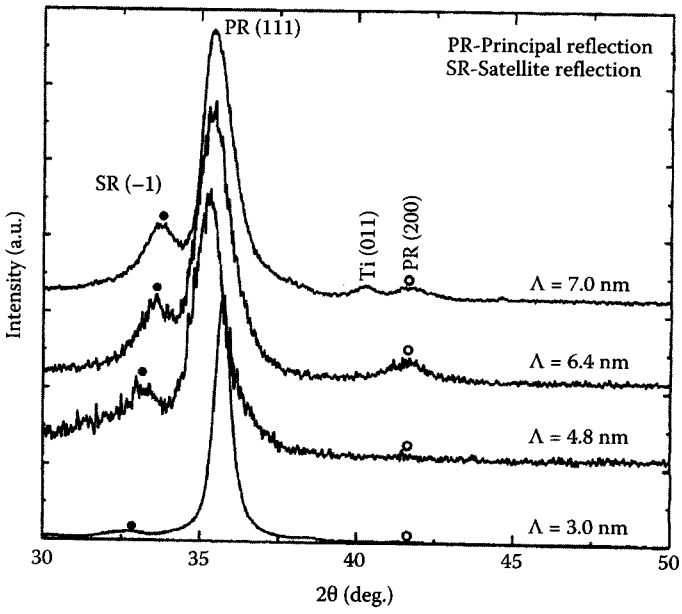

FIGURE 10.4 XRD patterns of TiN/NbN multilayer coatings at different modulation wavelengths. The spectra show (111) principal reflection which is flanked by 1st order negative satellite reflection. (From Barshilia, H.C. and Rajam, K.S., *Surf. Coat. Technol.*, 183, 174, 2004. With permission.)

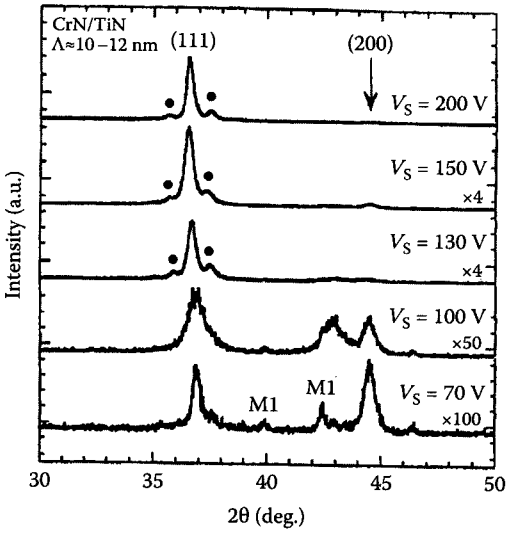

FIGURE 10.5 XRD patterns of CrN/TiN superlattices deposited at various substrate bias voltages. First order satellite peaks around the (111) Bragg peak are observed for $V_S \geq 130$ V, represented by •. M1 represents peaks from the tool steel substrate. (From Yashar, P. et al., *J. Vac. Sci. Technol. A*, 16, 2913, 1998. With permission.)

The characterization of transition metal nitride coatings using XRD provides information on the overall identification of the crystalline phases. However, these nitrides exist in different forms and are not always stoichiometric. Their reactivity to oxygen also affects the stoichiometry. This problem is more serious for ternary and multi-phase nitrides. In addition, minor phases of atomic-molecular dimensions constituting the interface between the crystalline grains may not be detected using

XRD. Therefore, it is necessary to determine the exact chemical composition of the transition metal nitride based coatings. Conventionally, energy dispersive x-ray analysis is used to determine the composition but estimation of the chemical composition of low atomic number elements (such as N, O, C, etc.) is not accurate because of low x-ray energies. Similarly, a glow-discharge optical emission spectroscopy and an electron probe micro-analyzer require appropriate standards, which may contain minor unknown impurities. Other techniques such as an electron energy loss spectroscopy combined with transmission electron microscopy (TEM) and Rutherford backscattering are reliable but complex and time consuming. Electron spectroscopies, in particular, Auger electron spectroscopy (AES) and x-ray photoelectron spectroscopy (XPS), have proved to be versatile techniques for the determination of the chemical composition of thin coatings. The quantification of various elements in a given coating using AES and XPS can be performed using existing models [84]. XPS is more accurate than AES since the signal-to-noise ratio is very high and is, therefore, routinely used to characterize the nitride coatings.

The use of XPS allows for obtaining information on the chemical structure and bonding states in the outermost ~5 nm of the thin coating. The chemical state of the nitride coatings is usually characterized by the binding energy position of the N 1*s* and the respective metal or nitride-forming element lines. The N 1*s* line recorded on a chemically well-defined nitride is of a single Gaussian shape with a full-width-at-half maximum (FWHM) of approximately 1.6–1.9 eV [85]. Any significant broadening is usually indicative of the presence of a new chemical state. The XPS core level spectra of such samples need to be deconvoluted in order to obtain chemical states of different phases. As the samples are usually exposed to air prior to the XPS measurements, the XPS spectra may contain information on surface oxide contamination. Of course, if the partial pressure of oxygen is not sufficiently low during the deposition ($<10^{-5}$ Pa), there are chances of formation of oxy-nitrides/oxides, which can be very easily detected in the XPS data. Sputter cleaning is generally used to eliminate the effect of surface oxide contamination on the XPS spectra of a given coating. In Table 10.1, we summarize the binding energy values of N 1*s*, O 1*s*, metal, nitride, and oxide compounds of important hard coating materials. This table may be used as a quick reference to find out the binding energies of spectral lines of various nitrides. Detailed characterization of transition metal nitride coatings using XPS can be found elsewhere [84–86].

10.2.1.3 Interface Characterization

The properties of the multilayer coatings are determined by the modulation wavelength and the thickness fluctuations between the two component layers [105]. The multilayer coatings exhibit superior properties only at very low modulation wavelengths. Furthermore, the thickness fluctuation leads to accumulation of interface roughness, resulting in deterioration of properties of the multilayer coatings [106]. Therefore, determination of the modulation wavelength and the interface properties (interface roughness, width, etc.) of the multilayer coatings is very important. X-ray reflectivity (XRR) has been widely employed by a number of authors to determine the interface properties of metallic multilayer coatings [107–109]. However, there are only a few papers wherein detailed studies on interface properties of the transition metal nitride based multilayer coatings using XRR have been reported [110–112].

The reflectivity in a multilayer depends on the difference in the electron densities between the two layers [107]. The refractive index (n) in materials for x-rays of wavelength around 0.1 nm is slightly less than unity. While passing from the air ($n=1$) to the material ($n<1$), it is possible to reflect the beam if the incident angle θ_m (which is the angle between the surface of the sample and incident beam) is small enough. This is known as the total external reflection of x-rays and the angle is called critical angle. If one or more thin films of different electron densities are present, interference oscillations are observed in the reflectivity profile. From the XRR data, the modulation wavelength of a multilayer is determined using the modified Bragg's law, expressed as [110,112]

TABLE 10.1
Core Level Binding Energy Values of Various Transition Metal Nitride Coatings

Element	Metallic (eV)	Nitride (eV)	N 1*s* (eV)	Oxide (eV)	O 1*s* (eV)	References
Ti	Ti $2p_{3/2}$ 453.8 Ti $2p_{1/2}$ 459.9	TiN: Ti $2p_{3/2}$ 455.1 Ti $2p_{1/2}$ 461.0	TiN: 397.4	TiO_2: Ti $2p_{3/2}$ 458.5 Ti $2p_{1/2}$ 464.6 TiO: Ti $2p_{3/2}$ 455.0 Ti $2p_{1/2}$ 461.0	TiO_2: 530.4	[84–89]
Cr	Cr $2p_{3/2}$ 574.3 Cr $2p_{1/2}$ 583.5[a]	CrN: Cr $2p_{3/2}$ 574.7 Cr $2p_{1/2}$ — Cr_2N: Cr $2p_{3/2}$ 574.5 Cr $2p_{1/2}$ —	CrN: 396.6 Cr_2N: 397.5	Cr_2O_3: Cr $2p_{3/2}$ 576.6 Cr $2p_{1/2}$ 586.4 CrO_2: Cr $2p_{3/2}$ 576.4 Cr $2p_{1/2}$ 586.1 CrO_3: Cr $2p_{3/2}$ 580.1 Cr $2p_{1/2}$ 589.2	Cr_2O_3: 530.0 CrO_2: 529.3 CrO_3: 529.7	[84–86,90–93]
Nb	Nb $3d_{5/2}$ 202.2 Nb $3d_{3/2}$ 205.0	NbN: Nb $3d_{5/2}$ 203.8 Nb $3d_{3/2}$ —	NbN: 397.7	Nb_2O_5: Nb $3d_{5/2}$ 207.2 Nb $3d_{3/2}$ 210.7 NbO_2: Nb $3d_{5/2}$ 205.9 Nb $3d_{3/2}$ — NbO: Nb $3d_{5/2}$ 203.0 Nb $3d_{3/2}$ —	Nb_2O_5: 530.8 NbO_2: 530.6 NbO: 530.7	[86,94,95]
B	B1*s* 186.5	BN: B 1*s* 190.5	BN: 398.1	B_2O_3: B 1*s* 193.1	B_2O_3: 533.2	[84–86, 96,97]
Al	Al 2*p* 72.6	AlN: Al 2*p* 73.6	AlN: 397.0	Al_2O_3: Al 2*p* 74.7	Al_2O_3: 531.0	[84–86]
Hf	Hf $4f_{7/2}$ 13.9 Hf $4f_{5/2}$ 15.6	HfN: Hf $4f_{7/2}$ 15.0 Hf $4f_{5/2}$ 16.7	HfN: 396.0	HfO_2: Hf $4f_{7/2}$ 17.3 Hf $4f_{5/2}$ 18.9	HfO_2: 532.8	[98,99]
Zr	Zr $3d_{5/2}$ 178.5 Zr $3d_{3/2}$ 181.1	ZrN: Zr $3d_{5/2}$ 179.8 Zr $3d_{3/2}$ 182.2	ZrN: 397.5	ZrO_2: Zr $3d_{5/2}$ 182.9 Zr $3d_{3/2}$ 185.3	ZrO_2: 530.7	[87,100]
V	V $2p_{3/2}$ 512.1 V $2p_{1/2}$ 519.9	VN: V $2p_{3/2}$ 514.3 V $2p_{1/2}$ —	VN: 397.2[a]	V_2O_3: V $2p_{3/2}$ 515.7 V $2p_{1/2}$ 523.3 V_2O_5: V $2p_{3/2}$ 517.4 V $2p_{1/2}$ 524.9 VO_2: V $2p_{3/2}$ 515.9 V $2p_{1/2}$ 523.3	V_2O_3: 530.1 V_2O_5: 529.8 VO_2: 529.7	[86,101,102]
W	W $4f_{7/2}$ 31.0 W $4f_{5/2}$ 33.1	WN: W $4f_{7/2}$ 33.0 W $4f_{5/2}$ 35.0	WN: 397.3	WO_2: W $4f_{7/2}$ 32.7 W $4f_{5/2}$ 34.9 WO_3: W $4f_{7/2}$ 35.7 W $4f_{5/2}$ 37.9	WO_2: 531.0 WO_3: 530.6	[86,103]
Si	Si 2*p* 99.1	Si_3N_4: Si 2*p* 102.0	Si_3N_4: 397.7	SiO_2: Si 2*p* 103.4	SiO_2: 533.1	[84–86,104]

Source: Values taken from NIST x-ray photoelectron spectroscopy database, Version 3.5 (National Institute of Standards and Technology, Gaithersburg, 2003); http://srdata.nist.gov/xps/

$$\sin^2\theta_m = (m\lambda/2\Lambda)^2 + 2\delta \tag{10.4}$$

where

m is the order of reflection
λ is the wavelength of x-rays
δ is related to the average refractive index

According to Equation 10.4, a linear fit to the observed data can be made by plotting $(m\lambda)^2$ versus $\sin^2\theta_m$. The slope of the resulting line is then equal to $4\Lambda^2$, and from this Λ can be derived. The XRR pattern also contains information on the individual layer thicknesses and interface and surface roughnesses *[112,113].*

Typical XRR scans of TiN/CrN multilayer coatings at different modulation wavelengths are shown in Figure 10.6. Simulations of the experimentally observed XRR data are required in order to

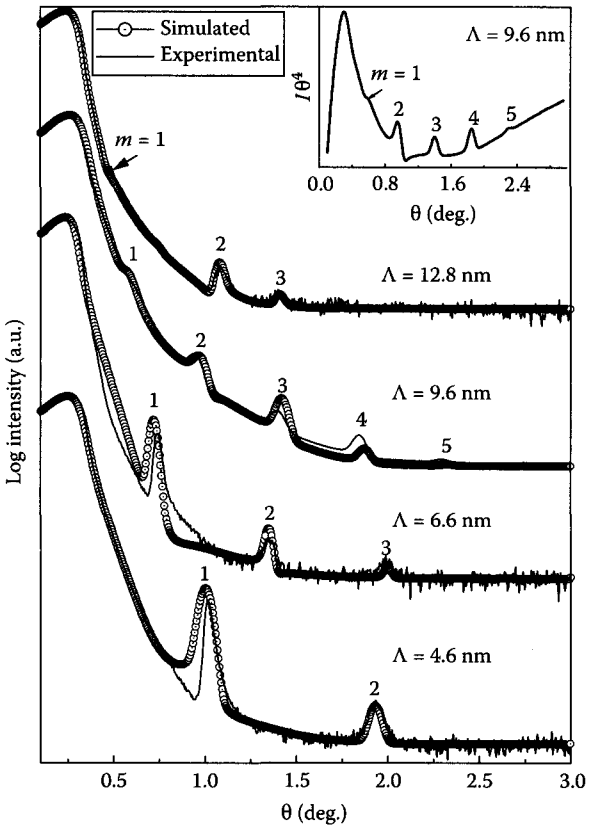

FIGURE 10.6 Experimental and simulated low angle XRR patterns of TiN/CrN multilayer coatings deposited at various modulation wavelengths. Also shown is a plot of θ versus $I\theta^4$ for the multilayer with a modulation wavelength of 9.7 nm. (From Barshilia, H.C. et al., *J. Phys. D Appl. Phys.*, 41, 205409, 2008. With permission.)

obtain the information on interface properties. The simulation of the XRR data is generally carried out employing the well-known Parrat formalism for specular x-ray reflection [107]. The Parrat formalism is based on a successive reflection of low angle x-rays at many interfaces as in the case of a superlattice. The simulated data for TiN/CrN multilayer coatings is shown using dotted curves in Figure 10.6. Detailed discussions on the effect of various process parameters on the interface properties of transition metal nitride based multilayers can be found elsewhere [112]. To summarize, the phase and amplitude of the reflected x-rays are functions of many parameters such as electron density, interface roughness, surface roughness, and individual layer thickness. The interface roughness in a multilayer depends upon (1) the number of bilayers, (2) the bilayer thickness, and (3) the ratio of individual layer thicknesses [113]. For thin films (that is a single layer), theoretically, it has been shown that the width of the interface (ε) scales with thickness (t) by the general relation $\varepsilon \approx t^{\beta}$ with $\beta = 0.2–0.5$ [109]. Furthermore, for the sputtered films, the substrate temperature (50°C–450°C) is low compared with the melting temperature of the deposited materials (e.g., 2950°C for TiN and 1500°C for CrN); the expected surface morphology consists of columns with a characteristic length ξ, which scales with thickness as $\xi \approx t^{p}$ with p as the scaling exponent [109]. For multilayer coatings, however, the roughness evolution is more complex because of the existence of many buried interfaces [114]. It has been reported that for a multilayer, the intensity of the XRR peaks is reduced by a Debye-Waller-like factor $\exp(-2k_1k_2\,\sigma'^2)$, where k_1 and k_2 are wave vectors in the constituent layers and σ′ is the interface roughness [109]. The higher order XRR peaks are sensitive to

roughness and a decrease in the intensities of the higher order peaks is observed with an increase in the interface roughness. There are other causes for a reduction in the intensity of XRR peaks; these include long-range waviness of the sample beyond the limits of resolution of the diffractometer and surface roughness [115]. Interface broadening is also attributed to inter-diffusion and intermixing. Intermixing is the mixing of interfaces due to energetic particle bombardment, whereas inter-diffusion is the thermally activated transport of material across the interface. Because of the low substrate temperature generally used during the deposition of transition metal nitride multilayers, inter-diffusion between the component layers is insignificant [116,117]. The surface roughness of PVD deposited transition metal nitrides is mainly attributed to the columnar microstructure and formation of oxides on the surface of the coating when exposed to ambient. In general, a decrease in the surface roughness is observed at a low modulation wavelength, which is attributed to the interruption of columnar grains because of the alternating deposition of constituent layers [52]. Furthermore, the thickness fluctuations (discrete and continuous) give rise to cumulative disorder and destroy the long-range order of the superlattice, resulting in main Bragg-peak broadening and dampening of higher order Bragg-peak intensities [82].

10.2.1.4 Microstructural Characterization

Cross-sectional transmission electron microscopy (XTEM) is an ideal tool for studying ultra-thin layers of the multilayer coatings even though it is a destructive technique and the sample preparation is tedious [118,119]. The sample preparation for XTEM has been reviewed by Bravman and Sinclair [118]. XTEM yields direct information about layer thickness, uniformity of the layer, interface roughness, and interfacial defects (e.g., misfit dislocations and voids) [62,65]. XTEM has been employed to study the microstructure including grain size, orientation, and texture as well as the types and distribution of defects (dislocations, stacking faults) [62,65]. Furthermore, high-resolution transmission electron microscopy (HRTEM) allows imaging on an atomic scale with the possibility of locally determining crystal structure, inter-planar spacing, and interface characteristics such as coherency, morphology, and epitaxial relationships between the layers. The crystal structure and the lattice parameter of a multilayer can also be obtained from selected area electron diffraction (SAD).

A number of metal/metal [120–122], metal/ceramic [53], and ceramic/ceramic [123–128] superlattices have been characterized using XTEM. XTEM images provide detailed information on the microstructure and evolution of the layers from the interface to the outer surface as is shown in Figure 10.7 for a TiN/NbN multilayer coating along with a Ti interlayer deposited on a Si substrate in which the superlattice period is approximately 6–8 nm. The XTEM image shows that the composition modulation did not vary along the growth direction i.e., with the thickness of the coating, and bulk thermal diffusion or ion-induced intermixing between the layers is minimal. The interdiffusion between the layers, however, can be studied more precisely using electron energy loss spectroscopy and chemical mapping. The absence of any inter-lamella cracking indicates good adhesion between the multilayers and the substrate. The layers are well defined, but exhibit some non-planarity. These results are markedly different from epitaxial TiN/NbN superlattices, where the layers are reported to be nearly planar [62]. It must be emphasized that the lack of multiple XRD superlattice peaks in the case of TiN/NbN polycrystalline superlattices, as discussed Section 10.2.1.3, is due to the non-uniform and non-planar nature of the polycrystalline layers. The XTEM micrograph (Figure 10.7) clearly shows alternating layers of TiN and NbN. The layers can be easily recognized since TiN layers are visible as bright bands and NbN layers are visible as dark bands because of a higher average atomic number for NbN [62]. The

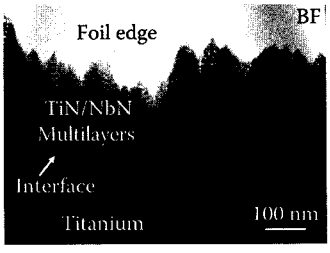

FIGURE 10.7 Cross-sectional bright field TEM image of a TiN/NbN multilayer coating along with Ti interface. (From Barshilia, H.C. et al., *Surf. Coat. Technol.*, 200, 4586, 2006. With permission.)

micrograph suggests that the interface between the Ti interlayer and the multilayers has a wavy nature and the multilayers are grown with a columnar microstructure. At the column boundary, the layers are typically curved towards the substrate; the origin of which is not known and has been observed for a variety of strained films [57,62,65,129]. It is known that the PVD coatings deposited at a low substrate temperature and a low gas pressure exhibit a columnar microstructure [130]. The wavy nature and the columnar microstructure of the transition metal nitride multilayer coatings affect the mechanical properties significantly. The columnar microstructure of the TiN/NbN multilayers is displayed more clearly in Figure 10.8, exhibiting a fully dense structure, i.e., no grain boundary porosity between the columns and low-angle columnar grains oriented along the growth direction with column widths of approximately 100–200 nm. The presence of the low-angle columnar grains is a common feature in lattice mismatched films (e.g., 3.6% mismatch between TiN and NbN) [128]. The dense structure of the multilayers is attributed to ion bombardment as a suitable substrate bias is generally used to densify the microstructure of transition metal nitride superlattices [58,64]. The ion bombardment also smoothens the film surface [13]. Porous boundaries have been observed for TiN/NbN multilayer films prepared at a low substrate bias [56]. The micrograph in Figure 10.8 also shows that the superlattice layer thicknesses do not vary measurably either along the layers or through the film thickness, and the layers are continuous across the column boundaries. A large amount of layer roughness is evident from the TEM micrograph presented in Figure 10.8. The bilayer period and relative layer thickness ratio can also be determined from the TEM data as shown in bright field (BF) XTEM image of a TiN/NbN multilayer coating taken at a very high magnification (Figure 10.9).

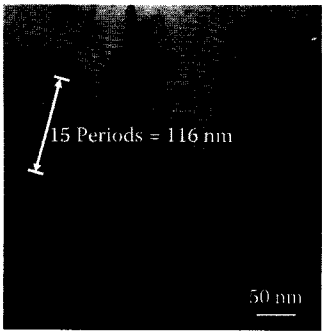

FIGURE 10.8 Cross-sectional TEM image of TiN/NbN multilayers at relatively higher magnification showing columnar growth. (From Barshilia, H.C. et al., *Surf. Coat. Technol.*, 200, 4586, 2006. With permission.)

The crystalline nature of the multilayers can be examined using HRTEM and SAD. For example, the HRTEM image of a TiN/NbN multilayer coating presented in Figure 10.10 clearly shows that the layers are crystalline with no amorphous regions. A typical SAD pattern of a polycrystalline TiN/NbN multilayer coating shown in Figure 10.11 exhibits a spotty, discontinuous ring pattern, indicating small randomly oriented grains. As the lattice parameters of TiN (0.424 nm) and NbN (0.439 nm) are very close, the diffraction rings from the multilayers are broader, resulting from the superposition of the reflections from TiN and NbN. The rings marked as 1, 2, 3, and 4 in Figure 10.11 correspond to (111), (200), (220), and (311) planes of TiN and NbN. It must be mentioned that the SAD pattern from a single crystalline epitaxial TiN/NbN multilayer coating shows satellite reflections along the Bragg reflection, from which the modulation wavelength can also be calculated [62]. However, in the case of polycrystalline multilayer coatings, the satellite peaks are not observed as is shown in Figure 10.11 for TiN/NbN multilayers.

FIGURE 10.9 Cross-sectional bright field TEM image of TiN/NbN multilayers at very high magnification showing distinct layers of TiN and NbN. (From Barshilia, H.C. et al., *Surf. Coat. Technol.*, 200, 4586, 2006. With permission.)

10.2.1.5 Mechanical Properties

The mechanical properties of the transition metal nitride based multilayer coatings are of great interest because these multilayers exhibit very high strength and hardness at very low modulation wavelengths. Over the last two decades, significant advances have been made in the measurement of mechanical properties of thin coatings using nanoindentation techniques coupled with scanning probe microscopy such as atomic force microscopy (AFM)

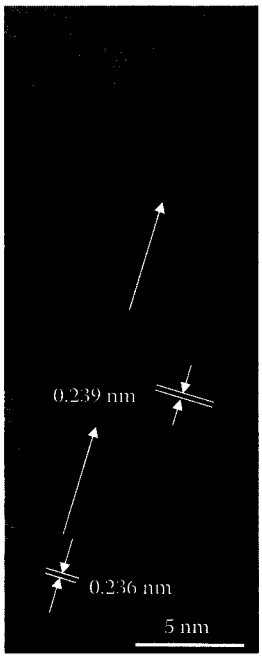

FIGURE 10.10 HRTEM image of a portion of TiN/NbN multilayers (30×12 nm), indicating crystalline nature of the TiN and NbN layers. (From Barshilia, H.C. et al., *Surf. Coat. Technol.*, 200, 4586, 2006. With permission.)

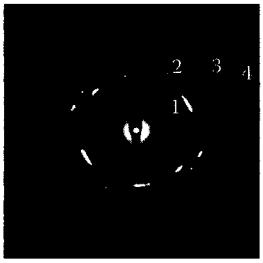

FIGURE 10.11 SAD pattern of TiN/NbN multilayer coating. (From Barshilia, H.C. et al., *Surf. Coat. Technol.*, 200, 4586, 2006. With permission.)

[131–133]. In the case of very thin coatings (e.g., nanolayered multilayer coatings), the intrinsic hardness becomes meaningful only if the influence of the substrate material is eliminated [134]. Thus, the indentation depth should not exceed about 1/10th of the total coating thickness. Applied loads in the range of 0.5–50 mN are desirable if the indentation depths are to remain in the nanometer range [131]. For the nanoindentation measurements, an indenter of known geometry is pressed onto the sample. After initial contact of the indenter on the sample surface, the load is increased at a predetermined rate to the desired maximum load (e.g., 5 mN) and then decreased at the same rate to zero. From the load versus displacement curves, the mechanical properties of the coatings are evaluated. The Oliver and Pharr method is the most commonly used approach for calculating the hardness (H) and the elastic modulus (E) from the nanoindentation measurements [132]. In this method, the hardness and the elastic modulus are calculated from the load–displacement data using the relationship

$$H = \frac{P_{\max}}{A} \tag{10.5}$$

$$E^* = \frac{E}{1-\nu^2} = \frac{\sqrt{\pi}}{2}\frac{S}{\sqrt{A}} \tag{10.6}$$

where

$P_{\max}$ is the peak indentation load
A is the projected contact area
E^* is the effective elastic modulus
ν is the Poisson ratio
S is the experimentally measured contact stiffness

In general, the loading data are influenced more by the plastic properties of the material and the unloading data are influenced more by the elastic properties [135]. It must be emphasized that the hardness values measured by the nanoindentation technique are sensitive functions of surface roughness, oxidation of the surface layer, and indenter size effect [131]. Therefore, these factors need to be considered for the accurate measurement of the hardness and the elastic modulus of the coatings.

In general, transition metal nitride based nanostructured coatings exhibit high toughness, however, at present there is neither a standard test procedure nor a standard methodology for assessment of the toughness of thin coatings. In recent years, efforts have been made by Zhang et al., and others toward the toughness measurements in thin coatings [47,136,137]. In this section, we will briefly discuss that qualitative information on toughness can also be inferred from the nanoindentation measurements. Load versus displacement curves for a typical TiN/NbN nanolayered multilayer coating deposited on a tool steel substrate at a load of 5 mN are shown in Figure 10.12. For a comparison, the data for the component layers (i.e., NbN and TiN) are also presented. Apart from the hardness and the elastic modulus of the coating, additional information on elastic/plastic deformation and toughness can also be inferred from the load versus displacement curves. The area between the loading and unloading curves of

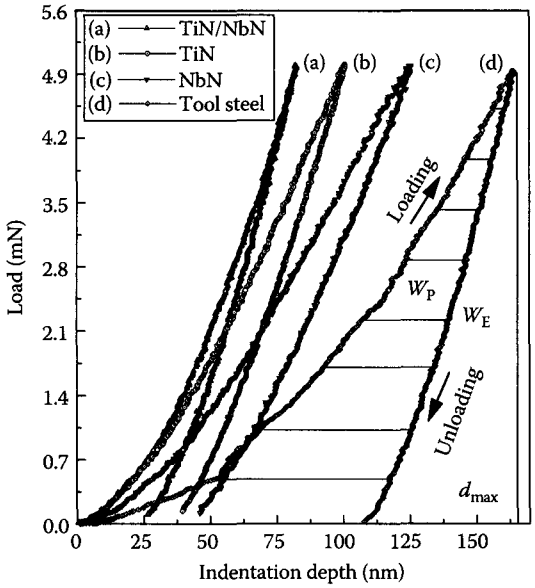

FIGURE 10.12 Load versus displacement curves for a typical TiN/NbN nanolayered multilayer coating at a load of 5 mN. Also shown are the curves for the tool steel substrate, single layer TiN coating and single layer NbN coating. The thicknesses of all the coatings were approximately 1.5 μm. (From Barshilia, H.C. and Rajam, K.S., *Surf. Coat. Technol.*, 183, 174, 2004. With permission.)

the nanoindentation data represents the energy dissipated in the coating due to plastic deformation (W_P) and the area between the unloading curve and maximum indentation depth (d_{max}) represents the energy for elastic deformation (W_E), as shown in Figure 10.12. The ratio $W_P/(W_P+W_E)$ gives a simple, rough but quick indication of the toughness of thin films [136]. Furthermore, the quantity H^3/E^{*2}, which is known as resistance to plastic deformation, has been correlated with the formation of cracks and their propagation, where $E^* = E/(1-\nu^2)$ is the effective elastic modulus [137]. It is clear from Figure 10.12 that the multilayer coating exhibits the largest resistance to plastic deformation and toughness as compared with the component layers.

The mechanical properties of both epitaxial and polycrystalline transition metal nitride superlattices have been studied widely [54–65,71,72]. The epitaxial superlattices have been used for fundamental studies since the effects of grain boundary, orientation dependence, and defects are minimized in these superlattices [65]. The selection of component layers in a multilayer system leading to enhanced properties is based upon the nature of bonding between the two component layers, thermal expansion coefficients, lattice parameters, elastic coefficients, and the thicknesses of the component layers. Apart from these, a number of factors affect the mechanical properties of sputter deposited polycrystalline nitride superlattices. These include: the stoichiometry of the component layers, texturing, quality of the interfaces, and modulation wavelength. It has been reported that the nitride multilayer superlattice coatings exhibit the highest hardness corresponding to the stoichiometric phase of the component layers [56,61]. For both under- and over-stoichiometric component layers, a decrease in the hardness has been reported. The hardness of sputter deposited transition metal nitride multilayer coatings also depends upon the substrate bias; the hardness is reported to increase first with the substrate bias and then decrease [63]. Enhancement in the hardness of multilayer coating with substrate bias has been attributed to ion bombardment leading to a dense microstructure [58]. As mentioned earlier, the ion bombardment leads to a small crystallite size due to high ad-atom mobility and preferential sputtering of the growing film, which densifies the microstructure of the coating. The lower hardness at a higher substrate bias has been attributed to a decrease in the compressive stress in the coating [63].

It is well-known that most of the sputter deposited polycrystalline transition metal nitride superlattices exhibit a preferred orientation [138]. The mechanical properties of the multilayer coatings are reported to depend on the preferred orientation [64]. For example, for TiN/CrN superlattices, Yang et al. report that the (200)-oriented superlattices exhibit a much higher hardness enhancement at low modulation wavelengths than the (111)-oriented superlattices [64]. This enhancement has been explained in terms of the critical shear stress required for dislocations to glide within the individual layer and/or across layer interfaces during indentation-testing induced plastic deformation. The dislocation glide on the secondary slip system has been reported to contribute significantly to the hardness enhancement compared with the primary slip system for the (200)-oriented superlattices than (111)-oriented superlattices. Similar results have been reported by Yashar et al. for the TiN/CrN superlattices [63]. The quality of the interfaces has also been reported to affect the mechanical properties of the multilayer coatings although it has not been studied widely for transition metal nitride multilayer coatings [112,139]. It has been reported that the flattening of each layer leads to higher nucleation density of the next layer to be deposited [139]. This also decreases the number of voids and the void volume fraction at the interfaces resulting in improved mechanical properties.

The effect of the modulation wavelength on the mechanical properties of the transition metal nitride superlattices has been studied extensively [54–65,71,72]. The hardness variations for polycrystalline TiAlN/CrAlN, TiN/CrN, TiN/NbN, and TiAlN/TiN multilayer coatings as a function of the modulation wavelength are shown in Figure 10.13. The maximum hardness values reported for these systems as well as for some of the other promising multilayer systems are summarized in Table 10.2. As can be seen from Figure 10.13, all the multilayer coatings exhibit a maximum hardness only at low bilayer thicknesses in the range of 4–12 nm. For all the multilayer systems, the maximum hardness obtained is very high as compared with that of the rule-of-mixtures value calculated using Equation 10.1. TiN and NbN exhibit hardness values of 20 and 14 GPa, respectively [58]. The rule-of-mixtures value, therefore, would be approximately 17 GPa considering the equal volume fractions of TiN and NbN. The maximum hardness value for the TiN/NbN multilayer coating in Figure 10.13 is 40 GPa, which is approximately 2.4 times the rule-of-mixtures value. At low modulation wavelengths, the hardness, in general, decreases and has been related to intermixing at the interfaces, leading to alloying. Also, the superlattice tends toward an ordered compound in the limit of very thin layers, so the hardness drops to a value characteristic of that compound. At higher modulation wavelengths, the hardness decreases because of the loss of the superlattice structure as described in Section 10.2.1.2.

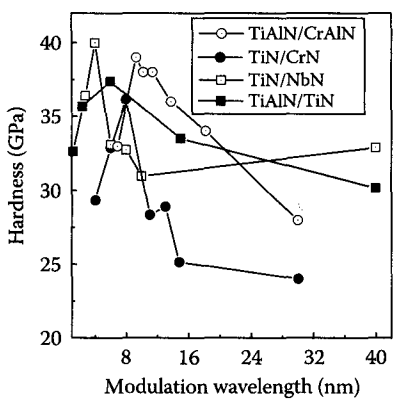

FIGURE 10.13 Variations of hardness of polycrystalline TiAlN/CrAlN, TiN/CrN, TiN/NbN and TiAlN/TiN multilayer coatings as a function of modulation wavelength. The thicknesses of all the coatings were approximately 1.5 μm. (From Barshilia, H.C. and Rajam, K.S., *Surf. Coat. Technol.*, 183, 174, 2004; Barshilia, H.C. et al., *Vacuum*, 72, 241, 2004; Barshilia, H.C. et al., *Thin Solid Films*, 503, 158, 2006; Barshilia, H.C. et al., *J. Vac. Sci. Technol. A*, 27, 29, 2009. With permission.)

TABLE 10.2
Maximum Hardness Reported for Various Transition Metal Nitride-Based Superlattice Coatings

Multilayer System	Λ (nm)	Hardness (GPa)	Reference
TiN/CrN	8	36	[54]
	2.3	35	[63]
	10	40	[64]
TiN/NbN	4.8	40	[58]
	4.6	49	[62]
TiN/VN	5–10	50	[56]
	5.2	56	[57]
TiAlN/CrN	6.4	39	[60]
	4.8	35	[68]
TiAlN/TiN	9.6	37.5	[59]
$TiN/V_xNb_{1-x}N$	6	48	[65]

Source: Values taken from NIST–X-ray photoelectron spectroscopy database, Version 3.5 (National Institute of Standards and Technology, Gaithersburg, 2003); http://srdata.nist.gov/xps/

A variety of mechanisms (namely, the effect of elastic anomalies, coherency strains, elastic modulus differences, Hall–Petch strengthening, etc.) have been used to explain the hardness enhancement in nanolayered multilayer coatings and have been reviewed extensively in the literature [36,43,45,140]. To summarize, it has been shown that the elastic anomalies are too small to explain the hardness enhancements and the coherency strain effects also appear to be relatively small [45]. Barnett and Shinn have shown that the elastic moduli differences are a critical factor in determining the hardness enhancement, as predicted by Koehler in his theoretical model [43,44]. According to Koehler's model, the critical stress required to move a dislocation across an abrupt interface is proportional to the following equation:

$$Q = (G_A - G_B)/(G_A + G_B) \tag{10.7}$$

where G_A and G_B are shear moduli of layers A and B. A superlattice in which the difference in the modulus between the two layers is large will therefore exhibit a large hardness enhancement. Further enhancement in the hardness of the nanolayered multilayer coatings arises from the fact that the thicknesses of the component layers are very small and dislocation generation mechanisms such as Frank–Read sources cannot operate inside a given layer [141]. According to the Hall–Petch model, the strengthening of polycrystalline materials results from the fact that grain boundaries are obstacles to the passage of slip across a boundary. Hence, slip cannot propagate freely from grain to grain. Since the slip cannot propagate freely across a boundary in a polycrystal, a slip band there can sustain a higher stress than in a single crystal [61]. Therefore, an increase in the hardness of a coating is expected with a decrease in the grain size. A decrease in the hardness with increasing modulation wavelength has been reported for metallic and metal/ceramic superlattices and has been fitted using the following equation:

$$H = H_o + a/\Lambda^{1/2} \tag{10.8}$$

where

H is the relative hardness

H_o and a are the constants [51,142]

The hardness behavior expressed by the above equation is similar to the empirical Hall–Petch relation [143,144]:

$$\sigma = \sigma_0 + kd'^{-1/2} \tag{10.9}$$

where
- σ is the fracture stress
- d' is the grain size
- σ_0 and k are the constants

It must be emphasized that the above models are not expected to apply for non-isostructural superlattices (e.g., TiN/AlN, TiN/Cr_2N, TiN/MoN, TiN/TaN, etc.) as the component layers have different dislocation glide systems [41,145]. Furthermore, an epitaxial stabilization effect is generally observed for non-isostructural superlattices at small layer thicknesses (<2 nm), leading to a metastable structure [41,66]. The mechanical properties of this metastable structure are generally unknown. Therefore, in order to understand more about the hardness enhancement in non-isostructural superlattices, information on various properties (such as shear modulus) of the component layers is required.

10.2.1.6 Wear Behavior

Wear is defined as the surface damage or removal of material from one or both of two solid surfaces in a sliding, rolling, or impact motion relative to one another [146]. For most of the tribological applications, the most commonly encountered wear types are: adhesive, abrasive, fatigue, and chemical (or corrosive). Other wear types include fretting and fretting corrosion, which are combinations of adhesive, corrosive, and abrasive wear [146]. Traditionally, transition metal nitride coatings such as TiN have been used to enhance the wear resistance of tribological materials [147–149]. However, the friction between TiN coating and the counter-bodies induces a tribo-chemical reaction, i.e., oxidation of TiN coating, thus affecting its wear behavior [150,151]. For many industrial applications, the wear-resistant coating is exposed to severe environmental conditions—the protective coating must therefore possess a combination of properties such as high hardness, high toughness, high corrosion, and oxidation resistance. It is impossible to achieve all these properties in binary transition metal nitride wear-resistant coatings and, therefore, alternative coatings are required to enhance the lifetime of coated components. The transition metal nitride based multilayer coatings offer improved mechanical properties such as hardness, toughness, etc., and are ideal candidates for a variety of tribological applications. Furthermore, because of their high thermal and chemical stability, these coatings are also being explored for dry machining applications (i.e., without coolant) [152,153].

It must be emphasized that in addition to the coating properties (e.g., hardness, toughness), the interface properties (e.g., adhesion) play an important role in determining the tribological behavior of the coated surfaces. Spalling and delamination also lead to failure of the coating. The delamination can be avoided by improved adhesion and also by minimizing stress in the coating. The adhesion of the coating on the substrate is generally improved by cleaning the surface of the substrate using *ex situ* and *in situ* treatments. In the case of *ex situ* treatments, the coated surfaces are cleaned with conventional chemical reagents employing ultrasonic agitation. *In situ* techniques such as physical cleaning (Ar plasma sputter cleaning) and physical plus chemical cleaning (H_2+Ar plasma etching) are used for the removal of impurities on the atomic scale [130,154]. Further improvement in the adhesion of the coating can be achieved by introducing a metallic interlayer between the substrate and the transition metal nitride coating.

In recent years, in order to study the surface mechanical properties of thin coatings, a lot of progress has been made in the development of the nanotribometer and nanoscratch tester [155]. In a nanotribometer, a flat, a pin, or a sphere is loaded onto the test sample with a precisely known force. The pin is mounted on a stiff lever designed as a frictionless force transducer. The friction

coefficient is determined during the test by measuring the deflection of the elastic arm. The wear ratio for the pin and disc materials are calculated from the volume of material lost during the test. In order to measure the adhesive strength, a nanoscratch tester is used in which a diamond tip is drawn across the coated surface with an increasing load, resulting in various types of failure at specific critical loads. The load at which the first damage (or chipping) of the coating occurs is called the first critical load. At the second critical load, the damage becomes continuous resulting in complete delamination of the coating. These critical loads are used to quantify the adhesive strength of a coating/substrate system.

As the transition metal nitride based multilayer coatings have recently been developed, their exact wear behavior is not very clear and is of current research interest [69,126,127,135,156–161]. In general, the multilayer coatings have been reported to outperform the single layer coatings. For example, Zhou et al. report that the wear volume of TiN/CrN multilayers decreases significantly in comparison with that of single layer coatings (see Figure 10.14) [159]. The enhanced wear resistance of TiN/CrN multilayer coatings has been attributed to many factors such as high hardness, formation of Cr_2O_3 and CrO_3 layers (commonly known as tribo-oxidation) on the worn surface, and decrease in the coefficient of friction. The chromium oxide layer helps to build an additional protective coating on the worn surface, thus, improving the wear resistance. A decrease in the wear volume with an increase in the hardness has been reported in the literature and has been explained in terms of the Archard relationship in which the wear volume is inversely proportional to the hardness of the worn surface [160,162]. A lower coefficient of friction reported for the TiN/CrN multilayer system (see Figure 10.15) has been correlated to the exposure of the CrN layer to the atmosphere, leading to improved tribological properties of the multilayer coating [159]. Detailed TEM investigations by Luo et al. on the wear properties of TiAlN/CrN multilayer coatings have further demonstrated a lower wear rate for the multilayer coating than that of the monolayers [69,127]. The TEM studies confirmed a high resistance to plastic deformation in TiAlN/CrN multilayer coatings, leading to improved wear resistance. In addition to the above factors, the interfaces in a multilayer coating act as crack inhibitors, thereby increasing the fracture resistance due to crack deflection at the interfaces, crack tip shielding by plastic deformation, residual stress distribution, etc. [157,158].

Even though the transition metal nitride multilayer coatings exhibit superior tribological properties, their application to the substrate material cannot guarantee optimal tribological performance without the pretreatment of the substrate material due to plastic deformation of the substrate, which results in eventual coating failure. In recent years, duplex surface engineering methods have been

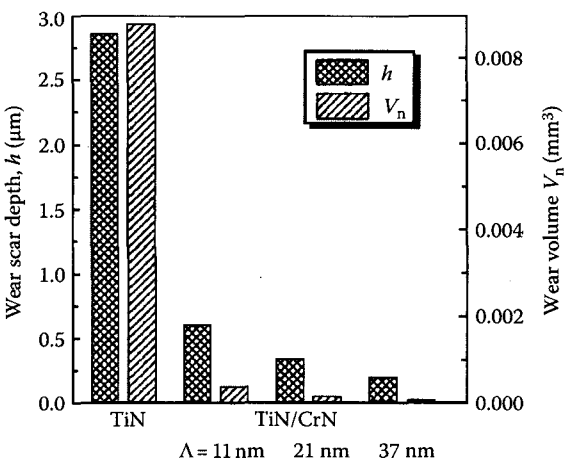

FIGURE 10.14 Comparison of the wear volume and the scar depth between TiN and TiN/CrN multilayer after 500-m sliding tests. (From Zhou, Y.M. et al., *Surf. Coat. Technol.*, 130, 9, 2000. With permission.)

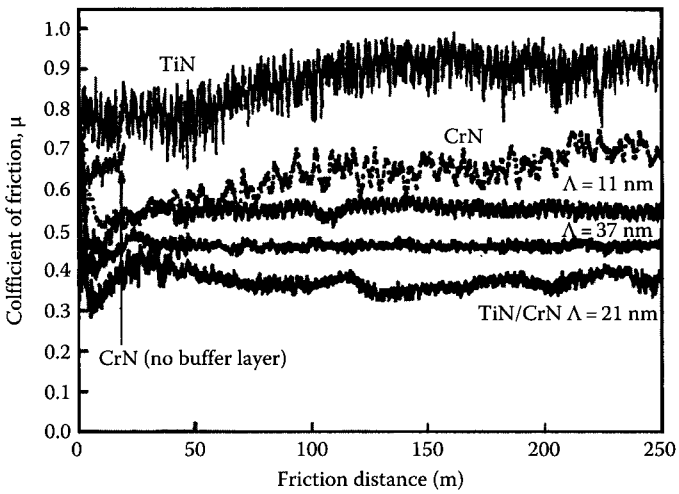

FIGURE 10.15 Coefficient of friction of TiN, CrN and TiN/CrN multilayers with different modulation periods. (From Zhou, Y.M. et al., *Surf. Coat. Technol.*, 130, 9, 2000. With permission.)

used to overcome this problem [163]. These include pretreatment of the substrate using either plasma nitriding or by carburizing followed by the application of PVD hard coatings such as transition metal nitride based multilayer coatings. The duplex surface engineering not only increases the load carrying capacity but also improves the fatigue strength of the coating/substrate system [163].

10.2.1.7 Oxidation Resistance and Thermal Stability

The study of the thermal stability of hard coatings is very important, as these coatings are potential candidates for wear resistance applications, such as cutting, forming, and stamping tools [14,152,153]. These tools are often operated at very high temperatures in the air and, therefore, the performance of the coated tools depends on the oxidation resistance of the protective coating [164]. The thermal stability of PVD hard coatings has been studied by various researchers [54,60,117,165–173]. An excellent review article on this subject has been written by Lars Hultman [117]. It has been reported that TiN, CrN, and TiAlN coatings exhibit thermal stability in the air up to 500°C, 600°C, and 750°C, respectively [18,19,25,166,174,175]. The oxidation energies of TiN, CrN, and TiAlN are reported to be 136, 224, and 456 kJ/mol, respectively [19]. The oxidation of TiN is believed to be controlled by the O or the N ion diffusion, which is enhanced by the grain boundary along the formed TiO_2 layer and the oxidation of CrN is controlled by the outward diffusion of Cr ions through the Cr_2O_3 layer formed on each CrN grain [17,19,174]. On the other hand, the oxidation behavior of TiAlN is mainly controlled by the Al content [19,175]. Experimentally, it has been demonstrated that Al forms a very thin amorphous Al_2O_3 surface layer, which makes oxygen diffusion through the coating difficult [19]. The superior oxidation behavior of TiAlN is also attributed to strongly differing values of Gibbs free energy for oxide formation [176]. Over a wide temperature range, Al_2O_3 is much more stable than TiO_2 (i.e., for Al_2O_3, $\Delta G° = -954$ kJ/mol and for TiO_2, $\Delta G° = -765$ kJ/mol; both values are for 500°C and per mole of O_2) [176].

In general, nanolayered multilayer coatings of transition metal nitrides exhibit superior oxidation resistance when compared with the single layer coatings [54,58,60,165]. However, exact mechanisms explaining the superior oxidation behavior of these multilayer coatings are still not very clear because of complex issues related to the presence of interfaces, inter-diffusion properties of various elements (such as Ti, Cr, Al, O, N, etc.) in the constituent layers, etc. In the case of single layer coatings, heating in the air can lead to oxide formation and the transformation of the phases. However,

in the case of multilayer coatings, apart from oxidation, heating can lead to complex phenomena such as: (1) interdiffusion, (2) coarsening of the layers, (3) reaction between the layers to form a new phase, and (4) transformation within one or both layers [117]. In view of these complex phenomena, a universal mechanism cannot be put forward to explain the thermal stability of transition metal nitride multilayer coatings. A large number of multilayer systems have been studied for this purpose using a variety of characterization techniques such as high-temperature x-ray diffraction, x-ray reflectivity, thermo-gravimetric analysis, micro-Raman spectroscopy, and x-ray photoelectron spectroscopy [116,165,170–173].

Hultman et al. [116,177] have reported that single-crystalline TiN/NbN superlattices exhibit a non-linear diffusion with different activation energies in different temperature regimes. For example, activation energies of 1.2, 2.6, and 4.5 eV have been reported for annealing temperatures $T_A \leq 830°C$, $875°C \geq T_A \geq 830°C$, and $930°C \geq T_A \geq 875°C$, respectively. The lower activation energy has been attributed to defect-mediated diffusion, whereas, the higher activation energies have been attributed to bulk diffusion. Different activation energies have been explained in terms of shift in relative layer thicknesses and different diffusion rates of Ti in NbN (fast) and Nb in TiN (slow). Lopez et al. also observed that annealing of TiN/NbN multilayers caused almost no intermixing up to 700°C, while the hardness, the adhesion/cohesion, and the structure remained unaffected [173]. Similar results have been reported by Barshilia and Rajam for polycrystalline TiN/NbN superlattices [58]. Typical high-temperature XRD plots obtained from a polycrystalline TiN/NbN multilayer sample ($\Lambda = 5.0$ nm) annealed at different temperatures in a vacuum are shown in Figure 10.16, exhibiting strong (111) principal reflection. The coating exhibits 1st and 2nd order negative satellites and 1st order positive satellite along the (111) principal peak. The position of the (111) principal reflection shifts to higher 2θ values, which can be attributed to stress relaxation as a result of annealing. The FWHM of the (111) peak decreases with annealing temperature, which is indicative of an increase in the crystallite size. The normalized intensity and FWHM of the 1st order negative satellite reflection of the XRD data have been used to determine the quality of the superlattice coating after annealing as the satellite reflections provide information on the nature of the interfaces (sharp or diffused) [116]. It has been reported that for polycrystalline TiN/NbN multilayer coatings, no degradation in the superlattice structure is observed for $T_A < 700°C$ [58]. The XRD data presented in Figure 10.16 also shows that the position of the satellite reflection did not change with the annealing temperature, indicating no change in the modulation wavelength. Hence, variations in the layer

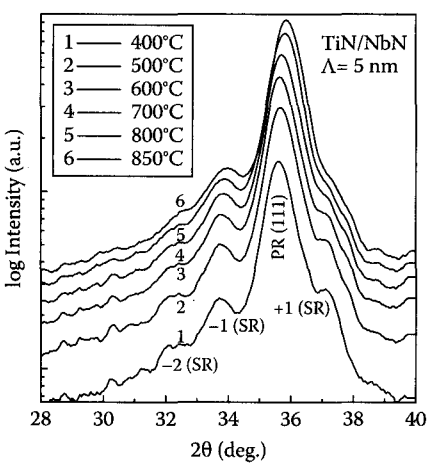

FIGURE 10.16 High-temperature XRD data of a TiN/NbN superlattice coating annealed at different temperatures in vacuum. (From Barshilia, H.C. and Rajam, K.S., *Surf. Coat. Technol.*, 183, 174, 2004. With permission.)

thicknesses are minimal during annealing. It must be emphasized that the diffusion behavior of the polycrystalline multilayer coatings also depends on other factors like variations in composition and growth-induced defect density [116]. For example, in the case of the transition metal nitride coatings with oversaturated nitrogen, annealing will drive excess N to find empty lattice sites or, as a competing process, precipitate at grain boundaries or as gas bubbles [117]. Furthermore, the transition metal nitride coatings (and also the multilayer coatings) are deposited well below their melting points and are expected to contain point defects. The defect density depends upon the deposition conditions. Annealing causes migration, redistribution, or annihilation of the defects, thus affecting the diffusion behavior [117].

The TiN/CrN multilayer is another interesting system that has been studied widely due to its superior mechanical properties [54,64,135]. In this section, we briefly discuss the oxidation resistance and the thermal stability of the TiN/CrN multilayer coatings. Figure 10.17 shows the XRD plots of TiN/CrN multilayer coating ($\Lambda = 8.0$ nm) and coatings heated in the air at 700°C, 750°C, and 800°C. The data shows the retention of the superlattice structure and the absence of titanium oxide and chromium oxide phases as a result of heating up to 700°C. However, evolution of oxide phases is observed at $T_A = 750$°C along with a weak superlattice structure. The superlattice structure disappears completely at 800°C. On the other hand, the formation of TiO_2 and Cr_2O_3 phases has been reported to be observed at 550°C and 600°C for CrN and TiN coatings, respectively [165]. These results demonstrate the superior oxidation resistance of TiN/CrN multilayer coatings as compared with TiN and CrN coatings. The onset of oxidation of the transition metal nitride multilayer coatings can be further increased by the addition of Al or Si [72,178]. The XRD data of the TiAlN/CrN multilayer coatings heat-treated at different temperatures in the air are shown in Figure 10.18, indicating that intense oxide peaks of Cr_2O_3, Al_2O_3, and TiO_2 are observed only at 900°C. Therefore, TiAlN/CrN coatings exhibit superior oxidation resistance as compared with TiN/CrN multilayer coatings. In addition, recent results on the TiAlN/CrAlN multilayer coatings indicate oxidation resistance up to 950°C [72].

It must be emphasized that the coating defects (such as droplets) also affect the oxidation behavior of the transition metal nitride multilayer coatings [179]. Münz et al. have carried out extensive studies on the growth and properties of TiAlN/CrN (and other) nanolayered multilayer coatings deposited using an industrial cathodic arc/unbalanced magnetron system [69,179]. In the combined cathodic arc/unbalanced magnetron sputtering process, the substrate cleaning is generally carried

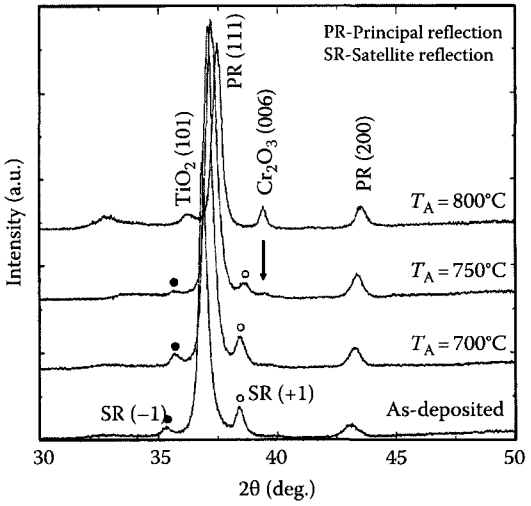

FIGURE 10.17 XRD patterns of as-deposited TiN/CrN multilayer coating and coatings heated at different temperatures in air. (From Barshilia, H.C. et al., *Vacuum*, 72, 241, 2004. With permission.)

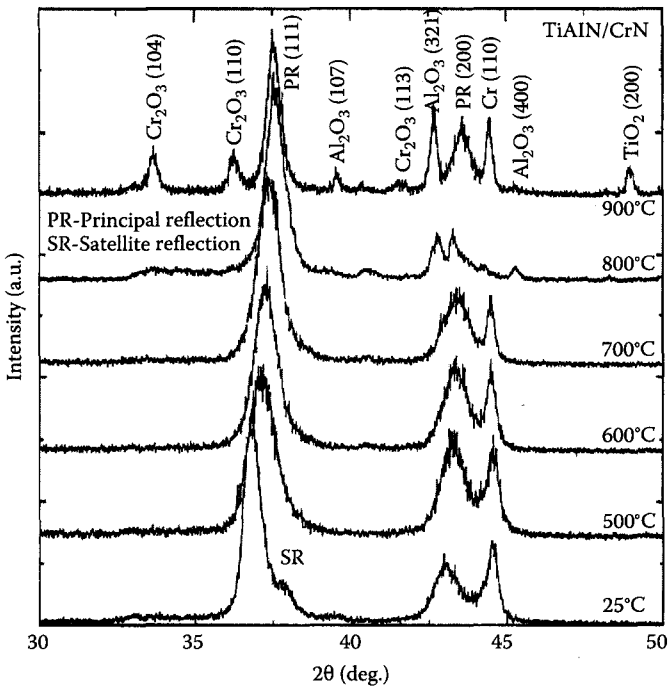

FIGURE 10.18 XRD patterns of as-deposited TiAlN coating and coatings heated at different temperatures in air. (From Barshilia, H.C. et al., *Vacuum*, 77, 169, 2005. With permission.)

out using cathodic arc chromium metal ion etching for improved adhesion of the coating. However, one of the major drawbacks of the cathodic arc process is the macro-particles generated in the metal ion etching stage, which can extend from the substrate surface to the coating surface. The droplets, observed in the industrial cathodic arc/unbalanced magnetron process, cause a shadowing effect underneath the droplet. The defect structure that surrounds the droplets leaves a low-density zone or even a gap between the growth defect grain structure and the coating [179]. Furthermore, the droplets may also be expelled from the coating during the film growth due to compressive stress generated by the growing film causing craters. The properties of the coating (such as hardness, oxidation behavior, etc.), therefore, are greatly influenced by these growth defects. To improve the oxidation behavior of the multilayer hard coatings, it is important to reduce the size and the density of these defects by optimizing the process parameters. Furthermore, it has been reported that the oxidation of TiAlN/CrN multilayer coatings depends upon the CrN layer thickness and thicker CrN layers reduce the onset and the rate of oxidation [172].

Recrystallization during annealing is another important issue that affects the oxidation behavior of the transition metal nitride multilayer coatings. The presence of a large number of interfaces in a multilayer coating controls the recrystallization process and the stress in the coating [170]. At very high temperatures, the volume of the coating increases, which induces stress in the coating. This stress results in cracks, which provide paths for oxygen transport. In the case of a single layer coating, the crack initiates at lower temperatures as compared with a multilayer coating because the stress at the oxide phase boundary becomes smaller for nanolayered multilayer coatings [170]. The oxidation of the coatings is also controlled by the micro-porosity of the coating [19]. As will be discussed in Section 10.2.1.8, most of the PVD coatings (especially sputtered deposited) contain significant amounts of micro-porosity because of the columnar microstructure. Layered deposition minimizes the columnar structure of the sputtered coatings. In the multilayer coatings, re-nucleation associated with the successive deposition of sub-layers reduces the grain size and prevents

the growth of pores and defects all through the coating. A reduced grain size and a large number of interfaces in a multilayer results in dense and homogeneous non-columnar microstructures, thus leading to improved oxidation behavior.

The foregoing discussion clearly highlights that the oxidation behavior of transition metal nitride based multilayer coatings is superior as compared with their single layer counterparts. For instance, TiN, CrN, TiAlN, TiN/CrN, and TiAlN/CrN coatings exhibit stability in the air up to 550°C, 650°C, 700°C, 700°C, and 800°C, respectively [19,58,60,174]. Therefore, the transition metal nitride multilayer coatings are promising candidates for high temperature machining applications. In order to check the suitability of these coatings for high temperature applications, it is important to measure their hot hardness (i.e., hardness at elevated temperatures). Currently, measuring nanoindentation hot hardness is difficult because of instrumental limitations and researchers generally measure the hot hardness after heat treatment of the coatings. There are a few reports on the investigation of the mechanical properties of the transition metal nitride multilayer coatings after heat treatment in vacuum and in air [54,60,116,173]. Hultman et al. report a decline in the hardness of single crystalline TiN/NbN superlattices for $T_A > 900°C$ in vacuum [116]. Similar results have been reported by Lopez et al. for polycrystalline TiN/NbN superlattices, wherein no changes in the nitrogen content and hardness of the coating have been observed after heat treatment in vacuum up to 700°C [173].

For TiN/CrN multilayer coatings heat-treated in air, Zeng et al. reported complete oxidation of TiN and CrN coatings, thus, resulting in sharp decreases in their hardness values and a moderate decrease in the hardness (33 to 30 GPa) of the TiN/CrN multilayers [169]. For CrN/AlN multilayers with $\Lambda = 4$ and 20 nm, after heat treatment at 800°C in air, the coatings are reported to maintain hardness as high as 23.5 and 20.2 GPa, respectively [168]. Similarly, for TiAlN/CrN multilayers, hardness does not change significantly for $T_A = 700°C$ and a progressive decline occurs for $T_A > 750°C$ [172]. Similar results have been reported by Barshilia et al. [60]. The variations of hardness values of a TiAlN coating and a TiAlN/CrN multilayer coating ($\Lambda = 5.6$ nm) as a function of annealing temperature are shown in Figure 10.19. As can be seen from the figure, the hardness values of both TiAlN coating and TiAlN/CrN multilayers are about 36 GPa at 500°C. The hardness decreases for $T_A > 500°C$ and this decrease in hardness is more for single layer TiAlN coating than for TiAlN/CrN multilayer coating. TiAlN/CrN multilayer coating retains hardness as high as 26 GPa (cf. 36 GPa for as-deposited coating) even after heating up to 800°C. It must be emphasized that in the case of multilayer coatings in addition to oxide layer formation, the hardness also decreases because of inter-diffusion between the constituent layers.

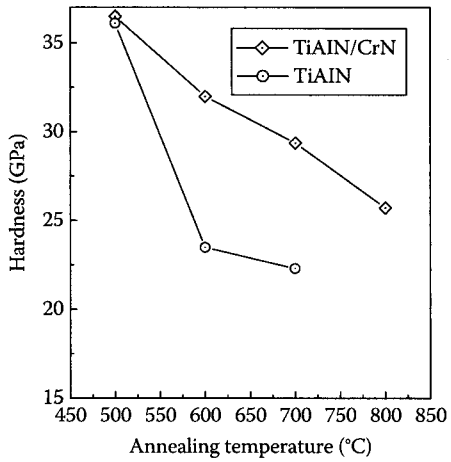

FIGURE 10.19 Variations of nanoindentation hardness of TiAlN/CrN and TiAlN coatings with annealing temperature. The thicknesses of all the coatings were approximately 1.5 μm. (From Barshilia, H.C. et al., *Vacuum*, 77, 169, 2005. With permission.)

10.2.1.8 Corrosion Behavior

Even though physical vapor deposited transition metal nitride hard coatings exhibit good wear resistance, chemical inertness, and high thermal stability, their corrosion behavior is unsatisfactory as these coatings are often not completely dense due to defects in the coating (such as micro-pores, pin holes, and cracks), which may be formed during deposition [16,180]. These defects may create channels for the aggressive medium to attack the substrate, thus affecting the corrosion behavior of the coatings. In order to improve the corrosion protection afforded by the PVD coatings, it is of great importance to inhibit the columnar growth, porosity, and other growth defects. In addition to impurities on the substrate surface, the substrate-state (roughness, scratches, etc.) and a large grain size can also induce porosity in the coating. Smaller grain size can be achieved by judicious control of the deposition parameters (e.g., ion bombardment during deposition). The corrosion behavior of PVD coatings is generally evaluated using potentiodynamic polarization studies [181]. Potentiodynamic polarization is performed using a galvanostat/potentiostat system and the tests are conducted in various environments such as NaCl, H_2SO_4, HNO_3, HCl, etc. [182–186]. The Tafel plots (that is, log i vs. E plot) are obtained from the potentiodynamic polarization measurements, and the corrosion potential (E_{corr}), corrosion current density (i_{corr}), and other important parameters are deduced from these plots [181]. It must be emphasized that the potentiodynamic polarization measurements alone are not sufficient to explain the detailed corrosion mechanism of the PVD hard coatings that takes place at the electrolyte/coating/metal interface. The electrochemical impedance spectroscopy (EIS) has been used for this purpose [183,184,187]. As a small amplitude sinusoidal signal is used throughout the EIS measurements, this technique does not significantly accelerate the corrosion reactions and, therefore, the coating surface is not affected too much and can be considered as a non-destructive method. Interpretation of the EIS data with an appropriate equivalent circuit can provide detailed information on the electrochemical reaction that takes place on the electrode. From the EIS data, the resistance of pores in the coating and the charge transfer resistance as well as the electrical double-layer capacitance at the electrolyte/substrate interface can be obtained. Detailed information on the EIS measurements on the PVD hard coatings can be found elsewhere [187,188].

A large number of studies have been carried out to evaluate the corrosion behavior of physical vapor deposited transition metal nitride coatings [16,180,182,187–190]. Various methods have been used to improve the corrosion resistance of the transition metal nitride coatings. These include increased coating thickness, alloying of nitrides (TiAlN, $TiCrN_x$, TiCN), and intermediate plasma etching during deposition [182–184,189–193]. It has been shown that, in general, TiN coatings do not exhibit good corrosion resistance due to their columnar microstructure, which weakens the protective nature of the coatings [190]. Pitting corrosion occurs if the thickness of the coating is less than approximately 6 μm [189]. CrN coatings exhibit a relatively dense microstructure and provide higher corrosion resistance than TiN. Ternary nitride coatings such as TiAlN show improved corrosion resistance as compared with the binary transition metal nitride coatings [182,192]. Incorporation of an interlayer (e.g., Ti, Cr) between the substrate and the coating helps in achieving good adhesion and also corrosion resistance. Brandl and Gendig studied the electrochemical behavior of PVD deposited Cr/CrN system and underlined the importance of a Cr interlayer for the improvement of corrosion resistance [193].

To illustrate the corrosion behavior of PVD hard coatings, Figure 10.20 shows the typical Tafel plots for the mild steel (MS) substrate, Cr interlayer, and single layer coatings of TiN, CrN, and TiAlN in a 3.5 wt % NaCl solution. As can be seen from the figure, the corrosion potential of the coated samples, when compared with the substrate, shows a shift towards the positive side. Furthermore, a decrease in the corrosion current is observed for the coated samples. The positive shift of E_{corr} and the low corrosion current indicates better corrosion resistance of the coated samples. From Figure 10.20, it is seen that the corrosion resistance of CrN is better than TiN because CrN has the ability to form a passive layer over the surface and exhibits a dense microstructure [187]. In addition, TiN

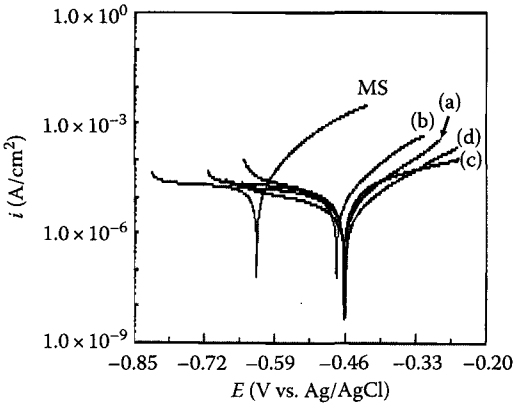

FIGURE 10.20 Potentiodynamic polarization curves of: (a) Cr interlayer, (b) TiN, (c) CrN and (d) TiAlN single layer coatings. Also shown is the polarization curve of the mild steel substrate. (From Grips, V.K.W. et al., *Thin Solid Films*, 514, 204, 2006. With permission.)

exhibits the columnar structure with pores between the inter-granular columns, forming a direct path for the corrosive medium to pass through the coating defects [192]. The TiAlN coatings exhibit superior corrosion behavior as compared with the TiN and the CrN coatings. It has been reported that the addition of a third element (such as Al) to the transition metal nitrides improves corrosion resistance [182]. During the chemical attack, Al easily forms an amorphous aluminum oxide layer on the surface of the coating, which passivates the surface and prevents further corrosion attack. The presence of a passive layer leads to an additional resistance to the corrosive medium passing through the pores. As mentioned previously, the PVD coatings contain cracks, pin holes, and pores that allow the corrosion media to enter the substrate, thus leading to pitting corrosion. The occurrence of pitting corrosion in the PVD coatings has been confirmed by examining the corroded samples under scanning electron microscope (SEM). Typical corrosion pits along micropores for a 104 nm thick TiN coating deposited on the MS substrate after corrosion in 0.5 M HCl solution are shown in Figure 10.21, displaying fully and partially open pits. The diameter of the pore determines the extent of the chemical attack. As can be seen from Figure 10.21a, the corrosion pit is fully open, which could be due to the flaking of the coating as a result of the chemical attack. The corrosion underneath the coating causes rust formation and consequently increases the interface volume, which results in delamination of the coating.

In order to limit the effect of defects and to enhance the corrosion resistance of the PVD coatings without changing their surface properties, an alternative protective interlayer (e.g., electroless nickel or electrodeposited nickel) can be deposited between the film and the substrate [184,194,195]. In particular, electroless nickel (Ni-P) is known to have excellent corrosion, wear, and abrasion resistance and provides uniformity in thickness of the deposits [184,195]. The combination of an electroless nickel interlayer and the PVD hard coating improves both the mechanical and the corrosion properties of the duplex coating. Very few studies have been reported in literature on the corrosion behavior of the PVD coating/Ni-P/MS system. Doong et al. have reported that TiN coatings with electroless nickel exhibited better corrosion resistance than TiN coatings in 0.5 M H_2SO_4 solution [196]. Similarly, Chen et al. have also reported that the CrN/Ni-Ni_3P/MS system exhibits a better corrosion resistance as compared with the CrN/MS system in 0.5 M NaCl solution [195].

Several studies on the corrosion behavior of transition metal nitride multilayer coatings are reported in literature [183–186,197–200]. The application of nanolayered multilayer coatings of transition metal nitrides on the substrate material has shown a significant improvement in corrosion resistance as compared with the single layered coatings [183–186,197–200]. Figure 10.22

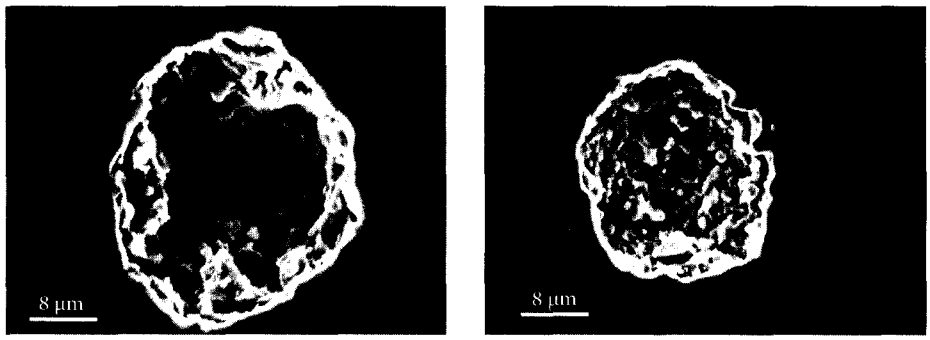

FIGURE 10.21 SEM micrographs of TiN coatings after corrosion testing exhibiting corrosion pits. The pit in (a) is fully open because of flaking of the coating as a result of corrosion attack. In (b) the corrosion is seen along a pore. (From Barshilia, H.C. et al., *Thin Solid Films*, 460, 133, 2004. With permission.)

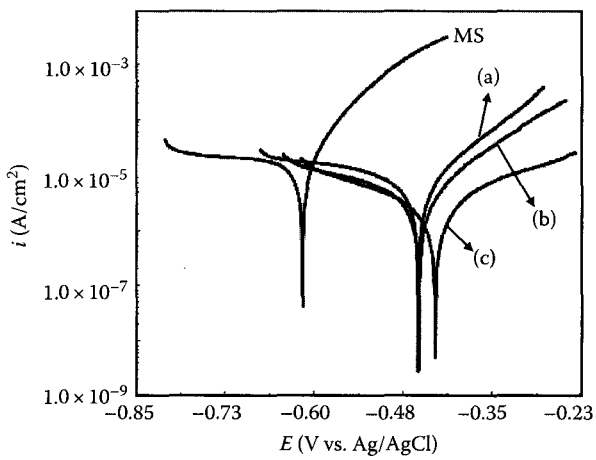

FIGURE 10.22 Potentiodynamic polarization curves of: (a) CrN, (b) TiAlN, and (c) TiAlN/CrN multilayer coatings. Also shown is the polarization curve of the mild steel substrate. The total coating thickness was approximately 2.0 μm for all the samples. (From Grips, V.K.W. et al., *Thin Solid Films*, 514, 204, 2006. With permission.)

shows the Tafel plots (3.5 wt % NaCl solution) of CrN, TiAlN, and TiAlN/CrN multilayer coatings deposited on MS substrates. The multilayer coatings show superior corrosion resistance than that of the single layer coatings of CrN and TiAlN. Figure 10.23 presents the Tafel plots of TiAlN/CrN multilayer coatings deposited at various modulation wavelengths (that is, at various number of interfaces, N). Even though no significant change in the corrosion potential was observed for TiAlN/CrN multilayer coatings prepared at different modulation wavelengths, a detailed investigation showed an overall improvement in the corrosion resistance of the multilayer coatings. For instance, i_{corr} values of 2.30 and 1.52 μA/cm^2 were observed for TiAlN/CrN multilayers with $N = 100$ and 430, respectively [183]. It has been reported that as the number of interfaces in a multilayer increases, more numbers of micro-pores are blocked, leading to improved corrosion behavior [186]. As discussed previously, a layered deposition minimizes the columnar structure of the PVD coatings and reduces the grain size. A reduced grain size and a large number of interfaces in a multilayer result in a dense and homogeneous microstructure, which leads to improved corrosion properties. Furthermore, multilayer coatings have lower residual stress mainly because of stress relaxation at

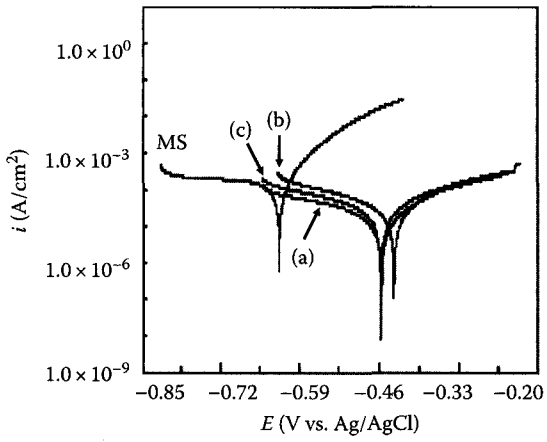

FIGURE 10.23 Potentiodynamic polarization curves of TiAlN/CrN multilayer coatings with different number of interfaces: (a) $N=100$, (b) $N=300$, and (c) $N=430$. The total coating thickness was approximately 2.0μm for all the samples. Also shown is the polarization curve of the mild steel substrate. (From Grips, V.K.W. et al., *Thin Solid Films*, 514, 204, 2006. With permission.)

the interfaces, thus inhibiting crack propagation as a result of a chemical attack. Recent reports suggest that the corrosion behavior of the transition metal nitride multilayer coatings can be further improved by incorporation of electroless nickel (or other metal layers) and by incorporating Nb or Si in the matrices of transition metal nitrides [197,200].

10.2.2 Nanocomposite Coatings

As discussed in Section 10.2.1, transition metal nitride based multilayer superlattice coatings represent a very important class of extrinsic superhard materials. The origin of the enhanced properties of these superlattices is currently fairly well understood. However, it has been shown that the hardness of these coatings strongly depends on the modulation wavelength [54–72]. Therefore, it is desirable to have small fluctuations in the layer thicknesses along and perpendicular to the growth directions in order to achieve uniform multilayer coating. For most of the industrial applications, it is practically impossible to achieve uniform layer thicknesses on complex-shaped objects such as cutting, forming, and stamping tools. Similarly, interdiffusion between the different layers at higher temperatures also degrades the properties of the multilayer coatings. As most of the cutting tools attain a very high temperature during machining operations, performance of the coated tools deteriorates because of the interdiffusion between the component layers of the multilayer coating. Therefore, it is desirable to develop a single layer coating with a combination of properties such as high hardness, toughness, oxidation resistance, etc. This has led to the development of superhard nanocomposite coatings, which represent a new generation of materials [37–39,46,201–208].

The nanocomposite coatings are composed of at least two separated phases: either two nanocrystalline phases or a nanocrystalline phase and an amorphous phase. The schematic diagram of a nanocomposite coating with a crystalline phase and an amorphous phase is shown in Figure 10.24. The research on superhard nanocomposite coatings was pioneered by Stan Veprek and coworkers and subsequently carried out by several other researchers [37–39,46,201–208]. In recent years, various superhard nanocomposite systems such as Ti-Si-N, Ti-B-N, W-Si-N, Ti-Al-Si-N, etc. have been investigated and the Ti-Si-N system is the most widely studied [201–208]. Even though Hirai et al. were the first to report the preparation of Si_3N_4-TiN composites in 1982, the generic concept for the design of superhard nanocomposites was first put forward by Veprek et al. in 1995 [201,209,210]. In

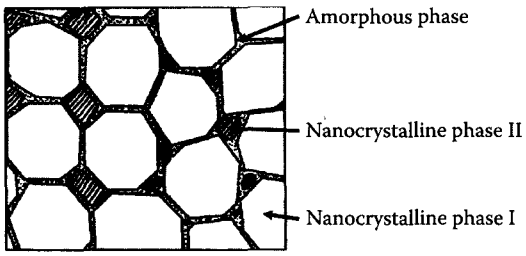

FIGURE 10.24 Schematic diagram of a nanocomposite coating with two nanocrystalline phases and an amorphous phase. (From Vepřek, S. et al., *Surf. Coat. Technol.*, 133–134, 152, 2000. With permission.)

this concept, the superhard nanocomposite coatings were prepared using a plasma assisted chemical vapor deposition (PACVD) process, wherein TiN nanocrystals were embedded in an amorphous Si_3N_4 matrix [201]. These coatings exhibited a hardness of the order of 50 GPa and were stable up to 800°C in the air.

In recent years, a variety of hard and superhard nanocomposite coatings have been studied by various researchers including TiN/*a*-Si_3N_4, CrN/*a*-Si_3N_4, W_2N/*a*-Si_3N_4, TiN/*a*-C, TiAlN/*a*-Si_3N_4, TiN/BN, TiAlN/*a*-AlN, ZrN/*a*-Si_3N_4, and *a*-CN/TiN [37–39,46,201–219]. These superhard coatings exhibit hardness in the range of 40–100 GPa. It is worthwhile to note that the validity of the measured hardness values reported by various groups for different superhard nanocomposite coatings was a subject of intense debate over the last few years. The nanocomposite coatings, in general, can be classified into two groups: *nc*-MN/hard phase (e.g., *a*-Si_3N_4, *a*-TiB_2, etc.) and *nc*-MN/soft phase (e.g., Cu, Ni, Y, Ag, etc.) [38,202]. Here *nc*- and *a*- denote the nanocrystalline phase and amorphous phase, respectively, and M = Ti, W, Cr, Zr, Mo, etc. The unique properties of the nanocomposite coatings are due to their high ratio of interface area to volume (i.e., surface-to-volume ratio) [40]. For example, for a one-shell cluster, an atom is surrounded by twelve atoms, therefore, the percentage of surface atoms is about 92. Similarly, for a two-shell cluster, the percentage of surface atoms is approximately 76, which decreases to 63 for a three-shell cluster. Therefore, with an increase in the number of shells (i.e., grain size) there is a decrease in the percentage of surface atoms [40]. Or in other words, in nanocomposite coatings, a large fraction of atoms are boundary atoms, compared with the polycrystalline coatings. Under these conditions, it has been reported that dislocations do not exist because grain boundaries prevent their formation [202]. Even though a dislocation might form in the crystalline phase, it cannot propagate into the amorphous phase and vice versa. Furthermore, the boundary regions play a decisive role in the deformation of the nanocomposite coatings and the grain boundary sliding is the dominant deformation mechanism [206]. The above factors result in new and unique properties of the nanocomposite coatings. It must be pointed out that unlike the heterostructures and nanocrystalline materials, which show softening behavior (i.e., reverse Hall–Petch effect) for crystallite size less than a critical value (generally 5–6 nm), the hardness of the nanocomposite coatings strongly increases with a decrease in the crystallite size in that range [30,220,221]. The softening behavior in the transition metal nitride based superhard nanocomposite coatings is generally observed at a very low crystallite size (typically < 2 nm). Recent advancements in the superhard nanocomposite coatings prepared using the PACVD and PVD processes have been reviewed by various researchers [37–39,202,203,206]. In this review, we briefly present the salient results pertaining to sputter deposited transition metal nitride based hard and superhard nanocomposite coatings.

10.2.2.1 Growth Processes and Microstructures

The choice of an appropriate system for the formation of superhard nanocomposites is determined by the immiscibility of the component phases, their oxidation behavior (thermodynamical stability), and the reactivity with nitrogen [201]. The immiscibility between the component phases is desirable for the segregation of the crystalline and the amorphous phases, leading to small crystallites with

sharp grain boundaries [37]. In addition, the component phases should also possess high strength and the cohesive energy of their interfaces should be high [208]. As has been discussed widely, the *nc*-MN/*a*-Si_3N_4 (BN, CN_x, etc.) system meets the above requirements for the formation of an extrinsic superhard nanocomposite coating. Initial work on the deposition of superhard nanocomposite coatings was carried out using a PACVD process [39,201,208,219]. High deposition rates and uniform coatings are the major advantages of PACVD. However, it suffers from drawbacks like high deposition temperature (500°C–600°C), use of gases like $SiCl_4$, $TiCl_4$, etc., which are highly corrosive and hazardous, and problems of scale-up [37]. To overcome these problems, both the PACVD and PVD (e.g., low pressure arc evaporation) processes have been combined to deposit superhard nanocomposite coatings for industrial applications [205].

In recent years, the reactive magnetron sputtering process has also been used for the deposition of superhard nanocomposite coatings [38,202,204,212–215]. A lot of work on the development of transition metal nitride based superhard nanocomposite coatings using reactive magnetron sputtering has been carried out by Vaz et al. [204,222–225] and Musil et al. [38,202,217,226,227]. In general, both balanced and unbalanced reactive magnetron sputtering processes have been used for the deposition of hard coatings. The unbalanced reactive magnetron sputtering is of great interest for the deposition of superhard nanocomposite coatings because ions from the dense secondary plasma formed in the region of the substrate can be used for bombardment of the growing film. Such bombardment is necessary to form a dense and well-adhered coating. Reactive sputtering is an ultra-clean process that can be carried out at low substrate temperatures (300°C–400°C). A wide variety of materials (refractory, insulating, etc.) can be deposited using sputtering and this technique is best suitable for large-scale industrial applications. Often an additional high-flux, low-energy ion bombardment is used for restricting the grain growth and for the formation of nanocrystalline coatings in this process. The energy and flux of the bombarding ions also control the orientation of the grains. However, the high-energy ion bombardment leads to incorporation of stress in the coating, affecting the mechanical properties of the nanocomposite coating [207]. Besides, it helps to improve the adhesion of the coating on various commercial substrates. The formation of a nanocrystalline phase and an amorphous phase in a sputtering process can be achieved by co-sputtering, wherein, two materials are reactively sputtered under a controlled environment and mixed in the gas phase on atomic scales. As most of the covalently bonded amorphous coatings (e.g., Si_3N_4, BN, etc.) are highly insulating in nature, conventional DC and RF reactive sputtering cannot be employed for the deposition of these coatings on a large scale because of arcing problem and low throughput. In particular, reactive DC sputtering of covalently bonded nitride coatings is difficult due to the formation of the insulating layer on the target surface, commonly known as "target poisoning" [73,74]. The RF sputtering enables reactive deposition of dielectric thin films but is unfavorable due to its poor energy efficiency, resulting in low growth rates [228].

Recent advancements in reactive DC pulsed sputtering have been reported to be beneficial for the deposition of highly insulating coatings such as AlN, Si_3N_4, etc. [73,213,214,229]. It is expected that the synergistic effect of low-energy ion bombardment and co-sputtering may lead to a nanocomposite coating with a controlled microstructure. A schematic diagram of a typical reactive unbalanced magnetron sputtering system used for deposition of superhard nanocomposite coatings is shown in Figure 10.25. The sputtering system consists of two sputtering guns, which are inclined at an angle to achieve co-sputtering of various materials. The sputtering system is also equipped with an ion beam facility (Kaufman ion source) for controlling the microstructure of the deposited coatings. Sputtering of nanocrystalline metal nitride and amorphous phases is carried out using DC (or pulsed DC) and pulsed DC power supplies, respectively. A number of superhard nanocomposite coatings such as: TiN/Si_3N_4 [213], TiAlN/Si_3N_4 [214], CrN/Si_3N_4 [215], CrAlN/Si_3N_4 [215], CN_x/TiN [218], etc., have been prepared using the reactive unbalanced magnetron sputtering process.

Various studies have been carried out to understand the microstructure of the superhard nanocomposite coatings [207,212,218,230,231]. Most of these indicate that the microstructure critically depends upon the content of the amorphous phase in the nanocomposite coating. In the case of

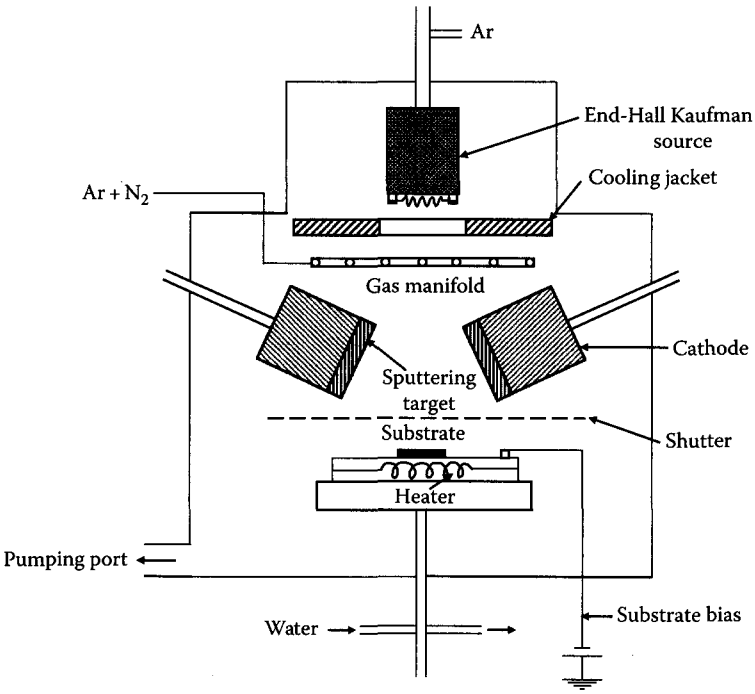

FIGURE 10.25 Schematic diagram of a typical unbalanced DC magnetron sputtering system used for the deposition of superhard nanocomposite coatings. (From Barshilia, H.C. et al., *Surf. Coat. Technol.*, 201, 329, 2006. With permission.)

sputter deposition, the content of amorphous and nanocrystalline phases can be controlled by regulating the sputtering power to the targets [230]. It has been reported that the crystallite size of the nanocrystalline phase decreases with an increase in the amorphous content [212,232]. At a very high amorphous content, the coating becomes totally amorphous and at a very low amorphous content, the nanocomposite coating exhibits a columnar microstructure. Typical bright-field (BF) and dark-field (DF) TEM micrographs of a TiN/*a*-C nanocomposite coating are shown in Figure 10.26. The micrographs show that TiN nanocrystals are dispersed homogenously in an amorphous carbon matrix. As can be seen from the micrograph, the TiN nanocrystals are elliptical in shape. Elongated nanocrystals have also been observed by Kauffman et al. for TiN/Si_3N_4 superhard nanocomposite coatings prepared at a higher Si content deposited using an industrial reactive magnetron sputtering system [232]. The average grain size of the TiN nanocrystals shown in Figure 10.26 is of the order of 7.8 nm and the corresponding crystallite size distribution is shown in Figure 10.27, which shows a fairly uniform crystallite size distribution. The average crystallite size measured from the TEM data can also be confirmed by XRD, in which the crystallite size can be determined from the FWHM of the reflections [233]. The presence of nanocrystalline and amorphous phases can further be confirmed using SAD and HRTEM studies. In Figure 10.28, we show a typical SAD pattern of a TiN/*a*-C superhard nanocomposite coating. The presence of a spotty-ring pattern with a halo confirms the presence of an amorphous phase (halo) and a nanocrystalline phase (spotty-ring). From the SAD pattern, one can actually calculate the *d* values from the diameter of different diffraction rings and compare them with the standard *d* values of the crystalline phase. The calculated *d* values matched closely with those of the cubic TiN phase and no phases of TiC were observed. In Figure 10.29, we show the HRTEM image from a TiN/*a*-C nanocomposite coating in which the nanocrystalline regions are demarcated numerically and resolved crystal planes are seen clearly.

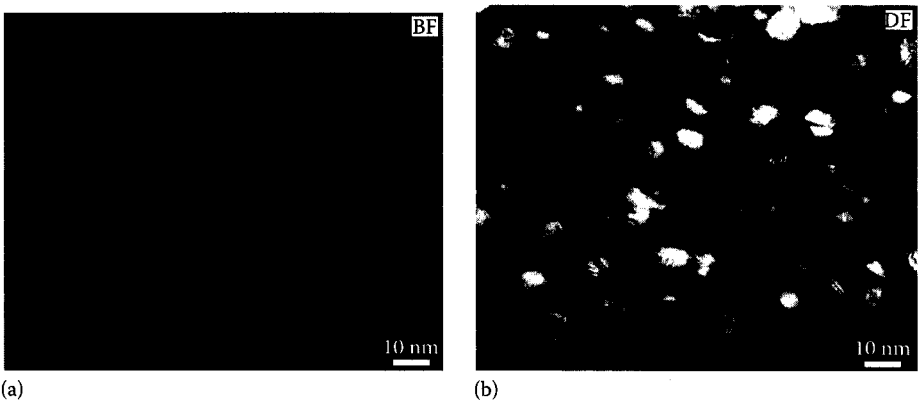

FIGURE 10.26 Typical bright field (a) and dark field (b) TEM images of TiN/*a*-C nanocomposite coating. (From Barshilia, H.C. et al., *Surf. Coat. Technol.*, 195, 147, 2005. With permission.)

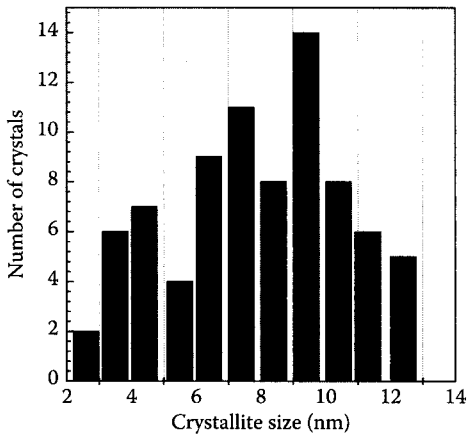

FIGURE 10.27 Crystallite size histogram of a typical TiN/a-C nanocomposite coating. (From Barshilia, H.C. et al., *Surf. Coat. Technol.*, 195, 147, 2005. With permission.)

The HRTEM data show that most of the nanocrystals are oriented along the {111} direction. The unmarked regions in Figure 10.29 actually represent the amorphous phase. These studies suggest that nanocomposite coatings with a controlled microstructure can be deposited using the magnetron sputtering process.

10.2.2.2 Mechanical and Tribological Properties

A large number of studies have been carried out on the mechanical properties of transition metal nitride based superhard nanocomposite coatings [212–217,223]. The effects of the substrate temperature, sputtering power, nitrogen partial pressure, and substrate bias on the mechanical properties of sputter deposited nanocomposite coatings have been reported [212–215,230]. All these studies indicate that hardness depends primarily on the amorphous phase content in the nanocomposite coating. This is illustrated in Figure 10.30, wherein the variation of hardness of sputter deposited TiN/Si_3N_4 nanocomposite coatings with silicon content is shown. The TiN and Si_3N_4 coatings

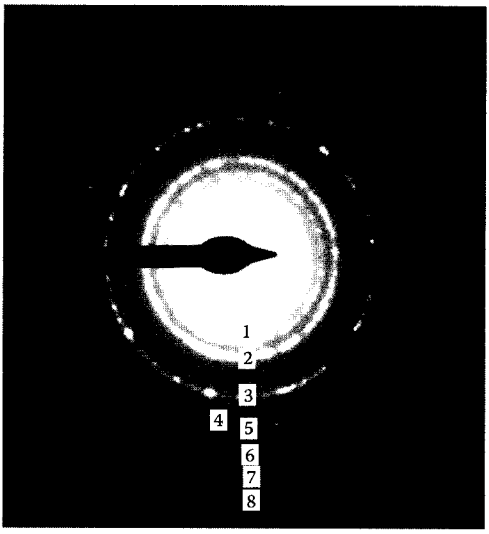

FIGURE 10.28 SAD pattern of a typical TiN/a-C nanocomposite coating, showing the presence of both amorphous and nanocrystalline phases in the coating. The diffraction rings, nos. 1–8, closely match with the d_{111}, d_{200}, d_{311}, d_{222}, d_{400}, d_{422}, and d_{333} of cubic TiN phase. (From Barshilia, H.C. et al., *Surf. Coat. Technol.*, 195, 147, 2005. With permission.)

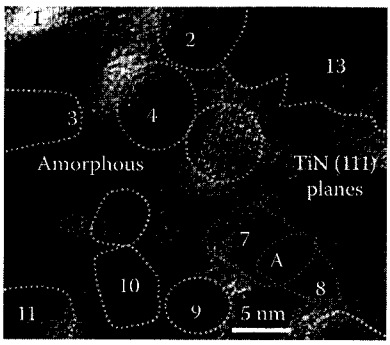

FIGURE 10.29 HRTEM micrograph showing the nanocrystals (marked as 1–13) of TiN phase embedded in an *a*-C matrix. (From Barshilia, H.C. et al., *Surf. Coat. Technol.*, 195, 147, 2005. With permission.)

exhibit hardness values of 28 and 26 GPa, respectively. For the nanocomposite coatings, the hardness is low at a lower silicon content (<12 at.%). It increases with an increase in the silicon content and exhibits a maximum hardness of 52 GPa for a silicon content of about 12 at.%. The maximum hardness of the nanocomposite coatings is very high as compared with the rule-of-mixtures value. The hardness of the nanocomposite coatings decreases significantly with further increase in the silicon content. For example, for a silicon content of approximately 27 at.%, the nanocomposite coating shows a hardness of 32 GPa. This decrease in the hardness is attributed to an increase in the amorphous Si_3N_4 content in the TiN matrix. Also shown in Figure 10.30 is the variation of elastic modulus with silicon content. It is interesting to note that the TiN/Si_3N_4 nanocomposite coating exhibits both high hardness and high elastic modulus.

The origin of hardness enhancement in the nanocomposite coatings has been reviewed extensively by Vepřek et al. [207]. It has been reported that the hardness of the nanocomposite coating depends on the nature of materials chosen and also on other strengthening mechanisms. It is a

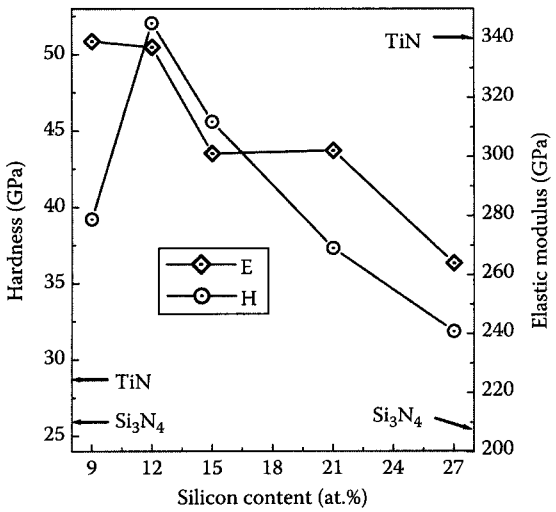

FIGURE 10.30 Variations of nanoindentation hardness and elastic modulus of TiN/Si_3N_4 nanocomposite coatings with silicon content. The thicknesses of all the coatings were approximately 1.5 μm. (From Barshilia, H.C. et al., *Surf. Coat. Technol.*, 201, 329, 2006. With permission.)

combination of factors like chemical bonding, solution hardening, Hall–Petch strengthening, and formation of a stable nanostructure due to spinodal decomposition that results in the high hardness of the nanocomposite coatings. It must be emphasized that unlike in the case of ternary nitrides (TiAlN, CrAlN, TiCN, etc.) whose hardness is based on solution hardening, the hardness of the transition metal nitride based nanocomposite coatings depends on grain boundary hardening, which is described by the well-known Hall–Petch relationship (see Equation 10.9). Due to the presence of a large number of grain boundaries in a nanocomposite coating, the dislocations that propagate through the grains are hindered at the grain boundaries, resulting in a dislocation pile-up. Increased stress is required to move the dislocations further, which results in an increase in the hardness of the nanocomposite coatings. However, it is important to note that at very small grain sizes (typically less than 2–3 nm) the universal dislocation pile-up mechanism is not valid because dislocations cannot be generated in small grains. The grain boundary sliding and grain boundary migration are believed to play important roles in lowering the hardness of the nanocomposite coatings at very low grain sizes, which is commonly known as the reverse Hall–Petch effect.

Unlike the conventional intrinsic superhard materials such as diamond and c-BN, which are brittle, the nanocomposite coatings exhibit superior fracture toughness due to the small grain size. According to the Griffith's theory of crack propagation, the critical stress required to cause fracture (σ_c) is inversely related to the square root of the crack length ($2c$) [141]:

$$\sigma_c = \sqrt{\frac{2\gamma Y}{\pi c}} \tag{10.10}$$

where

γ is the surface energy per unit area
Y is the Young's modulus

In a nanocomposite coating, the size of a crack is expected to be of the order of a few nanometers (<grain size). Therefore, increased critical stress is required for the crack propagation. Furthermore, even if the critical stress is increased and the crack starts growing, its growth is hindered by the

grain boundaries [39,207]. In addition, the origin of superhardness is attributed to a stable nanostructure of the nanocomposite coatings. It has been widely reported by Vepřek that a thermodynamically driven and diffusion rate controlled phase segregation in the nanocomposite coatings leads to the formation of a stable nanostructure by self organization. This is commonly known as spinodal phase segregation [39,207,234,235]. It is important to note that the phase segregation with sharp interfaces between the crystalline and the amorphous phases in the nanocomposite coatings can be achieved only under controlled deposition conditions such as high substrate temperature, high nitrogen partial pressure, low impurity levels (i.e., low oxygen partial pressure), ion bombardment, etc. Judicious control of these process parameters can be obtained only in PACVD and PVD processes, which are commonly employed for the deposition of the nanocomposite coatings.

Understanding the tribological behavior of the superhard nanocomposite coatings is very important for industrial applications. Despite the importance of hardness as a key parameter for wear-protective hard coatings, which has been studied widely, the tribological properties of the nanocomposite coatings have been discussed less extensively [236–243]. The tribological behavior of superhard nanocomposite coatings consisting of Ti-Si-N, Ti-B-N, Cr-Si-N, etc., has been studied in recent years [236–240]. Most of these studies suggest that the nanocomposite coatings display superior tribological behavior as compared with the corresponding nanocrystalline and amorphous components. For example, Figure 10.31 shows the wear data obtained using a conventional pin-on-disc wear tester (load=9.8 N) for an uncoated stainless steel pin and pins coated with TiN and TiN/Si_3N_4 nanocomposite coatings. The uncoated pin shows very high wear loss from the beginning, with a wear loss of about 75–100 μm. On the other hand, the TiN-coated pin does not show greater wear loss for a sliding distance of 300 m, as displayed in the inset. However, a significant improvement in the wear resistance is observed for the TiN/Si_3N_4 nanocomposite coatings. It has been observed that if the concentration of Si_3N_4 is increased in the nanocomposite coatings, the improvement in the wear resistance is very high. This improvement in the wear resistance for the TiN/Si_3N_4 nanocomposites could be attributed to a combination of factors such as high hardness as compared with TiN, lower coefficient of friction of Si_3N_4, and the formation of a self-lubricating protective layer. The decrease in the friction coefficient with an increase in silicon content is attributed to the formation of self-lubricating tribo-layers such as SiO_2 or $Si(OH)_2$, which are activated with increasing silicon content [244]. In addition to the beneficial effects of Si_3N_4 in the formation of self-lubricating tribo-layers, the amorphous structure of

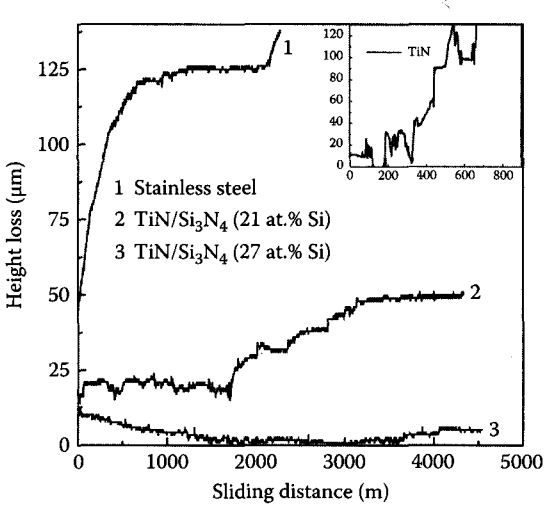

FIGURE 10.31 Wear data of the uncoated stainless steel pin and pins coated with TiN and TiN/Si_3N_4 nanocomposites. The thicknesses of all the coatings were approximately 1.5 μm. (From Barshilia, H.C. et al., *Surf. Coat. Technol.*, 201, 329, 2006. With permission.)

the nanocomposite coatings prepared with high silicon content plays an important role in improving wear resistance, as the amorphous materials exhibit better wear resistance as compared with crystalline ones due to their low reactivity [241].

The superhard nanocomposite coatings have been reported to show better wear behavior at elevated temperatures than the single component materials. For example, Ma et al. report a low wear rate of *nc*-TiN/*a*-Si_3N_4 coatings at 550°C of 10^{-4} to 10^{-5} mm^3/N m in comparison with that of TiN coatings of 10^{-3} mm^3/N m [245]. As mentioned previously, TiN coatings become oxidized at these temperatures, whereas the nanocomposite coatings exhibit a stable nanostructure at 550°C, leading to improved wear resistance. In order to further improve the oxidation and tribological behavior (the wear resistance, in particular) of the Ti-Si-N and Cr-Si-N nanocomposite coatings, addition of Al has also been reported [242]. The addition of amorphous carbon has also been explored to significantly decrease the friction coefficient of the superhard nanocomposite coatings [243,246]. A friction coefficient as low as 0.17–0.35 has been reported for Ti-Si-C-N superhard nanocomposite coatings [243]. However, the addition of amorphous carbon is expected to deteriorate the high temperature hardness of the superhard nanocomposite coatings due to the oxidation of amorphous carbon and evaporation of CO_x [243]. Clearly, there are a large number of possibilities for designing superhard nanocomposite coatings with a unique combination of properties and a lot of research is still required to fully exploit the potential of these coatings.

10.2.2.3 Stability under Extreme Environments

The characterization of the superhard nanocomposite coatings is primarily focused on nanostructure, chemical composition, and mechanical properties as a function of processing conditions. However, detailed studies on the oxidation and corrosion behaviors of these coatings are insufficient. This section briefly discusses the performance of these coatings under extreme environments. In order to use the superhard nanocomposite coatings for industrial applications such as cutting tools, their high temperature stability in the air is very important. The higher the temperature that these coatings can sustain, the higher the achievable machining speed. Higher machining speeds are required for efficient and high precision machining in the manufacturing industry. In general, the thermal stability of superhard nanocomposite coatings depends on their nanostructure and composition, and also on the properties of the constituent nanocrystalline and amorphous phases.

The oxidation resistance of TiN/Si_3N_4 superhard nanocomposite coatings has been studied in recent years [39,213]. It has been shown that Ti-Si-N nanocomposite coatings offer better protection against oxidation than TiN coatings. The *nc*-TiN/*a*-Si_3N_4 nanocomposite coatings have been reported to be stable up to 1100°C in the air [201]. The absence of Ostwald ripening in these coatings as a result of annealing in the air up to 1100°C indicates the absence of any Ti diffusion through the *a*-Si_3N_4 matrix [201]. Furthermore, a decrease in the oxidation rate of the Ti-Si-N system with an increase in the Si content (up to 10 at.%) has been reported [225,247]. As has been mentioned in Section 10.2.1.7, in TiN coatings, the boundaries between the columns and the grain boundaries between the TiN crystallites offer a path for the diffusion of oxygen. However, in the case of TiN/Si_3N_4 nanocomposite coatings, the Si_3N_4 phase surrounding the TiN crystallites acts as a diffusion barrier due to its covalent bonding characteristics. The stable oxidation product SiO_2 is also believed to act as an oxygen diffusion barrier [248]. In addition, higher thermal stability of the superhard nanocomposite coatings is also due to the inherent thermodynamic stability of the nanostructure at the percolation threshold as a result of strong bonding at the interfaces [208]. However, the exact reason for this thermodynamic stability of the nanostructure is not clearly known and may be related to the quantum confinement phenomena [208,249].

Oxidation resistance of the TiN/Si_3N_4 nanocomposite coatings is reported to be better than for the TiAlN coatings. As discussed previously, in the latter case, the Al ions easily diffuse to the surface and cause the formation of a rich aluminum oxide surface layer, which acts as a diffusion barrier. However, in the former case, only a slight migration of Si atoms to the surface of the coating takes place because of low solubility of Si in the TiN lattice and also because of the strong Si-N

covalent bonds. Even though the measurements of mechanical properties after heat treatment of the superhard nanocomposite coatings are lacking, the recent results of Colligon et al. indicate that the TiN/Si_3N_4 nanocomposite coatings retain their hardness up to 1000°C after annealing in vacuum for 30 min [250]. Their TEM data also indicated no changes in the nanostructure of these coatings after annealing up to 1000°C. These results highlight the significance of superhard nanocomposite coatings for dry machining. Similar improvements in the thermal stability of W-Si-N, Zr-Si-N, Ta-Si-N, etc., superhard nanocomposite coatings have also been reported [251–253].

Recent trends in the development of superhard nanocomposite coatings with high thermal stability include the addition of Al in the transition metal nitride based nanocomposite coatings [214,222,254–256]. In particular, the addition of Al in the TiN/Si_3N_4 nanocomposite coatings has been reported to improve the oxidation behavior. Interest in the development of the Ti-Al-Si-N nanocomposite system has been motivated by the superior high temperature cutting performance of TiAlN [77,167]. The Ti-Al-Si-N nanocomposite coatings retain their properties (e.g., hardness) up to 1100°C [255]. It must be emphasized that in spite of the accelerated developments in the deposition and characterization of the superhard nanocomposite coatings during the last decade, there are still a large number of unanswered questions regarding their structural stability at higher temperatures. Both theoretical and experimental studies are required to fully understand the superior thermal stability of superhard nanocomposite coatings.

Unlike the thermal stability, the electrochemical behavior of superhard nanocomposite coatings has not been investigated in detail [214,257]. The corrosion behavior of superhard nanocomposite coatings is expected to be similar to that of the nanolayered multilayer coatings. As has been discussed in Section 10.2.1.4, the binary and the ternary transition metal nitride coatings deposited by PVD techniques exhibit a columnar microstructure with pores between the inter-granular columns, forming a direct path for the corrosive medium to pass through the coating defects [187]. Hence, these coatings exhibit low corrosion resistance, whereas, amorphous coatings (such as a-Si_3N_4, a-BN_x, a-C, etc.) exhibit high corrosion resistance because of their dielectric nature and dense microstructure without preferential corrosion paths like grain boundaries and other structural defects. Recent literature suggests that the superhard nanocomposite coatings exhibit improved corrosion resistance as compared with the conventional transitional metal nitride PVD hard coatings [213,214]. For instance, about 1.5 μm thick sputter deposited TiN/Si_3N_4 nanocomposite coating with a silicon content of approximately 27 at.% improves the corrosion resistance of the stainless steel substrate by a factor of 6 [213]. Similar results have also been reported for $TiAlN/Si_3N_4$ nanocomposite coatings [214].

Several factors are believed to be responsible for the enhanced corrosion behavior of the nanocomposite coatings including: non-columnar and dense microstructure, the reduced crystallite size of the nanocomposite coatings, and poor electrical conductivity of the amorphous constituent in the nanocomposite coating (e.g., Si_3N_4 in TiN/Si_3N_4 nanocomposites). For the sputtered coatings, the dense microstructure and reduced crystallite size of the nanocomposite coatings are attributed to the ion bombardment during deposition and incorporation of the amorphous phase in the nanocrystalline matrix. For example, addition of a-Si_3N_4 in the TiN matrix is known to change the surface morphology from a pronounced columnar microstructure to a dense structure at low silicon contents [240,258]. It has been reported that the magnetron sputtered TiN coatings exhibit columns of 60–80 nm in diameter, which almost disappear with the addition of 9 at.% Si, indicating the presence of a dense microstructure in the nanocomposite coatings [258]. The densification effect as a result of ion bombardment has already been discussed in great detail in Section 10.2.1.4. The addition of the amorphous component in the crystalline matrix has also been reported to decrease the crystallite size of the nanocomposite coatings [213]. For example, addition of 27 at.% Si in the TiN matrix reduces the crystallite size from approximately 12 to 3 nm [213]. Both the densification effect and the reduced crystallite size observed in the nanocomposite coatings are, therefore, believed to be responsible for their enhanced corrosion behavior.

From the foregoing discussion, it is evident that the nanocomposite coatings not only exhibit superior mechanical properties (e.g., high hardness and toughness) but also have high structural stability under extreme environments. Therefore, the superhard nanocomposite coatings have a great potential for high-temperature machining applications.

10.3 APPLICATIONS, OUTLOOK, AND SUMMARY

Superhard nanolayered multilayer coatings and nanocomposite coatings are useful in several industrial sectors. They are needed wherever rapidly moving parts come into contact with a hot or corrosive environment or when high friction and impact are created. The applications of these coatings include: cutting tools for normal or high-speed machining (including dry machining), stamping tools, moulds and dies, bearings, wear components, aerospace and automotive parts, etc., to name a few. However, at present, a majority of these applications are in the field of high-speed machining of difficult-to-cut materials. It is expected that with the progress in understanding the properties of transition metal nitride based new generation hard coatings as well as the development of newer and simpler deposition technologies, these coatings may find applications in several other industrial sectors in the future. Figure 10.32 shows photographs of some of the sputter deposited transition metal nitride based hard and superhard coatings on high-speed steel (HSS) drill bits and other small engineering components, using a semi-industrial sputtering system shown in Figure 10.2. Significant improvement in the life of the coated tools (e.g., HSS drill bits) has been observed as compared with uncoated tools [77,259].

It must be noted that the selection of a coating for a given application depends upon a variety of factors. For example, in the case of cutting tools, the selection criteria is based on: the property of the tool material, pretreatment of the tool, deposition parameters (e.g., substrate temperature), microstructure of the coating, adhesion, the stress state of the coating, post-deposition treatment (e.g., annealing), and of course the performance evaluation methods (e.g., machining speed, feed

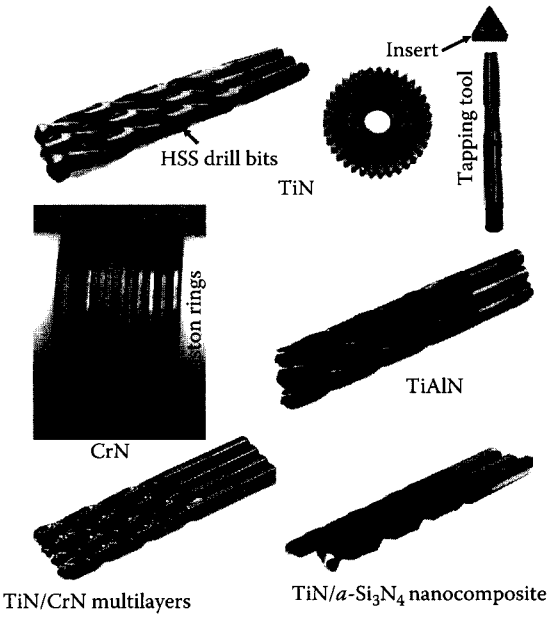

FIGURE 10.32 Photographs of HSS drill bits and other small engineering components coated with transition metal nitride based hard and superhard coatings using a semi-industrial unbalanced magnetron sputtering system in the authors' laboratory.

rate, nature of coolant, depth of cut, properties of the material to be machined, etc.). Therefore, one has to optimize these parameters to achieve the best results for a given application. Tables 10.3 and 10.4 list some of the applications of the transition metal nitride based nanolayered multilayer coatings and nanocomposite coatings, respectively. The information presented in the tables has been taken from recently published literature. The list is not necessarily complete as some of the coatings are marketed without revealing their microstructure, composition, etc. to protect intellectual property rights. The interested readers are advised to refer to websites of various reputed PVD coaters such as: Oerlikon Balzers, Platit AG Advanced Coating Systems, Hauzer Techno Coating BV, SHM Ltd., Teer Coatings Ltd., Swiss Tek Coatings, Inc., Ceme Con, Crystallume, Ion Bond, Hitachi Tool Eng., Ltd., Unimerco, etc.

As can be seen from the information presented in Tables 10.3 and 10.4, the transition metal nitride based nanolayered multilayer coatings and nanocomposite coatings are already being used for a variety of industrial applications. In addition, these coatings have great potential in other manufacturing/processing applications. These include (but are not limited to): sliding, rolling and rotating tribological surfaces, metal/polymer bearing surfaces, engine and drive-train components, fuel injectors, power transmission components, gears, bearings, can-roller followers, piston pins, valves, tappets, etc. These coatings may also find applications in micro electro-mechanical systems due to their superior wear resistance and low friction. Their metallic nature as well as very high thermal stability may be utilized for interconnects in solid oxide fuel cell applications. However, in order to fully exploit the potential of these coatings, newer deposition technologies need to be developed. In

TABLE 10.3
Applications of Transition Metal Nitride Based Nanolayered Multilayer Coatings

Coating System	Application	References
TiN/NbN	Machining of stainless steel	[260]
	Rolling contact fatigue of M-50 steel	[261]
TiAlN/CrN	Protection of titanium aluminides used in aerospace industry	[138]
	Moulds for high temperature Cu semi-solid processing	[262]
CrN/NbN	Printing industry, leather industry and surgical blades	[138]
	Textile industry (combing rollers, scissors, blades, etc.)	[138]
	Cutlery industry	[263]
TiAlN/VN	Dry high-speed machining of low-alloyed and Ni-based steels	[138]
	Dry high-speed machining of Al alloys	[138]
	Machining of Al alloys for aerospace and automotive components	[264]
TiN/AlTiN	Machining of inconel superalloys	[265,266]
	High-speed machining of stainless steel	[267]
$TiAl_xN/TiAl_yN$	Dry machining of gray and ductile cast iron	[268]
$TiAlN_x/TiAlN_y$	Machining of difficult-to-cut materials (CrNiMoTi, CrMo, etc.)	[269]
TiN/CrN	Moulds for high temperature Cu semi-solid processing	[262]
TiN/TaN	Machining of stainless steel	[260]
TiN/SiN_x	Hard disk and tribological applications	[270]
TiN/CrN-Ti/Cr-TiN/CrN	Periodontal instruments	[271]
TiAlCrN/TiAlYN	Dry high-speed machining of steels	[138]
	Coatings on moulds for glass industry	[138]
	Protection of titanium aluminides used in aerospace industry	[138]
TiAlCrN/NbN	Dry high-speed machining of hardened H 13 steel	[272]
$CrN_x/a\text{-}Si_3N_4$	Water hydraulic components	[273]

Source: Values taken from NIST–X-ray photoelectron spectroscopy database, Version 3.5 (National Institute of Standards and Technology, Gaithersburg, 2003); http://srdata.nist.gov/xps

TABLE 10.4
Applications of Transition Metal Nitride Based Superhard Nanocomposite Coatings

Coating System	Application	References
TiSiN	Diffusion barrier liners for gigascale copper interconnect applications	[274]
	High-speed cutting tool machining	[275]
TiAlSiN	High-speed machining of ASTM 1043 steel	[203,205]
	Machining of commercial alloy steel	[216]
	High-speed machining of high hardened die steel	[254]
	Stamping tools	[276]
	High-speed machining of alloyed cold work steel X155CrVMo12–1 DIN 1.2379	[276]
	Machining of hard and tough sintered Co-alloy	[276]
	Dry tapping	[276]
	High-speed machining of cast iron GGC-40	[276]
	High-speed machining of Inconel	[276]
	High-speed machining of hardened AISI D2 steel	[277]
AlSiTiN	High-speed machining of M2 die steel	[242]
	Dry milling of AISI M2 die steel	[278]
	High-speed machining of hardened steel	[279]
	Machining of titanium-based alloys	[280]
TiAlBN	Machining of mild steel	[281]
TiBN	Machining of hardened steel at high cutting speed	[203,205]
$(Ti_{1-x}Al_x)N/a\text{-}Si_3N_4+TiN$	High-speed machining of HSS AISI M2 steel	[282]
CrSiN	Green machining of brass	[239]
	Hydraulic piston pump used in electro-hydrostatic actuators	[283]
	High-speed micro-drilling of circuit board	[284]
CrAlSiN	High-speed micro-drilling of circuit board	[284]
	Dry turning of cast iron and aluminum alloy	[285]
AlCrSiN	High-speed machining of M2 die steel	[242]
$nc\text{-}(Al_{1-x}Cr_x)N/Si_3N_4$ (nACRo®)	Hobbing	[276]

Source: Values taken from NIST–X-ray photoelectron spectroscopy database, Version 3.5 (National Institute of Standards and Technology, Gaithersburg, 2003); http://srdata.nist.gov/xps

addition, hybrid coating technologies can be used to develop novel coatings with superior properties. These coating technologies should be modeled and tailored for specific applications at affordable costs. Nevertheless, to develop newer coatings, a synergistic and deeper understanding of the constitution and microstructure of the coatings, and also deposition methodologies are required.

In the search for newer extrinsic superhard coatings, efforts should also be directed towards the oxide materials and a combination of oxide/nitride materials. This is because of the fact that most of the transition metal nitride based nanolayered multilayer coatings and nanocomposite coatings have limitations for very high temperature applications. Therefore, extrinsic superhard coatings consisting of highly stable oxide materials such as Al_2O_3, Y_2O_3, ZrO_2, etc., that are stable at very high temperatures (e.g., melting point = 2700°C, 2000°C, and 2400°C for ZrO_2, Al_2O_3, and Y_2O_3, respectively) need to be explored. Few reports have been published on the mechanical properties of the oxide multilayer coatings [286,287]. For example, it has been shown that ZrO_2/Al_2O_3 and ZrO_2/Y_2O_3 nanolayered multilayer coatings exhibit hardnesses as high as 30 and 28 GPa, respectively, which are very high as compared with the rule-of-mixture values (15 and 13 GPa, respectively for ZrO_2/Al_2O_3 and ZrO_2/Y_2O_3) [287]. Furthermore, it has been demonstrated that crystalline/amorphous multilayers

based on ZrO_2 and Al_2O_3 exhibit very high resistance to plastic deformation with a structural stability up to 1100°C [287]. However, there is no published literature on nanocomposite coatings based on oxide materials. In the future, it may be possible to design oxide based nanolayered multilayer coatings and nanocomposite coatings consisting of several combinations of oxide materials, which will exhibit outstanding mechanical, thermal, and chemical properties.

In summary, we have reviewed state-of-the-art techniques in the deposition and the characterization of the transition metal nitride based nanolayered multilayer coatings and nanocomposite coatings. We have discussed in detail the structural and the mechanical properties of these coatings and also the performance of these coatings under extreme environments. It has been shown that these coatings can operate across multiple extreme environments. It has been demonstrated that reactive sputtering is a promising technique for the deposition of these coatings on small engineering components (such as cutting tools). However, the development of these coatings on large areas and deposition at production scale at an affordable cost still needs considerable efforts. Furthermore, studies correlating the deposition conditions and the resulting properties are desirable. It is believed that use of *in situ* techniques should be useful in this direction. In addition, theoretical simulations may be necessary to provide details on the atomic structure and subsequent property enhancement of these coatings. Considerable efforts also need to be made to improve the toughness and the adhesion of these coatings. Finally, both nanolayered multilayer coatings and nanocomposite coatings provide enormous flexibility in choice of material and therefore provide an opportunity to design novel coating properties. In addition to the applications discussed above, there exists a large number of possibilities yet to be explored. The ever increasing number of researchers working in this field (including the industry) will enable us to exploit the vast potential of these coatings in the near future.

ACKNOWLEDGMENTS

The authors are grateful to all their students, coworkers, and collaborators. Special mention should be made to Dr. D.V. Sridhara Rao of DMRL, Hyderabad and Dr. Sujeet Chaudhary of IIT, Delhi. Dr. Anjana Jain, Mr. V. K. William Grips, Mr. N. Selvakumar, Mrs. V. Ezhil Selvi, Mr. G. H. Jakeer Khan, Mr. Siju, Mr. V. Praveen Kumar, and Mr. N. T. Manikandanath all from National Aerospace Laboratories (NAL), Bangalore are thanked for their help at various stages of the work partially presented in this review. This work was supported in part by NAL, Bangalore, Council of Scientific and Industrial Research (CSIR), New Delhi, and Department of Science and Technology, New Delhi. We wish to thank the Director, NAL (CSIR) for his constant support and permission to publish this book chapter.

ABBREVIATIONS

AES	Auger electron spectroscopy
AFM	Atomic force microscopy
BF	Bright field
DC	Direct current
DF	Dark field
EIS	Electrochemical impedance spectroscopy
FWHM	Full-width-at-half maximum
HRTEM	High resolution transmission electron microscopy
HSS	High-speed steel
MS	Mild steel
PACVD	Plasma assisted chemical vapor deposition
PR	Principal reflection
PVD	Physical vapor deposition
RF	Radio frequency

SAD	Selected area diffraction
SEM	Scanning electron microscopy
SR	Satellite reflection
TEM	Transmission electron microscopy
XPS	X-ray photoelectron spectroscopy
XRD	X-ray diffraction
XRR	X-ray reflectivity
XTEM	Cross-sectional transmission electron microscopy

SYMBOLS

A	Projected contact area in nanoindentation
C	Crack length
d	Inter-atomic distance
$\overline{d}$	Average lattice spacing
d'	Average crystallite size
d_{max}	Maximum indentation depth
E	Elastic modulus
E	Width of the interface
E^*	Effective elastic modulus
E_{corr}	Corrosion potential
E_h	Covalent band gap
G	Shear modulus
H	Hardness
i_{corr}	Corrosion current density
n	Refractive index
N	Number of interfaces in a multilayer
P_{max}	Peak indentation load
S	Stiffness
T_A	Annealing temperature
V_S	Substrate bias voltage
W_E	Elastic deformation energy
W_P	Plastic deformation energy
Y	Young's modulus
Γ	Surface energy per unit area
θ_m	Incident angle
θ_{PR}	Position of the principal reflection
θ_{SR}	Position of the satellite reflection
ν	Poisson's ratio
λ	Wavelength of x-rays
Λ	Modulation wavelength
σ	Fracture stress
σ'	Interface roughness
σ_c	Critical stress required to cause fracture

REFERENCES

1. Holleck, H. 1999. Design of nanostructured thin films for tribological applications. In *Surface Engineering: Science and Technology I*, eds. A. Kumar, Y.-W. Chung, J. J. Moore, and J. E. Smugeresky, pp. 207–218. Warrendale, PA: The Minerals, Metals and Materials Society.
2. Burakowski, T. and Wierzchoñ, T. 1999. *Surface Engineering of Metals*. Boca Raton, FL: CRC Press.

3. Byrne, G., Dornfeld, D., and Denkena, B. 2003. Advanced cutting technology. *Ann. CIRP* 52: 483–507.
4. Taga, Y. 1999. Review of plasma thin-film technology in automobile industry. *Surf. Coat. Technol.* 112: 339–346.
5. Erkens, G., Cremer, R., Hamoudi, T. et al. 2003. Supernitrides: A novel generation of PVD hard coatings to meet the requirements of high demanding cutting applications. *Ann. CIRP* 52: 65–68.
6. Bull, S. J. 2006. Physical vapor deposition methods for protection against wear. In *Surface Coatings for Protection Against Wear*, ed. B. G. Mellor, pp. 146–183. Cambridge, U.K.: Woodhead Publishing Limited.
7. Holleck, H. 1986. Material selection for hard coatings. *J. Vac. Sci. Technol. A* 4: 2661–2669.
8. Toth, L. E. 1971. *Transition Metal Carbides and Nitrides*. New York: Academic Press.
9. Holleck, H. 1990. Basic principles of specific applications of ceramic materials as protective layers. *Surf. Coat. Technol.* 43–44: 245–258.
10. Sundgren, J.-E. and Hentzell, H. T. G. 1986. A review of the present state of art in hard coatings grown from the vapor phase. *J. Vac. Sci. Technol. A* 4: 2259–2279.
11. Musil, J., Kadlec, S., Valvoda, V., Kuzel Jr., R. and Cerny, R. 1990. Ion-assisted sputtering of TiN films. *Surf. Coat. Technol.* 43–44: 259–269.
12. Musil, J., Bardos, L., Rajsky, A. et al. 1986. TiN_x coatings prepared by D.C. reactive magnetron sputtering. *Thin Solid Films* 136: 229–239.
13. Petrov, I., Hultman, L., Helmersson, U., Sundgren, J.-E., and Greene, J. E. 1989. Microstructure modification of TiN by ion bombardment during reactive sputter deposition. *Thin Solid Films* 169: 299–314.
14. Randhawa, H. 1986. TiN-coated high-speed steel cutting tools. *J. Vac. Sci. Technol. A* 4: 2755–2758.
15. Kwak, M. Y., Shin, D. H., Kang, T. W., and Kim, K. N. 1999. Characteristics of TiN barrier layer against Cu diffusion. *Thin Solid Films* 339: 290–293.
16. Jehn, H. A. 2000. Improvement of the corrosion resistance of PVD hard coating-substrate systems. *Surf. Coat. Technol.* 125: 212–217.
17. Wittmer, M., Noser, J., and Melchior, H. 1981. Oxidation kinetics of TiN thin films. *J. Appl. Phys.* 52: 6659–6664.
18. Münz, W. D. 1986. Titanium aluminum nitride films: A new alternative to TiN coatings. *J. Vac. Sci. Technol. A* 4: 2717–2725.
19. Ichimura, H. and Kawana, A. 1993. High-temperature oxidation of ion-plated TiN and TiAlN films. *J. Mater. Res.* 8: 1093–1100.
20. PalDey, S. and Deevi, S. C. 2003. Single layer and multilayer wear resistant coatings of (Ti,Al)N: A review. *Mater. Sci. Eng. A* 342: 58–79.
21. Mo, J. L., Zhu, M. H., Lei, B., Leng, Y. X., and Huang, N. 2007. Comparison of tribological behaviors of AlCrN and TiAlN coatings-deposited by physical vapor deposition. *Wear* 263: 1423–1429.
22. Berg, G., Friedrich, C., Broszeit, E., and Berger, C. 1996. Development of chromium nitride coatings substituting titanium nitride. *Surf. Coat. Technol.* 86–87: 184–191.
23. Sue, J. A. and Chang, T. P. 1995. Friction and wear behavior of titanium nitride, zirconium nitride and chromium nitride coatings at elevated temperatures. *Surf. Coat. Technol.* 76–77: 61–69.
24. Engel, P., Schwarz, G., and Wolf, G. K. 1998. Corrosion and mechanical studies of chromium nitride films prepared by ion-beam-assisted deposition. *Surf. Coat. Technol.* 98: 1002–1007.
25. Barshilia, H. C., Selvakumar, N., Deepthi, B., and Rajam, K. S. 2006. A comparative study of reactive direct current magnetron sputtered CrAlN and CrN coatings. *Surf. Coat. Technol.* 201: 2193–2201.
26. Endrino, J. L., Fox-Rabinovich, G. S., and Gey, C. 2006. Hard AlTiN, AlCrN PVD coatings for machining of austenitic stainless steel. *Surf. Coat. Technol.* 200: 6840–6845.
27. Barshilia, H. C., Deepthi, B., Rajam, K. S., Bhatti, K. P., and Chaudhary, S. 2008. Structure and properties of reactive direct current magnetron sputtered niobium aluminum nitride coatings. *J. Mater. Res.* 23: 1258–1268.
28. Sanjinés, R., Sandu, C. S., Lamni, R., and Lévy, F. 2006. Thermal decomposition of $Zr_{1-x}Al_xN$ thin films deposited by magnetron sputtering. *Surf. Coat. Technol.* 200: 6308–6312.
29. Howe, B., Bareño, J., Sardela, M. et al. 2007. Growth and physical properties of epitaxial metastable $Hf_{1-x}Al_xN$ alloys deposited on MgO(001) by ultrahigh vacuum reactive magnetron sputtering. *Surf. Coat. Technol.* 202: 809–814.
30. Nieh, T. G. and Wadsworth, J. 1991. Hall-Petch relation in nanocrystalline solids. *Scr. Metall.* 25: 955–958.
31. Hultman, L., Helmersson, U., Barnett, S. A., Sundgren, J.-E., and Greene, J. E. 1987. Low-energy ion irradiation during film growth for reducing defect densities in epitaxial TiN (100) films deposited by reactive-magnetron sputtering. *J. Appl. Phys.* 61: 552–555.

32. Ljungcrantz, H., Hultman, L., Sundgren, J.-E., and Karlsson, L. 1995. Ion induced stress generation in arc-evaporated TiN films. *J. Appl. Phys.* 78: 832–837.
33. Yoder, M. N. 1993. Diamond properties and applications. In *Diamond Films and Coatings—Development, Properties and Applications*, ed. R. F. Davis, pp. 1–30. Park Ridge, NJ: Noyes Publications.
34. Ehrhardt, H. 1995. New developments in the field of superhard coatings. *Surf. Coat. Technol.* 74–75: 29–35.
35. Zerr, A. and Riedel, R. 2000. Introduction: Novel ultrahard materials. In *Handbook of Ceramic Hard Materials*, Vol. 1, ed. R. Riedel, XLV–LXXVII. Weinheim, Germany: Wiley-VCH.
36. Barnett, S. A. and Madan, A. 1998. Superhard superlattices. *Physics World.* January Issue: 45–50.
37. Vepřek, S. 1999. The search for novel, superhard materials. *J. Vac. Sci. Technol. A* 17: 2401–2420.
38. Musil, J. 2000. Hard and superhard nanocomposite coatings. *Surf. Coat. Technol.* 125: 322–330.
39. Vepřek, S., Haussmann, M., Reiprich, S., Shizhi, L., and Dian, J. 1996. Novel thermodynamically stable and oxidation resistant superhard coating materials. *Surf. Coat. Technol.* 86–87: 394–401.
40. Tjong, S. C. and Chen, H. 2004. Nanocrystalline materials and coatings. *Mater. Sci. Eng. R* 45: 1–88.
41. Yashar, P. C. and Sproul, W. D. 1999. Nanometer scale multilayered hard coatings. *Vacuum* 55: 179–190.
42. Ruud, J. A., Jervis, T. R., and Spaepen, F. 1994. Nanoindentation of Ag/Ni multilayered thin films. *J. Appl. Phys.* 75: 4969–4974.
43. Barnett, S. A. and Shinn, M. 1994. Plastic and elastic properties of compositionally modulated thin films. *Annu. Rev. Mater. Sci.* 24: 481–511.
44. Koehler, J. S. 1970. Attempt to design a strong solid. *Phys. Rev. B* 2: 547–551.
45. Chu, X. and Barnett, S. A. 1995. Model of superlattice yield stress and hardness enhancements. *J. Appl. Phys.* 77: 4403–4411.
46. Voevodin, A. A., Zabinski, J. S., and Muratore, C. 2005. Recent advances in hard, tough, and low friction nanocomposite coatings. *Tsinghua Sci. Technol.* 10: 665–679.
47. Zhang, S., Sun, D., Fu, Y., and Du, H. 2005. Toughening of hard nanostructural thin films: A critical review. *Surf. Coat. Technol.* 198: 2–8.
48. Lehoczky, S. L. 1978. Retardation of dislocation generation and motion in thin layered metal laminates. *Phys. Rev. Lett.* 41: 1814–1818.
49. Greer, A. L. and Somekh, R. E. 1991. Metallic multilayers. In *Materials Science and Technology: A Comprehensive Treatment*, eds. R. W. Cahn, P. Haasen, and E. J. Kramer. pp. 329–370. Weinheim, Germany: VCH.
50. Barshilia, H. C. and Rajam, K. S. 2002. Characterization of Cu/Ni multilayer coatings by nanoindentation and atomic force microscopy. *Surf. Coat. Technol.* 155: 195–202.
51. Shih, K. K. and Dove, D. B. 1992. Ti/Ti-N, Hf/Hf-N and W/W-N multilayer films with high mechanical hardness. *Appl. Phys. Lett.* 61: 654–656.
52. Wang, X., Kolitsch, A., and Möller, W. 1997. Roughness improvement and hardness enhancement in nanoscaled Al/AlN multilayered thin films. *Appl. Phys. Lett.* 71: 1951–1953.
53. Madan, A., Chu, X., and Barnett, S. A. 1996. Growth and characterization of epitaxial Mo/NbN superlattices. *Appl. Phys. Lett.* 68: 2198–2200.
54. Barshilia, H. C., Jain, A., and Rajam, K. S. 2004. Structure, hardness and thermal stability of nanolayered TiN/CrN multilayer coatings. *Vacuum* 72: 241–248.
55. Barshilia, H. C. and Rajam, K. S. 2003. Deposition of TiN/CrN hard superlattices by reactive d.c. magnetron sputtering. *Bull. Mater. Sci.* 26: 233–237.
56. Chu, X., Wong, M. S., Sproul, W. D., and Barnett, S. A. 1999. Deposition, structure and hardness of polycrystalline transition metal nitride superlattice films. *J. Mater. Res.* 14: 2500–2507.
57. Helmersson, U., Todorova, S., Barnett, S. A., Sundgren, J. E., Markert, L. C., and Greene, J. E. 1987. Growth of single crystal TiN/VN strained layer superlattices with extremely high mechanical hardness. *J. Appl. Phys.* 62: 481–484.
58. Barshilia, H. C. and Rajam, K. S. 2004. Structure and properties of reactive DC magnetron sputtered TiN/NbN hard superlattices. *Surf. Coat. Technol.* 183: 174–183.
59. Barshilia, H. C., Rajam, K. S., Jain, A., Gopinadhan, K., and Chaudhary, S. 2006. A comparative study on the structure and properties of nanolayered TiN/NbN and TiAlN/TiN multilayer coatings prepared by reactive direct current magnetron sputtering. *Thin Solid Films* 503: 158–166.
60. Barshilia, H. C., Prakash, M. S., Jain, A., and Rajam, K. S. 2005. Structure, hardness and thermal stability of TiAlN and nanolayered TiAlN/CrN multilayer films. *Vacuum* 77: 169–179.
61. Chu, X., Barnett, S. A., Wong, M. S., and Sproul, W. D. 1993. Reactive unbalanced magnetron sputter deposition of polycrystalline TiN/NbN superlattice coatings. *Surf. Coat. Technol.* 57: 13–18.

62. Shinn, M., Hultman, L., and Barnett, S. A. 1992. Growth, structure and microhardness of epitaxial TiN/NbN superlattices. *J. Mater. Res.* 7: 901–911.
63. Yashar, P., Barnett, S. A., Rechner, J., and Sproul, W. D. 1998. Structure and mechanical properties of polycrystalline CrN/TiN superlattices. *J. Vac. Sci. Technol. A* 16: 2913–2918.
64. Yang, Q., He, C., Zhao, L. R., and Immarigeon, J.-P. 2002. Preferred orientation and hardness enhancement of TiN/CrN superlattice coatings deposited by reactive magnetron sputtering. *Scr. Mater.* 46: 293–297.
65. Mirkarimi, P. B., Barnett, S. A., Hubbard, K. M., Jervis, T. R., and Hultman, L. 1994. Structure and mechanical properties of epitaxial $TiN/V_{0.3}Nb_{0.7}N(100)$ superlattices. *J. Mater. Res.* 9: 1456–1467.
66. Madan, A., Kim, I. W., Cheng, S. C., Yashar, P., Dravid, V. P., and Barnett, S. A. 1997. Stabilization of cubic AlN in epitaxial AlN/TiN superlattices. *Phys. Rev. Lett.* 78: 1743–1746.
67. Knutsson, A., Johansson, M. P., Persson, P. O. A., Hultman, L., and Odén, M. 2008. Thermal decomposition products in arc evaporated TiAlN/TiN multilayers. *Appl. Phys. Lett.* 93: 143110–143112.
68. Lewis, D. B., Wadsworth, I., Münz, W.-D., KuzelJr, R., and Valvoda, V. 1999. Structure and stress of TiAlN/CrN superlattice coatings as a function of CrN layer thickness. *Surf. Coat. Technol.* 116–119: 284–291.
69. Luo, Q., Rainforth, W. M., and Münz, W.-D. 1999. TEM observations of wear mechanisms of TiAlCrN and TiAlN/CrN coatings grown by combined steered-arc/unbalanced magnetron deposition. *Wear* 225–229: 74–82.
70. Hovsepian, P. E., Lewis, D. B., Münz, W.-D., Rouzaud, A., and Juliet, P. 1999. Chromium nitride/niobium nitride superlattice coatings deposited by combined cathodic-arc/unbalanced magnetron technique. *Surf. Coat. Technol.* 116–119: 727–734.
71. Barshilia, H. C., Deepthi, B., Selvakumar, N., Jain A., and Rajam, K. S. 2007. Nanolayered multilayer coatings of CrN/CrAlN prepared by reactive DC magnetron sputtering. *Appl. Surf. Sci.* 253: 5076–5083.
72. Barshilia, H. C., Deepthi, B., Rajam, K. S., Bhatti, K. P., and Chaudhary, S. 2009. Growth and characterization of TiAlN/CrAlN superlattices prepared by reactive direct current magnetron sputtering. *J. Vac. Sci. Technol. A* 27: 29–36.
73. Barshilia, H. C. and Rajam, K. S. 2006. Reactive sputtering of hard nitride coatings using asymmetric-bipolar pulsed DC generator. *Surf. Coat. Technol.* 201: 1827–1835.
74. Sproul, W. D. 1996. New routes in the preparation of mechanically hard films. *Science* 273: 889–892.
75. Safi, I. 2000. Recent aspects concerning DC reactive magnetron sputtering of thin films: A review. *Surf. Coat. Technol.* 127: 203–219.
76. Weast, R. C. and Astle, M. J. 1982. *CRC Handbook of Chemistry and Physics*. Boca Raton, FL: CRC Press, Inc.
77. Barshilia, H. C., Yogesh, K., and Rajam, K. S. 2008. Deposition of TiAlN coatings using reactive bipolar-pulsed direct current unbalanced magnetron sputtering. *Vacuum* 83: 427–434.
78. Hurkmans, T., Hauzer, F., Buil, B., Engel, K., and Tietema, R. 1997. A new large volume PVD coating system using advanced controlled arc and combined arc/unbalanced magnetron (ABS™) deposition techniques. *Surf. Coat. Technol.* 92: 62–68.
79. Fullerton, E. E., Schuller, I. K., Vanderstraeten, H., and Bruynseraede, Y. 1992. Structural refinement of superlattices from X-ray diffraction. *Phys. Rev. B* 45: 9292–9310.
80. Stearns, M. B. 1988. Microcrystalline and interface structure of metallic multilayers from x-ray spectra. *Phys. Rev. B* 38: 8109–8113.
81. Clemens, B. M. and Gay, J. G. 1987. Effect of layer-thickness fluctuations on superlattice diffraction. *Phys. Rev. B* 35: 9337–9340.
82. Lamelas, F. J., He, H. D., and Clarke, R. 1991. Numerical modeling of superlattice x-ray scattering intensities. *Phys. Rev. B* 43: 12296–12303.
83. Madan, A., Yashar, P., Shinn, M., and Barnett, S. A. 1997. An x-ray diffraction study of epitaxial TiN/NbN superlattices. *Thin Solid Films* 302: 147–154.
84. Briggs, D. and Seah, M. P. 1990. *Practical Surface Analysis, Vol. 1., Auger and X-ray Photoelectron Spectroscopy*. New York: John Wiley & Sons.
85. Bertóti, I. 2002. Characterization of nitride coatings by XPS. *Surf. Coat. Technol.* 151–152: 194–203.
86. Wagner, C. D., Riggs, W. M., Davis, L. E., Moulder, J. F., and Muilenberg, G. E. 1979. *Handbook of X-Ray Photoelectron Spectroscopy*. Eden Prairie, MN: Perkin Elmer Corporation, Physical Electronics Division.
87. Höchst, H., Bringans, R. D., Steiner, P., and Wolf, T. 1982. Photoemission study of the electronic structure of stoichiometric and sub-stoichiometric TiN and ZrN. *Phys. Rev. B* 25: 7183–7191.

88. Hofmann, S. 1986. Characterization of nitride coatings by Auger electron spectroscopy and x-ray photoelectron spectroscopy. *J. Vac. Sci. Technol. A* 4: 2789–2796.
89. Göpel, W., Anderson, J. A., Frankel, D. et al. 1984. Surface defects of TiO_2(110): A combined XPS, XAES and ELS study. *Surf. Sci.* 139: 333–346.
90. Milošev, I., Strehblow, H.-H., and Navinšek, B. 1995. XPS in the study of high-temperature oxidation of CrN and TiN hard coatings. *Surf. Coat. Technol.* 74–75: 897–902.
91. Lippitz, A. and Hübert, T. 2005. XPS investigations of chromium nitride thin films. *Surf. Coat. Technol.* 200: 250–253.
92. Emery, C., Chourasia, A. R., and Yashar, P. 1999. A study of CrN_x thin films by x-ray photoelectron spectroscopy. *J. Electron Spectrosc. Relat. Phenom.* 104: 91–97.
93. Cheng, R., Borca, C. N., Pilet, N. et al. 2002. Oxidation of metals at the chromium oxide interface. *Appl. Phys. Lett.* 81: 2109–2111.
94. Darlinski, A. and Halbritter, J. 1987. Angle-resolved XPS studies of oxides at NbN, NbC and Nb surfaces. *Surf. Interface Anal.* 10: 223–237.
95. Havey, K. S., Zabinski, J. S., and Walck, S. D. 1997. The chemistry, structure, and resulting wear properties of magnetron-sputtered NbN thin films. *Thin Solid Films* 303: 238–245.
96. Ruby, C., Ott, R., Huang, F., Weaver, M. L., and Barnard, J. A. 2000. XPS study of reactively sputtered Ti-B-N hard coatings. *Surf. Interface Anal.* 29: 823–828.
97. Joyner, D. J. and Hercules, D. M. 1980. Chemical bonding and electronic structure of B_2O_3, H_3BO_3, and BN: An ESCA, Auger, SIMS and SXS study. *J. Chem. Phys.* 72: 1095–1108.
98. Arranz, A. 2004. Synthesis of hafnium nitride thin films by 0.5-5 keV nitrogen implantation of metallic Hf: An X-ray photoelectron spectroscopy and factor analysis study. *Surf. Sci.* 563: 1–12.
99. He, G., Liu, M., Zhu, L. Q., Chang, M., Fang, Q., and Zhang, L. D. 2005. Effect of postdeposition annealing on the thermal stability and structural characteristics of sputtered HfO_2 films on Si (100). *Surf. Sci.* 576: 67–75.
100. Morant, C., Sanz, J. M., Galán, L., Soriano, L. and Rueda, F. 1989. An XPS study of the interaction of oxygen with zirconium. *Surf. Sci.* 218: 331–345.
101. Swatzky, G. A. and Post, D. 1979. X-ray photoelectron and Auger spectroscopy study of some vanadium oxides. *Phys. Rev. B* 20: 1546–1555.
102. Mendialdua, J., Casanova, R., and Barbaux, Y. 1995. XPS studies of V_2O_5, V_6O_{13}, VO_2 and V_2O_3. *J. Electron. Spectrosc. Relat. Phenom.* 71: 249–261.
103. Chiu, H.-T. and Chuang, S.-H. 1993. Tungsten nitride thin films prepared by MOCVD. *J. Mater. Res.* 8: 1353–1360.
104. Jeong, S.-H., Kim, J.-K., Kim, B.-S., Shim, S.-H., and Lee, B.-T. 2004. Characterization of SiO_2 and TiO_2 films prepared using rf magnetron sputtering and their application to anti-reflection coating. *Vacuum* 76: 507–515.
105. Sugawara, M., Kondo, M., Yamazaki, S., and Nakajima, K. 1988. Exact determination of superlattice structures by small-angle x-ray diffraction method. *Appl. Phys. Lett.* 52: 742–744.
106. Payne, A. P. and Clemens, B. M. 1993. Influence of roughness distributions and correlations on x-ray diffraction from superlattices. *Phys. Rev. B* 47: 2289–2300.
107. Parratt, L. G. 1954. Surface studies of solids by total reflection of x-rays. *Phys. Rev.* 95: 359–369.
108. Miceli, P. F., Neumann, D. A., and Zabel, H. 1986. X-ray refractive index: A tool to determine the average composition in multilayer structures. *Appl. Phys. Lett.* 48: 24–26.
109. Fullerton, E. E., Pearson, J., Sowers, C. H., Bader, S. D., Wu, X. Z., and Sinha, S. K. 1993. Interfacial roughness of sputtered multilayers: Nb/Si. *Phys. Rev. B* 48: 17432–17444.
110. Yang, Q. and Zhao, L. R. 2008. Characterization of nano-layered multilayer coatings using modified Bragg law. *Mater. Charact.* 59: 1285–1291.
111. Logothetidis, S., Kalfagiannis, N., Sarakinos, K., and Patsalas, P. 2006. Investigation of bilayer period and individual layer thickness of CrN/TiN superlattices by ellipsometry and x-ray techniques. *Surf. Coat. Technol.* 200: 6176–6180.
112. Barshilia, H. C., Selvakumar, N., Rajam, K. S., Gopinadhan, K., and Chaudhary, S. 2008. Investigation of interface properties of sputter deposited TiN/CrN superlattices by low angle x-ray reflectivity. *J. Phys. D Appl. Phys.* 41: 205409–205418.
113. Paul, A. and Lodha, G. S. 2002. Interface roughness correlation due to changing layer period in Pt/C multilayers. *Phys. Rev. B* 65: 245416-1–245416-9.
114. Liu, Z.-J. and Shen, Y. G. 2004. Oscillating growth of surface roughness in multilayer films. *Appl. Phys. Lett.* 84: 5121–5123.

115. Eriksson, F., Johansson, G. A., Hertz, H. M., and Birch, J. 2002. Enhanced soft x-ray reflectivity of Cr/Sc multilayers by ion-assisted sputter deposition. *Opt. Eng.* 41: 2903–2909.
116. Hultman, L., Engström, C., and Odén, M. 2000. Mechanical and thermal stability of TiN/NbN superlattice thin films. *Surf. Coat. Technol.* 133–134: 227–233.
117. Hultman, L. 2000. Thermal stability of nitride thin films. *Vacuum* 57: 1–30.
118. Bravman, J. C. and Sinclair, R. 1984. The preparation of cross-section specimens for transmission electron microscopy. *J. Electron Microsc. Tech.* 1: 53–61.
119. Helmersson, U. and Sundgren, J.-E. 1991. Cross-section preparation for TEM of film-substrate combinations with a large difference in sputtering yields. *J. Electron. Microsc. Tech.* 4: 361–369.
120. Han, K. and Zhang, K. Y. 2004. Transmission electron microscopy study of metallic multilayers. *Scr. Mater.* 50: 781–786.
121. Baxter, C. S. and Stobbs, W. M. 1986. Artifacts in transmission electron microscope images of artificially layered metallic superlattices. *Appl. Phys. Lett.* 48: 1202–1204.
122. Flevaris, N. K. and Karakostas, T. 1988. A columnar-growth mode in strained compositionally modulated Cu-Ni: Cross-sectional electron microscopy. *J. Appl. Phys.* 63: 1228–1230.
123. Panjan, M., Šturm, S., Panjan, P., and Čekada, M. 2007. TEM investigation of TiAlN/CrN multilayer coatings prepared by magnetron sputtering. *Surf. Coat. Technol.* 202: 815–819.
124. Meidia, H., Cullis, A. G., Schönjahn, C., Münz, W.-D., and Rodenburg, J. M. 2002. Investigation of intermixing in TiAlN/VN nanoscaled multilayer coatings by energy-filtered TEM. *Surf. Coat. Technol.* 151–152: 209–213.
125. Hultman, L., Shinn, M., Mirkarimi, P. B. and Barnett, S. A. 1994. Characterization of misfit dislocations in epitaxial (001)-oriented TiN, NbN, VN and (Ti,Nb)N film heterostructures by transmission electron microscopy. *J. Cryst. Growth* 135: 309–317.
126. Luo, Q. and Hovsepian, P. E. 2006. Transmission electron microscopy and energy dispersive x-ray spectroscopy on the worn surface of nano-structured TiAlN/VN multilayer coating. *Thin Solid Films* 497: 203–209.
127. Luo, Q., Rainforth, W. M., and Münz, W.-D. 2001. TEM studies of the wear of TiAlN/CrN superlattice coatings. *Scr. Mater.* 45: 399–404.
128. Barshilia, H. C., Rajam, K. S., and Rao, D. V. S. 2006. Characterization of low temperature deposited nanolayered TiN/NbN multilayer coatings by cross-sectional transmission electron microscopy. *Surf. Coat. Technol.* 200: 4586–4593.
129. Snyder, C. W., Orr, B. G., Kessler, D., and Sander, L. M. 1991. Effect of strain on surface morphology in highly strained InGaAs films. *Phys. Rev. Lett.* 66: 3032–3035.
130. Thornton, J. A. and Penfold, A. S. 1978. Cylindrical magnetron sputtering. In *Thin Film Processes*, eds. J. L. Vossen and W. Kern, pp. 75–113. New York: Academic Press, Inc.
131. Fischer-Cripps, A. C. 2004. *Nanoindentation*, 2nd edn. New York: Springer-Verlag.
132. Oliver, W. C. and Pharr, G. M. 1992. An improved technique for determining hardness and elastic modulus using load and displacement sensing indentation experiments. *J. Mater. Res.* 7: 1564–1583.
133. Randall, N. X. and Bozet, J. L. 1997. Nanoindentation and scanning force microscopy as a novel method for the characterization of tribological transfer films. *Wear* 212: 18–24.
134. Tsui, T. Y. and Pharr, G. M. 1999. Substrate effects on nanoindentation mechanical property measurement of soft films on hard substrates. *J. Mater. Res.* 14: 292–301.
135. Zhou, Y., Asaki, R., Soe, W.-H., Yamamoto, R., Chen, R., and Iwabuchi, A. 1999. Hardness anomaly, plastic deformation work and fretting wear properties of polycrystalline TiN/CrN multilayers. *Wear* 236: 159–164.
136. Zhang, S., Sun, D., Fu, Y., and Du, H. 2005. Toughness measurement of thin films: A critical review. *Surf. Coat. Technol.* 198: 74–84.
137. Musil, J. and Jirout, M. 2007. Toughness of hard nanostructured ceramic thin films. *Surf. Coat. Technol.* 201: 5148–5152.
138. Hovsepian, P. E. and Münz, W.-D. 2006. Synthesis, structure and applications of nanoscale multilayer/superlattice structured PVD coatings. In *Nanostructured Coatings*, eds. A. Cavaleiro and J. T. M. De Hosson, pp. 555–644. New York: Springer Science.
139. Thobor, A., Rousselot, C., Clement, C. et al. 2000. Enhancement of mechanical properties of TiN/AlN multilayers by modifying the number and quality of interfaces. *Surf. Coat. Technol.* 124: 210–221.
140. Barnett, S. A. 1993. Deposition and mechanical properties of superlattice thin films. In *Physics of Thin Films*, Vol. 17, eds. M. H. Francombe and J. L. Vossen, pp. 1–77. Boston, MA: Academic Press, Inc.
141. Dieter, G. E. 1976. *Mechanical Metallurgy*, 2nd edn. New York: McGraw-Hill, Inc.

142. Cammarata, R. C., Schlesinger, T. E., Kim, C., Qadri, S. B., and Edelstein, A. S. 1990. Nanoindentation study of the mechanical properties of copper-nickel multilayered thin films. *Appl. Phys. Lett.* 56: 1862–1864.
143. Hall, E. O. 1951. The deformation and ageing of mild steel: III Discussion of results. *Proc. Phys. Soc. Lond.* 64: 747–753.
144. Petch, N. J. 1953. The cleavage strength of polycrystals. *J. Iron Steel Inst.* 174: 25–28.
145. Xu, J., Kamiko, M., Zhou, Y., Yamamoto, R., Li, G., and Gu, M. 2001. Superhardness effects of heterostructure NbN/TaN nanostructured multilayers. *J. Appl. Phys.* 89: 3674–3678.
146. Bhushan, B. 1999. *Principles and Applications of Tribology*. New York: John Wiley & Sons, Inc.
147. Matthes, B., Broszeit, E., and Kloos, K. H. 1990. Fundamental and tribological properties of r.f. sputtered TiN coatings in plastic manufacturing model wear tests. *Surf. Coat. Technol.* 43–44: 688–698.
148. Takadoum, J. and Bennani, H. H. 1997. Influence of substrate roughness and coating thickness on adhesion, friction and wear of TiN films. *Surf. Coat. Technol.* 96: 272–282.
149. Sue, J. A. and Troue, H. H. 1990. Friction and wear properties of titanium nitride coating in sliding contact with AISI 01 steel. *Surf. Coat. Technol.* 43–44: 709–720.
150. Vancoille, E., Blanpain, B., Xingpu, Y., Celis, J.-P., and Roos, J. R. 1994. Tribo-oxidation of a TiN coating sliding against corundum. *J. Mater. Res.* 9: 992–998.
151. Cho, C.-W. and Lee, Y.-Z. 2003. Effects of oxide layer on the friction characteristics between TiN coated ball and steel disk in dry sliding. *Wear* 254: 383–390.
152. Kustas, F. M., Fehrehnbacher, L. L., and Komanduri. R. 1997. Nanocoatings on cutting tools for dry machining. *CIRP Ann. Manuf. Technol.* 46: 39–42.
153. Prengel, H. G., Pfouts, W. R., and Santhanam, A. T. 1998. State of the art in hard coatings for carbide cutting tools. *Surf. Coat. Technol.* 102: 183–190.
154. Budtz-Jørgensen, C. V., Kringhøj, P., and Bøttiger, J. 1999. The critical role of hydrogen for physical sputtering with Ar-H_2 glow discharges. *Surf. Coat. Technol.* 116–119: 938–943.
155. Löffler, F. 1999. Methods to investigate mechanical properties of coatings. *Thin Solid Films* 339: 181–186.
156. Larsson, M., Bromark M., Hedenqvist, P., and Hogmark, S. 1997. Mechanical and tribological properties of multilayered PVD TiN/NbN coatings. *Surf. Coat. Technol.* 91: 43–49.
157. Nordin, M., Larsson, M., and Hogmark, S. 1999. Mechanical and tribological properties of multilayered PVD TiN/CrN. *Wear* 232: 221–225.
158. Holleck, H. and Schier, V. 1995. Multilayer PVD coatings for wear protection. *Surf. Coat. Technol.* 76–77: 328–336.
159. Zhou, Y. M., Asaki, R., Higashi, K., Soe, W. H., and Yamamoto, R. 2000. Sliding wear behavior of polycrystalline TiN/CrN multilayers against an alumina ball. *Surf. Coat. Technol.* 130: 9–14.
160. An, J. and Zhang, Q. Y. 2007. Structure, hardness and tribological properties of nanolayered TiN/TaN multilayer coatings. *Mater. Charact.* 58: 439–446.
161. Chang, C.-L., Jao, J.-Y., Ho, W.-Y., and Wang, D.-Y. 2007. Influence of bi-layer period thickness on the residual stress, mechanical and tribological properties of nanolayered TiAlN/CrN multilayer coatings. *Vacuum* 81: 604–609.
162. Archard, J. F. 1953. Contact and rubbing of flat surfaces. *J. Appl. Phys.* 24: 981–988.
163. Zeghni, A. E. and Hashmi, M. S. J. 2004. The effect of coating and nitriding on the wear behavior of tool steels. *J. Mater. Process. Technol.* 155–156: 1918–1922.
164. Trent, E. M. and Wright, P. K. 2000. *Metal Cutting*, 4th edn. Boston, MA: Butterworth-Heinemann.
165. Barshilia, H. C. and Rajam, K. S. 2004. Raman spectroscopy studies on the thermal stability of TiN, CrN, TiAlN coatings and nanolayered TiN/CrN, TiAlN/CrN multilayer coatings. *J. Mater. Res.* 19: 3196–3205.
166. Panjan, P., Navinšek, B., Cvelbar, A., Zalar, A., and Milošev, I. 1996. Oxidation of TiN, ZrN, TiZrN, CrN, TiCrN and TiN/CrN multilayer hard coatings reactively sputtered at low temperature. *Thin Solid Films* 281–282: 298–301.
167. Raveh, A., Zukerman, I., Shneck, R., Avni, R., and Fried, I. 2007. Thermal stability of nanostructured superhard coatings: A review. *Surf. Coat. Technol.* 201: 6136–6142.
168. Tien, S.-K. and Duh, J.-G. 2006. Effect of heat treatment on mechanical properties and microstructure of CrN/AlN multilayer coatings. *Thin Solid Films* 494: 173–178.
169. Zeng, X. T., Zhang, S., Sun, C. Q., and Liu, Y. C. 2003. Nanometric-layered CrN/TiN thin films: Mechanical strength and thermal stability. *Thin Solid Films* 424: 99–102.
170. Andrievski, R. A., Anisimova, I. A., Anisimov, V. P., Makarov, V. P., and Popova, V. P. 1995. Grain size and recrystallization of TiN, ZrN, NbN, and CrN alloyed and multilayer films. *Thin Solid Films* 261: 83–86.

171. Panjan, P., Navinšek, B., Cvelbar, A., Zalar, A., and Vlcek, J. 1998. High-temperature oxidation of TiN/CrN multilayers reactively sputtered at low temperatures. *Surf. Coat. Technol.* 98: 1497–1502.
172. Wadsworth, I., Smith, I. J., Donohue, L. A., and Münz, W.-D. 1997. Thermal stability and oxidation resistance of TiAlN/CrN multilayer coatings. *Surf. Coat. Technol.* 94–95: 315–321.
173. Lopez, S., Wong, M.-S., and Sproul, W. D. 1995. Thermal behavior of carbon nitride and TiN/NbN superlattice films. *J. Vac. Sci. Technol. A* 13: 1644–1648.
174. Ichimura, H. and Kawana, A. 1994. High temperature oxidation of ion-plated CrN films. *J. Mater. Res.* 9: 151–155.
175. Mclntyre, D., Greene, J.-E., Håkansson, G., Sundgren, J.-E., and Münz, W.-D. 1990. Oxidation of metastable single-phase polycrystalline $Ti_{0.5}Al_{0.5}N$ films: Kinetics and mechanisms. *J. Appl. Phys.* 67: 1542–1553.
176. Tanaka, Y., Gür, T. M., Kelly, M. et al. 1992. Properties of $(Ti_{1-x}Al_x)N$ coatings for cutting tools prepared by the cathodic arc ion plating method. *J. Vac. Sci. Technol. A* 10: 1749–1756.
177. Engström, C., Birch, J., Hultman, L. et al. 1999. Interdiffusion studies of single crystal TiN/NbN superlattice thin films, *J. Vac. Sci. Technol. A* 17: 2920–2927.
178. Jeong, J. J., Hwang, S. K., and Lee, C. 2002. Hardness and adhesion properties of HfN/Si_3N_4 and NbN/Si_3N_4 multilayer coatings. *Mater. Chem. Phys.* 9314: 1–7.
179. Lembke, M. I., Lewis, D. B., and Münz, W.-D. 2000. Localised oxidation defects in TiAlN/CrN superlattice structured hard coatings grown by cathodic arc/unbalanced magnetron deposition on various substrate materials. *Surf. Coat. Technol.* 125: 263–268.
180. Cunha, L. and Andritschky, M. 1999. Residual stress, surface defects and corrosion resistance of CrN hard coatings. *Surf. Coat. Technol.* 111: 158–162.
181. Scully, J. R. 2003. The polarization resistance method for determination of instantaneous corrosion rates. In *Electrochemical Techniques in Corrosion Science and Engineering*, eds. R. G. Kelly, J. R. Scully, D. W. Shoesmith, and R. G. Buchheit, pp. 125–150. New York: Marcel-Dekker, Inc.
182. Cunha, L., Andritschky, M., Rebouta, L., and Pischow, K. 1999. Corrosion of CrN and TiAlN coatings in chloride-containing atmospheres. *Surf. Coat. Technol.* 116–119: 1152–1160.
183. Grips, V. K. W., Barshilia, H. C., Selvi, V. E., Kalavati, and Rajam, K. S. 2006. Electrochemical behavior of single layer CrN, TiN, TiAlN coatings and nanolayered TiAlN/CrN multilayer coatings prepared by reactive direct current magnetron sputtering. *Thin Solid Films* 514: 204–211.
184. Grips, V. K. W., Selvi, V. E., Barshilia, H. C., and Rajam, K. S. 2006. Effect of electroless nickel interlayer on the electrochemical behavior of single layer CrN, TiN, TiAlN coatings and nanolayered TiAlN/CrN multilayer coatings prepared by reactive dc magnetron sputtering. *Electrochim. Acta* 51: 3461–3468.
185. Barshilia, H. C., Prakash, M. S., Poojari, A., and Rajam, K. S. 2004. Corrosion behavior of nanolayered TiN/NbN multilayer coatings prepared by reactive direct current magnetron sputtering process. *Thin Solid Films* 460: 133–142.
186. Nordin, M., Herranen, M., and Hogmark, S. 1999. Influence of lamellae thickness on the corrosion behavior of multilayered PVD TiN/CrN coatings. *Thin Solid Films* 348: 202–209.
187. Liu, C., Bi, Q., and Matthews, A. 2001. EIS comparison on corrosion performance of PVD TiN and CrN coated mild steel in 0.5 N NaCl aqueous solution. *Corros. Sci.* 43: 1953–1961.
188. Liu, C., Leyland, A., Lyon, S., and Matthews, A. 1995. Electrochemical impedance spectroscopy of PVD-TiN coatings on mild steel and AISI316 substrates. *Surf. Coat. Technol.* 76–77: 615–622.
189. Lang, F. and Yu, Z. 2001. The corrosion resistance and wear resistance of thick TiN coatings deposited by arc ion plating. *Surf. Coat. Technol.* 145: 80–87.
190. Brown, R., Alias, M. N., and Fontana, R. 1993. Effect of composition and thickness on corrosion behavior of TiN and ZrN thin films. *Surf. Coat. Technol.* 62: 467–473.
191. Fenker, M., Balzer, M., Jehn, H. A. et al. 2002. Improvement of the corrosion resistance of hard wear resistant coatings by intermediate plasma etching or multilayered structure. *Surf. Coat. Technol.* 150: 101–106.
192. Souto, R. M. and Alanyali, H. 2000. Electrochemical characteristics of steel coated with TiN and TiAlN coatings. *Corros. Sci.* 42: 2201–2211.
193. Brandl, W. and Gendig, C. 1996. Corrosion behaviour of hybrid coatings. *Thin Solid Films* 290–291: 343–347.
194. Vacandio, F., Massiani, Y., Eyraud, M., Rossi, S., and Fedrizzi, L. 2001. Influence of various nickel underlayers on the corrosion behaviour of AlN films deposited by reactive sputtering. *Surf. Coat. Technol.* 137: 284–292.
195. Chen, J.-S., Duh, J.-G., and Wu, F.-B. 2002. Microhardness and corrosion behavior in CrN/electroless Ni/mild steel complex coating. *Surf. Coat. Technol.* 150: 239–245.
196. Doong, J. C., Duh, J. G., Tsai, S. Y., Wang, J. H., and Chiou, B. S. 1993. Corrosion behaviour of electroless nickel plating modified TiN coating. *Surf. Coat. Technol.* 58: 157–161.

197. Lewis, D. B., Creasey, S. J., Wüstefeld, C., Ehiasarian, A. P., and Hovsepian, P. E. 2006. The role of the growth defects on the corrosion resistance of CrN/NbN superlattice coatings deposited at low temperatures. *Thin Solid Films* 503: 143–148.
198. Liu, C., Leyland, A., Bi, Q., and Matthews, A. 2001. Corrosion resistance of multi-layered plasma-assisted physical vapor deposition TiN and CrN coatings. *Surf. Coat. Technol.* 141: 164–173.
199. Lin, C. S., Ke, C. S., and Peng, H. 2001. Corrosion of CrN and CrN/TiN coated heat-resistant steels in molten A356 aluminum alloy. *Surf. Coat. Technol.* 146–147: 168–174.
200. Chang, C.-L., Chen, W.-C., Tsai, P.-C., Ho, W.-Y., and Wang, D.-Y. 2007. Characteristics and performance of TiSiN/TiAlN multilayers coating synthesized by cathodic arc plasma evaporation. *Surf. Coat. Technol.* 202: 987–992.
201. Vepřek, S., Reiprich, S., and Shizhi, L. 1995. Superhard nanocrystalline composite materials: The TiN/Si_3N_4 system. *Appl. Phys. Lett.* 66: 2640–2642.
202. Musil, J. and Vlček. J. 2001. Magnetron sputtering of hard nanocomposite coatings and their properties. *Surf. Coat. Technol.* 142–144: 557–566.
203. Holubar, P., Jilek, M., and Sima, M. 2000. Present and possible future applications of superhard nanocomposite coatings. *Surf. Coat. Technol.* 133–134: 145–151.
204. Vaz, F., Rebouta, L., Almeida, B. et al. 1999. Structural analysis of $Ti_{1-x}Si_xN_y$ nanocomposite films prepared by reactive magnetron sputtering. *Surf. Coat. Technol.* 120–121: 166–172.
205. Holubár, P., Jílek, M., and Šíma, M. 1999. Nanocomposite nc-TiAlSiN and nc-TiN-BN coatings: Their applications on substrates made of cemented carbide and results of cutting tests. *Surf. Coat. Technol.* 120–121: 184–188.
206. Zhang, S., Sun, D., Fu, Y., and Du, H. 2003. Recent advances of superhard nanocomposite coatings: A review. *Surf. Coat. Technol.* 167: 113–119.
207. Vepřek, S., Vepřek-Heijman, M. G. J., Karvankova, P., and Prochazka, J. 2005. Different approaches to superhard coatings and nanocomposites. *Thin Solid Films* 476: 1–29.
208. Vepřek, S., Haussmann, M., and Reiprich, S. 1996. Superhard nanocrystalline W_2N/amorphous Si_3N_4 composite materials. *J. Vac. Sci. Technol. A* 14: 46–51.
209. Hirai, T. and Hayashi, S. 1982. Preparation and some properties of chemically vapour-deposited Si_3N_4-TiN composite. *J. Mater. Sci.* 17: 1320–1328.
210. Hayashi, S., Hirai, T., Hiraga, K., and Hirabayashi, M. 1982. Microstructure of Si_3N_4-TiN composites prepared by chemical-vapour deposition. *J. Mater. Sci.* 17: 3336–3340.
211. Shizhi, L., Yulong, S., and Hongrui, P. 1992. Ti-Si-N films prepared by plasma-enhanced chemical vapor deposition. *Plasma Chem. Plasma Process.* 12: 287–297.
212. Barshilia, H. C., Prakash, M. S., Rao, D. V. S., and Rajam, K. S. 2005. Superhard nanocomposite coatings of TiN/a-C prepared by reactive DC magnetron sputtering. *Surf. Coat. Technol.* 195: 147–153.
213. Barshilia, H. C., Deepthi, B., Arun Prabhu, A. S., and Rajam, K. S. 2006. Superhard nanocomposite coatings of TiN/Si_3N_4 prepared by reactive direct current unbalanced magnetron sputtering. *Surf. Coat. Technol.* 201: 329–337.
214. Barshilia, H. C., Deepthi, B., and Rajam, K. S. 2006. Deposition and characterization of TiAlN/Si_3N_4 superhard nanocomposite coatings prepared by reactive direct current unbalanced magnetron sputtering. *Vacuum* 81: 479–488.
215. Barshilia, H. C., Deepthi, B., and Rajam, K. S. 2007. Deposition and characterization of CrN/Si_3N_4 and CrAlN/Si_3N_4 nanocomposite coatings prepared using reactive DC unbalanced magnetron sputtering. *Surf. Coat. Technol.* 201: 9468–9475.
216. Carvalho, S., Ribeiro, E., Rebouta, L. et al. 2004. Microstructure, mechanical properties and cutting performance of superhard (Ti,Si,Al)N nanocomposite films grown by d.c. reactive magnetron sputtering. *Surf. Coat. Technol.* 177–178: 459–468.
217. Musil, J. and Hrubý, H. 2000. Superhard nanocomposite $Ti_{1-x}Al_xN$ films prepared by magnetron sputtering. *Thin Solid Films* 365: 104–109.
218. Li, D., Lin, X. W., Cheng, S.-C. et al. 1996. Structure and hardness studies of CN_x/TiN nanocomposite coatings. *Appl. Phys. Lett.* 68: 1211–1213.
219. Vepřek, S., Niederhofer, A., Moto, K. et al. 2000. Composition, nanostructure and origin of ultrahardness in nc-TiN/a-Si_3N_4/a- and nc-$TiSi_2$ nanocomposites with $H_v = 80$ to ≥ 105 GPa. *Surf. Coat. Technol.* 133–134: 152–159.
220. Chokshi, A. H., Rosen, A., Karch, J., and Gleiter, H. 1989. On the validity of the Hall-Petch relationship in nanocrystalline materials. *Scr. Metall.* 23: 1679–1684.
221. Schiøtz, J., Tolla, F. D. D., and Jacobsen, K. W. 1998. Softening of nanocrystalline metals at very small grain sizes. *Nature* 391: 561–563.

222. Vaz, F., Rebouta, L., Andritschky, M., da Silva, M. F., and Soares, J. C. 1998. Oxidation resistance of (Ti, Al, Si) N coatings in air. *Surf. Coat. Technol.* 98: 912–917.
223. Vaz, F., Rebouta, L., Ramos, S., da Silva, M. F., and Soares, J. C. 1998. Physical, structural and mechanical characterization of $Ti_{1-x}Si_xN_y$ films. *Surf. Coat. Technol.* 108–109: 236–240.
224. Vaz, F., Rebouta, L., Goudeau, P. et al. 2000. Characterization of $Ti_{1-x}Si_xN_y$ nanocomposite films. *Surf. Coat. Technol.* 133–134: 307–313.
225. Vaz, F., Rebouta, L., Andritschky, M., da Silva, M. F., and Soares, J. C. 1999. The effect of addition of Al and Si on the physical and mechanical properties of titanium nitride. *J. Mater. Process. Technol.* 92–93: 169–176.
226. Musil, J. and Vlček, J. 1998. Magnetron sputtering of films with controlled texture and grain size. *Mater. Chem. Phys.* 54: 116–122.
227. Musil, J., Kunc, F., Zeman, H., and Poláková, H. 2002. Relationships between hardness, Young's modulus and elastic recovery in hard nanocomposite coatings. *Surf. Coat. Technol.* 154: 304–313.
228. Vossen, J. L. and Cuomo, J. J. 1978. Glow discharge sputter deposition. In *Thin Film Processes*, eds. J. L. Vossen and W. Kern, pp. 75–113. New York: Academic Press, Inc.
229. Barshilia, H. C., Deepthi, B., and Rajam, K. S. 2008. Growth and characterization of aluminum nitride coatings prepared by pulsed-direct current reactive unbalanced magnetron sputtering. *Thin Solid Films* 516: 4168–4174.
230. Zhang, S., Sun, D., Fu, Y., and Du, H. 2004. Effect of sputtering target power on microstructure and mechanical properties of nanocomposite nc-TiN/a-SiN_x thin films. *Thin Solid Films* 447–448: 462–467.
231. Martin, P. J., Bendavid, A., Cairney, J. M., and Hoffman, M. 2005. Nanocomposite Ti-Si-N, Zr-Si-N, Ti-Al-Si-N, Ti-Al-V-Si-N thin film coatings deposited by vacuum arc deposition. *Surf. Coat. Technol.* 200: 2228–2235.
232. Kauffmann, F., Ji, B., Dehm, G., Gao, H., and Arzt, E. 2005. A quantitative study of the hardness of a superhard nanocrystalline titanium nitride/silicon nitride coating. *Scr. Mater.* 52: 1269–1274.
233. Cullity, B. D. 1978. *Elements of X-Ray Diffraction*. London, U.K.: Addison-Wesley.
234. Vepřek, S. and Argon, A. S. 2002. Towards the understanding of mechanical properties of super- and ultrahard nanocomposites. *J. Vac. Sci. Technol. B* 20: 650–664.
235. Zhang, R. F. and Vepřek, S. 2006. On the spinodal nature of the phase segregation and formation of stable nanostructure in the Ti-Si-N system. *Mater. Sci. Eng. A* 424: 128–137.
236. Ma, S., Procházka, J., Karvánkova, P. et al. 2005. Comparative study of the tribological behavior of superhard nanocomposite coatings nc-TiN/a-Si_3N_4 with TiN. *Surf. Coat. Technol.* 194: 143–148.
237. Park, O.-N., Park, J. H., Yoon, S.-Y., Lee, M.-H., and Kim, K. H. 2004. Tribological behavior of Ti-Si-N coating layers produced by a hybrid system of arc ion plating and sputtering techniques. *Surf. Coat. Technol.* 179: 83–88.
238. He, J. L., Miyake, S., Setsuhara, Y. et al. 2001. Improved anti-wear performance of nanostructured titanium boron nitride coatings. *Wear* 249: 498–502.
239. Kim, C., Kang, M. C., Kim, J. S., Kim, K. H., Shin, B. S., and Je, T. J. 2009. Mechanical properties and cutting performance of nanocomposite Cr-Si-N coated tool for green machining. *Curr. Appl. Phys.* 9: S145–S148.
240. Diserens, M., Patscheider, J., and Lévy, F. 1998. Improving the properties of titanium nitride by incorporation of silicon. *Surf. Coat. Technol.* 108–109: 241–246.
241. Pilloud, D., Pierson, J. F., and Takadoum, J. 2006. Structure and tribological properties of reactively sputtered Zr-Si-N films. *Thin Solid Films* 496: 445–449.
242. Settineri, L., Faga, M. G., Gautier, G., and Perucca, M. 2008. Evaluation of wear resistance of AlSiTiN and AlSiCrN nanocomposite coatings for cutting tools. *CIRP Ann. Manuf. Technol.* 57: 575–578.
243. Ma, D., Ma, S., Dong, H., Xu, K., and Bell, T. 2006. Microstructure and tribological behavior of superhard Ti-Si-C-N nanocomposite coatings deposited by plasma enhanced chemical vapor deposition. *Thin Solid Films* 496: 438–444.
244. Takadoum, J., Houmid-Bennani, H., and Mairey, D. 1998. The wear characteristics of silicon nitride. *J. Eur. Ceram. Soc.* 18: 553–556.
245. Ma, D., Ma, S., and Xu, K. 2005. The tribological and structural characterization of nano-structured Ti-Si-N films coated by pulsed-d.c. plasma enhanced CVD. *Vacuum* 79: 7–13.
246. Lin, J., Mishra, B., Moore, J. J., Pinkas, M., and Sproul, W. D. 2008. Structure and properties of Ti-B-C-N nanocomposite coatings synthesized using pulsed closed field unbalanced magnetron sputtering (P-CFUBMS). *Surf. Coat. Technol.* 203: 588–593.
247. Choi, J. B., Cho, K., Kim, Y., Kim, K. H., and Song, P. K. 2003. Microstructure effect on the high-temperature oxidation resistance of Ti-Si-N coating layers. *Jpn. J. Appl. Phys.* 42: 6556–6559.

248. Kim, K. H. and Park, B. H. 1999. Mechanical properties and oxidation behavior of Ti-Si-N films prepared by plasma-assisted CVD. *Chem. Vap. Deposition* 6: 275–279.
249. Vepřek, S. 1997. Electronic and mechanical properties of nanocrystalline composites when approaching molecular size. *Thin Solid Films* 297: 145–153.
250. Colligon, J. S., Vishnyakov, V., Valizadeh, R., Donnelly, S. E., and Kumashiro, S. 2005. Study of nanocrystalline TiN/Si_3N_4 thin films deposited using a dual ion beam method. *Thin Solid Films* 485: 148–154.
251. Cavaleiro, A. and Louro, C. 2007. Thermal behavior of hard nanocomposite coatings within the W-Si-N system in oxidant and protective atmospheres. *Surf. Coat. Technol.* 201: 6154–6160.
252. Daniel, R., Musil, J., Zeman, P., and Mitterer, C. 2006. Thermal stability of magnetron sputtered Zr-Si-N films. *Surf. Coat. Technol.* 201: 3368–3376.
253. Zeman, P., Musil, J., and Daniel, R. 2006. High-temperature oxidation resistance of Ta-Si-N films with a high silicon content. *Surf. Coat. Technol.* 200: 4091–4096.
254. Kim, J. S., Kim, G. J., Kang, M. C., Kim, J. W., and Kim, K. H. 2005. Cutting performance of Ti-Al-Si-N-coated tool by a hybrid-coating system for high-hardened materials. *Surf. Coat. Technol.* 193: 249–254.
255. Vepřek, S., Männling, H.-D., Jilek, M., and Holubar, P. 2004. Avoiding the high-temperature decomposition and softening of $(Al_{1-x}Ti_x)N$ coatings by the formation of stable superhard nc-$(Al_{1-x}Ti_x)N$/a-Si_3N_4 nanocomposite. *Mater. Sci. Eng. A* 366: 202–205.
256. Chang, Y.-Y., Chang, C.-P., Wang, D.-Y., Yang, S.-M., and Wu, W. 2008. High temperature oxidation resistance of CrAlSiN coatings synthesized by a cathodic arc deposition process. *J. Alloys Compd.* 461: 336–341.
257. Lin, C. H. and Duh, J. G. 2008. Corrosion behavior of $(Ti\text{-}Al\text{-}Cr\text{-}Si\text{-}V)_xN_y$ coatings on mild steels derived from RF magnetron sputtering. *Surf. Coat. Technol.* 203: 558–561.
258. Jiang, N., Shen, Y. G., Mai, Y.-W., Chan, T., and Tung, S. C. 2004. Nanocomposite Ti-Si-N films deposited by reactive unbalanced magnetron sputtering at room temperature. *Mater. Sci. Eng. B* 106: 163–171.
259. Barshilia, H. C. and Rajam, K. S. 2007. Performance evaluation of reactive direct current unbalanced magnetron sputter deposited nanostructured TiN coated high-speed steel drill bits. *Bull. Mater. Sci.* 30: 607–614.
260. Selinder, T. I., Sjöstrand, M. E., Nordin, M., Larsson, M., Östlund, A., and Hogmark, S. 1998. Performance of PVD TiN/TaN and TiN/NbN superlattice coated cemented carbide tools in stainless steel machining. *Surf. Coat. Technol.* 105: 51–55.
261. Liston, M.-J. A. 1998. Rolling contact fatigue properties of TiN/NbN superlattice coatings on M-50 steel. *ASTM Special Tech. Publ.* 1327: 499–510.
262. Lee, S. Y. and Lee, S. Y. 2006. Comparative evaluation of TiN/CrN, AlN/CrN, TiAlN/CrN multilayer films for the use of semi-solid processing of Cu alloys. In *Solid State Phenomana*, eds. C. G. Kang, S. K. Kim, and S. Y. Lee, vol. 116–117, pp. 124–127. Zurich, Switzerland: Trans Tech Publications Ltd.
263. Hovsepian, P. E., Münz, W.-D., Medlock, A., and Gregory, G. 2000. Combined cathodic arc/unbalanced magnetron grown CrN/NbN superlattice coatings for applications in the cutlery industry. *Surf. Coat. Technol.* 133–134: 508–516.
264. Hovsepian, P. E., Luo, Q., Robinson, G. et al. 2006. TiAlN/VN superlattice structured PVD coatings: A new alternative in machining of aluminum alloys for aerospace and automotive components. *Surf. Coat. Technol.* 201: 265–272.
265. Ducros, C., Benevent, V., and Sanchette, F. 2003. Deposition, characterization and machining performance of multilayer PVD coatings on cemented carbide cutting tools. *Surf. Coat. Technol.* 163–164: 681–688.
266. Dudzinski, D., Devillez, A., Moufki, A., Larrouquère, D., Zerrouki, V., and Vigneau, J. 2004. A review of developments towards dry and high speed machining of Inconel 718 alloy. *Int. J. Machine Tools Manuf.* 44: 439–456.
267. Penich, R. M., Hegde, P. L., and Inspektor, A. Nanolayered coated cutting tool and method for making the same. U.S. Patent 6,884,499, April 26, 2005.
268. Prengel, H. G., Jindal, P. C., Wendt, K. H., Santhanam, A. T., Hegde, P. L., and Penich, R. M. 2001. A new class of high performance PVD coatings for carbide cutting tools. *Surf. Coat. Technol.* 139: 25–34.
269. Hofmann, D. and Hensel, B. Multilayer Ti-Al-N coating for tools. U.S. Patent 5,330,853, July 19, 1994.
270. Lee, K. W., Li, D.-J., and Chung, Y.-W. 2002. Nanolayer coatings for hard disk and demanding tribological applications. *JOM* 54: 49–52.
271. Gorokhovsky, V., Heckerman, B., Watson, P., and Bekesch, N. 2006. The effect of multilayer filtered arc coatings on mechanical properties, corrosion resistance and performance of periodontal dental instruments. *Surf. Coat. Technol.* 200: 5614–5630.

272. Fox-Rabinovich, G. S., Yamamoto, K., Kovalev, A. I. et al. 2008. Wear behavior of adaptive nanomultilayered TiAlCrN/NbN coatings under dry high performance machining conditions. *Surf. Coat. Technol.* 202: 2015–2022.
273. Kim, G. S., Kim, B. S., and Lee, S. Y. 2005. High-speed wear behaviors of CrSiN coatings for the industrial applications of water hydraulics. *Surf. Coat. Technol.* 200: 1814–1818.
274. Eisenbraun, E., Upham, A., Dash, R. et al. 2000. Low temperature inorganic chemical vapor deposition of Ti-Si-N diffusion barrier liners for gigascale copper interconnect applications. *J. Vac. Sci. Technol. B* 18: 2011–2015.
275. Takeshi, I. 2004. Latest trends of nanocomposites. Progress of material technology and application development: Cases and topics. TiSiN coated tools drastically improved in strength and heat-resistance. *Eng. Mater.* 52: 52–56.
276. Vepřek, S. and Vepřek-Heijman, M. G. J. 2008. Industrial applications of superhard nanocomposite coatings. *Surf. Coat. Technol.* 202: 5063–5073.
277. Jeong, Y. K., Kang, M. C., Kwon, S. H., Kim, K. H., Kim, H. G., and Kim, J. S. 2009. Tool life of nanocomposite Ti-Al-Si-N coated end-mill by hybrid coating system in high speed machining of hardened AISI D2 steel. *Curr. Appl. Phys.* 9: S141–S144.
278. Faga, M. G., Gautier, G., Calzavarinin, R. et al. 2007. AlSiTiN nanocomposite coatings developed via arc cathodic PVD: Evaluation of wear resistance via tribological analysis and high speed machining operations. *Wear* 263: 1306–1314.
279. Tanaka, Y., Ichimiya, N., Onishi, Y., and Yamada, Y. 2001. Structure and properties of Al-Ti-Si-N coatings prepared by the cathodic arc ion plating method for high speed cutting applications. *Surf. Coat. Technol.* 146–147: 215–221.
280. Settineri, L. and Faga, M. G. 2008. Nanostructured cutting tools coatings for machining titanium. *Mach. Sci. Technol.* 12: 158–169.
281. Baker, M. A., Klose, S., Rebholz, C., Leyland, A., and Matthews, A. 2002. Evaluating the microstructure and performance of nanocomposite PVD TiAlBN coatings. *Surf. Coat. Technol.* 151–152: 338–343.
282. Settineri, L. and Faga, M. G. 2006. Laboratory tests for performance evaluation of nanocomposite coatings for cutting tools. *Wear* 260: 326–332.
283. Lee, S.-Y. and Hong, Y.-S. 2007. Effect of CrSiN thin film coating on the improvement of the low-speed torque efficiency of a hydraulic piston pump. *Surf. Coat. Technol.* 202: 1129–1134.
284. Kang, M. C., Je, S. K., Kim, K. H., Shin, B. S., Kwon, D. H., and Kim, J. S. 2008. Cutting performance of CrN-based coatings tool deposited by hybrid coating method for micro-drilling applications. *Surf. Coat. Technol.* 202: 5629–5632.
285. Abele, E., Schramm, B., and Scheerer, H. 2008. Dry machining using novel chromium based coatings. *Adv. Prod. Eng. Manag.* 3: 141–148.
286. Yashar, P. C., Barnett, S. A., Hultman, L., and Sproul, W. D. 1999. Deposition and mechanical properties of polycrystalline Y_2O_3/ZrO_2 superlattices. *J. Mater. Res.* 14: 3614– 3622.
287. Barshilia, H. C., Deepthi, B., and Rajam, K. S. 2008. Stabilization of tetragonal and cubic phases of ZrO_2 in pulsed sputter deposited ZrO_2/Al_2O_3 and ZrO_2/Y_2O_3 nanolayered thin films. *J. Appl. Phys.* 104: 113532 1–12.